Spring 5-8-2021

The Role of VGLL4 and MARK2-HDAC axis in Mitosis and Cancer

Yongji Zeng
University of Nebraska Medical Center

The Role of VGLL4 and MARK2-HDAC axis in Mitosis and Cancer

By

Yongji Zeng

A DISSERTATION

Presented to the Faculty of
the University of Nebraska Graduate College
in Partial Fulfillment of the Requirements
for the Degree of Doctor of Philosophy

Pathology & Microbiology Graduate Program

Under the Supervision of Professor Jixin Dong

University of Nebraska Medical Center
Omaha, Nebraska

April 2021

Supervisory Committee:
Rakesh Singh, Ph.D. Pankaj Singh, Ph.D.
Nicholas Woods, Ph.D.

ACKNOWLEDGMENTS

First and foremost, I would like to acknowledge the tireless work of Dr. Jixin Dong. He kindly took me into his mentorship. His indefatigable passion for science acts as a perfect role model for me and how a scientist should devote his/her life to the scientific research field. After a six-year-long journey in scientific research with his willingness to share his skills, knowledge, expertise, and patient mentor, I could now independently study a specific cancer disease in both clinic view and scientific research view.

Additionally, I would like to acknowledge my friends in the Dong lab, past and present, Xincheng Chen, Seth Staffer, Jiuli Zhou, Zhan Wang, Ling Yin, Renya Zeng, Yi Xiao, and Yuanhong Chen. Thank you for your support, when I pull you guys out of your work to help me to sharpen my mind and improve my scientific theories.

I would also like to acknowledge the mentorship and advice I have received over these six years from the amazing members of my dissertation committee: Dr. Rakesh Singh, Dr. Pankaj Singh, and Dr. Nicholas Woods. Thank you for your invaluable suggestions and constructive comments these years.

Moreover, I would like to show my sincere gratitude and appreciation to the encouragement and advice I have received over these six years from Dr. Keith Johnson. Your attendance in my student seminar and your challenging questions always spur me to do better in my scientific projects.

I want to thank my program coordinator Tuire Cechin for her help and support with my study.

I would like to acknowledge my parents, Shan Zeng and Guangying Wang. It is your great sacrifice that supports me to seek my career. I really hope someday scientists in cancer research can finally break the enigma code of cancer, and you will not suffer cancer anymore.

Finally, I owe a great debt of gratitude to my wife: Jian Cui. Without your support, I may not consider coming to the United States seeking a Ph.D. degree and going this deep into scientific research. It is because of you, I jumped out of the hospital and looked at the cancer disease in a much deeper way. Thank you for being with me on this long journey. I wouldn’t have made it this far without you.

ABSTRACT: THE ROLE OF VGLL4 AND MARK2-HDAC AXIS IN MITOSIS AND CANCER

Yongji Zeng, Ph.D.

University of Nebraska, 2021

Supervisor: Jixin Dong, Ph.D.

The Hippo pathway is an evolutionarily conserved signaling pathway that plays important roles in stem cell biology, tissue homeostasis, and cancer development. The Hippo core signaling pathway features a kinase cascade consisting of mammalian sterile-20 like protein 1/2 (Mst1/2) and large tumor suppressor 1/2 (Lats1/2). Inactivation of the Hippo pathway is correlated with the promotion of proliferation and anti-apoptosis through activation of the transcriptional co-activator Yes-associated protein (YAP). YAP functions through binding with TEA-domain transcription factors (TEAD1–4) to activate target genes.

Vestigial-like 4 (Vgll4) functions as a transcriptional co-repressor in the Hippo-Yes associated protein (YAP) pathway. Vgll4 inhibits cell proliferation and tumor growth by competing with YAP for binding to TEA-domain proteins (TEADs). However, the mechanisms by which Vgll4 itself is regulated are unclear. Here we identified a mechanism that regulates Vgll4's tumor-suppressing function. We found that Vgll4 is phosphorylated *in vitro* and *in vivo* by cyclin-dependent kinase 1 (CDK1) during antimitotic drug-induced mitotic arrest and also in normal mitosis. We further identified Ser-58, Ser-155, Thr-159, and Ser-280 as the main mitotic phosphorylation sites in Vgll4. We also noted that the non-phosphorylatable mutant Vgll4-4A (S58A/S155A/T159A/S280A) suppressed tumorigenesis in pancreatic cancer cells *in vitro* and *in vivo* to a greater extent than did wild-type Vgll4, suggesting that mitotic phosphorylation inhibits Vgll4's tumor-suppressive

activity. Consistent with these observations, the Vgll4-4A mutant possessed a higher-binding affinity to TEAD1 than wild-type Vgll4. Interestingly, Vgll4 and Vgll4-4A markedly suppressed YAP and -catenin signaling activity. Together, these findings reveal a previously unrecognized mechanism for Vgll4 regulation in mitosis and its role in tumorigenesis.

Paclitaxel is one of the anti-tubulin drugs and has been widely used in ovarian, breast, non-small cell lung cancers, and recently pancreatic cancer. Despite their wide use in cancer treatment, the patient response rate is still low, and drug resistance is a major clinical obstacle. Through a Phos-tag-based kinome-wide screen, we identified microtubule affinity-regulating kinase 2 (MARK2) as a critical regulator for Paclitaxel chemosensitivity in pancreatic ductal adenocarcinoma (PDAC). We show that MARK2 is phosphorylated by cyclin-dependent kinase 1 (CDK1) in response to anti-tubulin chemotherapeutics and in unperturbed mitosis in a kinase activity-independent manner. Phosphorylation is essential for MARK2 in regulating mitotic progression and Paclitaxel cytotoxicity in PDAC cells. Mechanistically, our findings also suggest that MARK2 controls Paclitaxel chemosensitivity by regulating class IIa histone deacetylase (HDACs). MARK2 directly phosphorylates HDAC4 specifically during anti-tubulin treatment. Phosphorylated HDAC4 promotes YAP activation and controls the expression of YAP target genes induced by Paclitaxel. Importantly, a combination of HDAC inhibition (by knockdown or Vorinostat) and Paclitaxel overcomes chemoresistance in preclinical PDAC animal models. Furthermore, the expression levels of MARK2, class IIa HDACs, and YAP are upregulated and positively correlated in PDAC patients. Inhibition of MARK2 or class IIa HDACs potentiates Paclitaxel cytotoxicity by inducing mitotic abnormalities in PDAC cells. Together, our findings identify the MARK2-HDAC axis as a druggable target for overcoming chemoresistance in PDAC.

TABLE OF CONTENTS

LIST OF FIGURES AND TABLES

LIST OF ABBREVIATIONS

32P	Phosphorus-32
AMPK	AMP-Activated Protein Kinase
ATCC	American Type Culture Collection
CAMKK	Calcium/Calmodulin-Dependent Protein Kinase Kinase
Cas9	CRISPR Associated Protein 9
CDC25C	Cell Division Cycle 25C
CDC27	Cell Division Cycle Protein 27
CDK1	Cyclin-Dependent Kinase 1
CDK2	Cyclin-Dependent Kinase 2
CDK4	Cyclin-Dependent Kinase 4
CDK5	Cyclin-Dependent Kinase 5
CDK6	Cyclin-Dependent Kinase 6
cDNA	Complimentary Deoxyribonucleic Acid
CTGF	connective tissue growth factor
CRISPR	Clustered Regularly Interspaced Short Palindromic Repeats
Cyr61	cysteine-rich angiogenic inducer 61
DAPI	4′,6-diamidino-2-phenylindole
DKO	Double-Knockout
DMSO	Dimethyl sulfoxide
DOX	doxycycline

EGF	Epidermal Growth Factor
EGFP	Enhanced Green Fluorescent Protein
EMT	Epithelial-Mesenchymal Transition
ERK	Extracellular Signal-Regulated Kinase
FAK	Focal adhesion kinase
G1	Gap 1 Phase
G2	Gap 2 Phase
GFP	Green Fluorescent Protein
GSK3	Glycogen Synthase Kinase 3
GST	Glutathione S-Transferase
HDACs	Histone Deacetylases
JNK1/2	C-Jun N-terminal Kinase-1/2
KIBRA	Kidney and Brain Expressed Protein
KD	kinase-dead
KO	Knockout
LATS 1/2	Large tumor suppressor kinase 1/2
LEF1	lymphoid enhancer-binding factor 1
LKB1	Liver Kinase B1
M	Mitosis
MAD2	Mitotic Arrest Deficient 2
MAPK1	Mitogen-Activated Protein Kinase 1
MARK 1-4	Microtubule Affinity Regulating Kinase 1-4

MCD	Mitotic Cell Death
MEK	MAP/ERK Kinase
Mst1/2	Mammalian sterile-20 like protein 1/2
MTT	3-(4,5-dimethylthiazol-2-yl)-2,5-diphenyltetrazolium bromide
NEBD	Nuclear Envelope Breakdown
Neo	Neomycin
Noco	Nocodazole
p38	P38 Mitogen Activated Protein Kinase
Puro	Puromycin
RNA-Seq	RNA Sequencing
RT-PCR	Reverse-Transcription Polymerase Chain Reaction
SAC	Spindle Assembly Checkpoint
shRNA	Short Hairpin Ribonucleic Acid
siRNA	Small Interfering Ribonucleic Acid
Snf1	Sucrose Non-Fermenting 1
Taxol	Paclitaxel
TGF	Transforming Growth Factor
VGLL 4	Vestigial Like Family Member 4
WW45	WW domain-containing protein, 45-kDa molecular mass
YAP	Yes-Associated Protein 1

CHAPTER 1 INTRODUCTION OF HIPPO PATHWAY, MITOSIS, AND TAXOL CYTOTOXICITY

The Hippo pathway is an evolutionarily conserved signaling pathway that controls organ size and tumorigenesis [1]. The Hippo core signaling pathway features a kinase cascade consisting of mammalian sterile-20 like protein 1/2 (Mst1/2) and large tumor suppressor 1/2 (Lats1/2) [1-3]. The Hippo pathway's inactivation is correlated with the promotion of proliferation and anti-apoptosis through activation of the transcriptional co-activator Yes-associated protein (YAP) [4]. YAP functions through binding with TEA-domain transcription factors (TEAD1–4) to activate target genes, including connective tissue growth factor (CTGF) [4] (Fig. 1-1). Hippo-YAP and Wnt/-catenin signaling pathways have a shared core feature: the phosphorylation-dependent control of the key transcriptional co-activators, YAP and β-catenin, respectively [5]. In addition to this similarity, recent studies showed multipoint cross-talk between the Hippo-YAP and Wnt/-catenin signaling pathways [6].

Mitosis must be precisely regulated. Mitotic aberrations result in tumor initiation and lost control of the cell cycle is critical for cancer cell evolution. Interestingly, some of the Hippo-YAP core components have been associated with the mitotic machinery and are phospho-regulated during mitosis. Dysregulation of many of the Hippo-YAP pathway members and regulators causes mitotic defects, which are common characteristics of a tumor cell. For instance, MST2 is critical for mitotic chromosomes' precise alignment[7]. LATS2 is pivotal in Aurora A and Aurora B signaling during mitosis. Cell expressing a LATS2 non-phosphorylated mutant S380A leads to chromosome missegregation and cytokinesis failure[8]. CDK1 phosphorylation of YAP promotes cell mitotic defects[9]. Therefore, we speculate that Hippo-YAP signaling may exert its oncogenic or suppressive function via mitosis dysregulation. Interestingly, the oncogene YAP is highly expressed in human pancreatic cancer tissue compared to non-neoplastic tissues[10].

The mitotic window has become the target of anticancer drugs for decades [11, 12]. Antitubulin agent Paclitaxel (Taxol) is one of the antimitotic drugs. Taxol entered clinical trials and was firstly administrated to patients in 1984 [13]. To date, Taxol has been widely used in ovarian, breast, non-small cell lung cancers, and recently pancreatic ductal adenocarcinoma (PDAC) [12, 14, 15]. However, approximately 69 to 75% of PDAC patients with adjuvant treatment relapse within two years [16, 17]. The overall response rate of pancreatic cancer to current therapies (paclitaxel plus gemcitabine) is still very low due to drug resistance, and attempts in reversing the resistance have not been successful in the clinic [18].

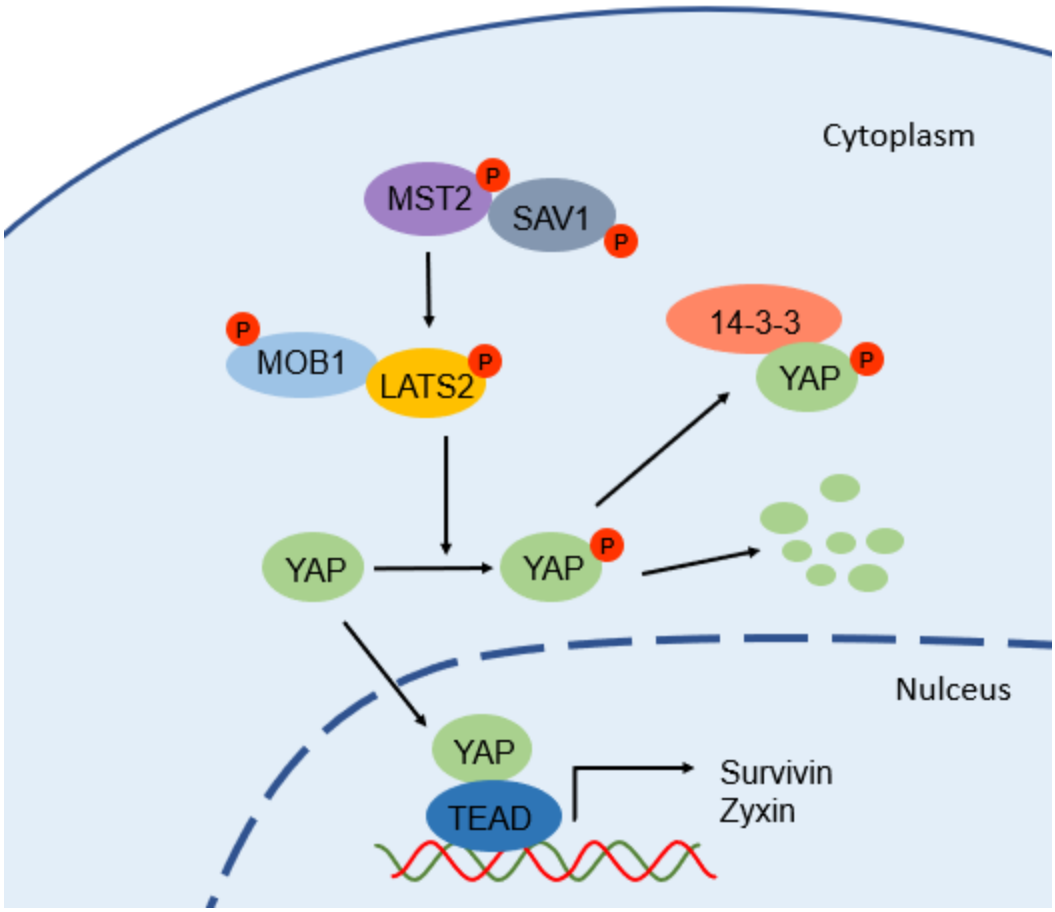

Figure 1-1. Schematic diagram of Hippo pathway

CHAPTER 2 CDK1-MEDIATED MITOTIC PHOSPHORYLATION OF THE TRANSCRIPTIONAL CO-REPRESSOR VGLL4 INHIBITS ITS TUMOR-SUPPRESSING ACTIVITY *

*The material presented in this chapter was previously published: Y. Zeng et al. J Biol Chem 2017; 292(36):15028-15038.

2.1. Abstract

The Hippo pathway is an evolutionarily conserved signaling pathway that plays important roles in stem cell biology, tissue homeostasis, and cancer development. Vestigial-like 4 (Vgll4) functions as a transcriptional co-repressor in the Hippo-Yes associated protein (YAP) pathway. Vgll4 inhibits cell proliferation and tumor growth by competing with YAP for binding to TEA-domain proteins (TEADs). However, the mechanisms by which Vgll4 itself is regulated are unclear. Here we identified a mechanism that regulates Vgll4's tumor-suppressing function. We found that Vgll4 is phosphorylated *in vitro* and *in vivo* by cyclin-dependent kinase 1 (CDK1) during antimitotic drug-induced mitotic arrest and also in normal mitosis. We further identified Ser-58, Ser-155, Thr-159, and Ser-280 as the main mitotic phosphorylation sites in Vgll4. We also noted that the non-phosphorylatable mutant Vgll4-4A (S58A/S155A/T159A/S280A) suppressed tumorigenesis in pancreatic cancer cells *in vitro* and *in vivo* to a greater extent than did wild-type Vgll4, suggesting that mitotic phosphorylation inhibits Vgll4's tumor-suppressive activity. Consistent with these observations, the Vgll4-4A mutant possessed a higher-binding affinity to TEAD1 than wild-type Vgll4. Interestingly, Vgll4 and Vgll4-4A markedly suppressed YAP and-catenin signaling activity. Together, these findings reveal a previously unrecognized mechanism for Vgll4 regulation in mitosis and its role in tumorigenesis.

2.2. Introduction

Vestigial-like protein 4 (Vgll4) (Tgi in Drosophila) is a newly identified protein in the Hippo pathway and is an antagonist of Yki/YAP [19]. Vgll4 functions as a transcriptional repressor by directly competing with YAP binding to TEADs [19]. Several reports

demonstrated that Vgll4 is a tumor suppressor in the lung, gastric, and colorectal cancer by negatively regulating the YAP-TEAD transcriptional complex and TCF4-TEAD4 transactivation [1, 2, 4, 5]. Furthermore, genetic screens in mice identified Vgll4 as a tumor suppressor candidate in pancreatic cancer, although its biological significance has not been examined [20]. Although extensive studies have demonstrated the Hippo-YAP pathway's fundamental roles in tumorigenesis, exploring the underlying mechanisms driving it is still incomplete.

The regulation of Vgll4 in mitosis and its possible role in cancer have remained elusive. This study found that the mitotic kinase cyclin-dependent kinase 1 (CDK1) phosphorylates Vgll4 at Ser-58, Ser-155/Thr-159, and Ser-280 during mitosis. Moreover, the mitotic phosphorylation-deficient mutant (Vgll4-4A, harboring S58A/S155A/T159A/S280A) possesses much stronger tumor-suppressive activity compared with wild-type Vgll4 in pancreatic cancer tumorigenesis *in vitro* and *in vivo*. Our findings reveal a novel layer of regulation for Vgll4 in mitosis and cancer development.

2.3. Materials and Methods

2.3.1. Cell culture and transfection

HEK293T, HeLa, HPAF-II, Capan-2, PANC-1, BxPC-3, and Hs776T cell lines were purchased from American Type Culture Collection (ATCC) and cultured as ATCC instructed. The cell lines were authenticated at ATCC and were used at low (<25) passages. The immortalized pancreatic epithelial cells (HPNE) were provided by Dr. Michel Ouellette (University of Nebraska Medical Center), who originally established the cell line and deposited it at ATCC [21]. The T3M4, S2.013, and Colo-357 pancreatic cancer cell lines were kindly provided by Dr. Michael (Tony) Hollingsworth. The cell lines

were maintained as described [10, 22]. Attractene (Qiagen) was used for transient overexpression of proteins in HEK293T and HEK293GP cells following the manufacturer's instructions. siRNA transfections were done with HiPerfect (Qiagen). The On-target SMART pool siRNA for Vgll4 was purchased from Dharmacon. Retrovirus or lentivirus packaging, infection, and subsequent selection were done as we have described previously[23]. Nocodazole (100 ng/ml for 16 h) and taxol (100 nM for 16 h) (Selleck Chemicals) were used to arrest cells in the G2/M phase unless otherwise indicated. Kinase inhibitors were purchased from Selleck Chemicals (VX680, ZM447439, BI2536, Purvalanol A, SP600125, rapamycin, and MK2206) ENZO life Sciences (RO3306 and roscovitine), or LC Laboratory (U0126, SB203580, and LY294002). MK5108 (Aurora-A inhibitor) was from Merck. All other chemicals were from either Sigma or Thermo Fisher.

2.3.2. Expression constructs

The human Vgll4 cDNA has been described [24]. To make the retroviral (TetOn-inducible) or Lentiviral Vgll4 expression constructs, the above full-length cDNA was cloned into the Tet-All [25] or pSIN4-FLAG-IRES-puro vector, respectively. The pSIN4-FLAG-IRES-puro vector was made by inserting a FLAG tag with multiple-cloning–site sequences into the pSIN4-IRESpuro vector, which was originally obtained from Addgene (Plasmid #61061) [26]. Myc-TEAD1 was also purchased from Addgene [4]. Point mutations were generated by the QuikChange site-directed PCR mutagenesis kit (Stratagene) and verified by sequencing.

2.3.3. Tet-On-inducible expression system

The wild-type or phosphorylation-deficient mutant (4A: S58A/S155A/T159A/S280A) or phosphorylation-mimetic mutant (4D: S58D/S155D/T159D/S280D) Vgll4 cDNA was cloned into the Tet-All vector [25] to generate Tet-On-inducible constructs. Vgll4, Vgll4-4A, or Vgll4-4D expression in BxPC3 cells was achieved by retroviral-mediated infection

and selection in a doxycycline-dependent manner. Cells were maintained in a medium containing the Tet system-approved fetal bovine serum (FBS) (Clontech Laboratories).

2.3.4. Quantitative real-time PCR

Total RNA isolation, RNA reverse transcription, and quantitative real-time PCR were done as we have described previously [23].

2.3.5. Recombinant protein purification and *in vitro* kinase assay

GST-tagged Vgll4 and Vgll4-4A were cloned in pGEX-5X-1, and the proteins were bacterially expressed and purified on GSTrap FF affinity columns (GE Healthcare) following the manufacturer's instructions. GST-Vgll4 (0.5–1 μg) was incubated with 10 units of recombinant CDK1–cyclin B complex (New England BioLabs) or 100 ng of CDK1–cyclin B (Signal-Chem) in kinase buffer (New England BioLabs) in the presence of 7.5 μCi of [γ-32P] ATP (3000 Ci/mmol, PerkinElmer Life Sciences). CDK5–p25, MEK1, ERK1, JNK1, JNK2, and p38α kinases were purchased from SignalChem. Phosphorylation (32P incorporation) was visualized by autoradiography followed by Western blotting or detected by phospho-specific antibodies.

2.3.6. Antibodies

The Vgll4 antibodies were purchased from Abnova (H00009686-B01P). Rabbit polyclonal phospho-specific antibodies against Vgll4 Ser-58, Ser-155/Thr-159, and Ser-280 were generated and purified by AbMart. The peptides used for immunizing rabbits were TGPPI-pS-PSKRK (Ser-58), RPAGLpS-PTL-pT-PGERQ (Ser-155/Thr-159), and RGQPA-pSPSAHM (Ser-280). The corresponding non-phosphorylated peptides were also synthesized and used for antibody purification and blocking assays. Anti-FLAG antibody was from Sigma. Anti-Myc, anti-β-actin, and anti-cyclin B antibodies were from Santa Cruz Biotechnology. Aurora-A, glutathione S-transferase

(GST), CDK3 and BubR1 antibodies were from Bethyl Laboratories. Phospho-Thr-288/Thr-232/Thr-198 Aurora-A/B/C, phospho-S10 H3, phospho-Ser-127 YAP, phospho-Ser-397 YAP, TAZ, TEAD1, CDC25C, CDK1, CDK4, CDK5, cyclin A2, cyclin E2, MAD2, phospho-Ser-795 Rb, β-catenin, phospho-Ser-33/Ser-37/Thr-41, β-catenin, phospho-Ser-675 β-catenin, Wee1, and phospho-S642 Wee1 antibodies were from Cell Signaling Technology. Anti-β-tubulin (Sigma) antibodies were used for immunofluorescence staining.

2.3.7. Phos-tag and Western blot analysis

Phos-tagTM was obtained from Wako Pure Chemical Industries, Ltd. (catalog #304-93521) and used at 10–20 μM (with 100 μM MnCl2) in 8% SDS-acrylamide gels as described [27]. Western blotting, immunoprecipitation, and λ-phosphatase treatment assays were done as previously described [23].

2.3.8. Migration and proliferation assays

Wound healing and Transwell assays were utilized for measuring migratory activity as previously described [28, 29]. Cell proliferation was determined by MTT (3-(4,5-dimethylthiazol-2-yl)-2,5-diphenyltetrazolium bromide) assays following the manufacturer's instructions (ATCC).

2.3.9. Animal studies

For *in vivo* xenograft studies, S2.013 cells expressing wildtype Vgll4 or Vgll4-4A or BxPC3 cells expressing TetOn-Vgll4 or TetOn-Vgll4-4A (non-phosphorylatable mutant) (1.0 x 106 cells each line) were subcutaneously injected into both flanks of 6-week-old male athymic nude mice (Ncr-nu/nu, Harlan). S2.013 cells were suspended in PBS, and BxPC3 cells were mixed with Matrigel at a 1:1 ratio (volume). Five animals were used per group. Doxycycline (0.5 mg/ml in 5% sucrose water) was administered beginning at the

time of cancer cell injection. Tumor sizes were measured twice a week using an electronic caliper starting when tumors in the Vgll4-4A group are palpable. Tumor volume (*V*) was calculated by the formula $V = 0.5 \times \text{length} \times \text{width}^2$ [10]. Mice were euthanized at the end of the experiment, and the tumors were excised for subsequent analysis. The animals were housed in pathogen-free facilities. All animal experiments were approved by the University of Nebraska Medical Center Institutional Animal Care and Use Committee.

2.3.10. Statistical analysis

Statistical significance was analyzed using a two-tailed, unpaired Student's t-test.

2.4. Results

2.4.1. Vgll4 was phosphorylated during antimitotic drug-induced G2/M arrest

We recently showed several regulators of the Hippo YAP signaling are phosphorylated during mitosis [23, 27, 28, 30-32]. We further explored whether the newly identified transcriptional repressor Vgll4 in the Hippo-YAP pathway is regulated by phosphorylation during mitosis. As shown in Fig. 2-1A, Vgll4 protein was up-shifted on a Phos-tag gel during taxol or nocodazole-induced G2/M arrest (Fig. 2-1A). Transiently transfected Vgll4 mobility was also retarded during taxol or nocodazole treatment (Fig. 2-1B). λ-Phosphatase treatment largely converted all up-shifted bands to fast-migrating bands, confirming that the mobility shift of Vgll4 during G2/M arrest is caused by phosphorylation (Fig. 2-1C).

2.4.2. Kinase identification for Vgll4 phosphorylation

Next, we used various kinase inhibitors to identify the candidate kinase for Vgll4 phosphorylation. Inhibition of Aurora-A, -B, and -C (with VX680) or JNK1/2 (with SP600125) kinases mildly reduced Vgll4 phosphorylation (Fig. 2-1D). Inhibition of MEK-

ERK kinases (with U0126), p38 (with SB203580), mTOR (with rapamycin), Akt (MK2206), Aurora-A (MK5108), or Plk1 (with BI2536) failed to alter the phosphorylation of Vgll4 during G2/M arrest (Fig. 2-1D). Interestingly, treatments with RO3306 (CDK1 inhibitor) or purvalanol A (CDK1/2/5 inhibitor) significantly inhibited the mobility shift/phosphorylation (Fig. 2-1D, fourth and seventh lanes). These data suggest that CDK1, a well-known master mitotic kinase, is likely the relevant kinase for Vgll4 phosphorylation induced during taxol or nocodazole treatment.

2.4.3. CDK1 phosphorylated Vgll4 *in vitro*

To determine whether CDK1 kinase can directly phosphorylate Vgll4, we performed *in vitro* kinase assays with GST-tagged Vgll4 proteins as substrates. Fig. 2-1A shows that purified CDK1– cyclin B kinase complex phosphorylated GST-Vgll4 proteins *in vitro* (Fig. 2-2A). We also included several other kinases that phosphorylate the same consensus sequence as CDK1 and found CDK5–p25 kinase complex could phosphorylate Vgll4 (Fig. 2-2A). These results indicate that CDK1 and -5 directly phosphorylate(s) Vgll4 *in vitro*.

2.4.4. CDK1–cyclin B complex phosphorylated Vgll4 at multiple sites

CDK1 phosphorylates substrates at a minimal proline-directed consensus sequence [33]. Human Vgll4 contains seven S/TP motifs (Ser-58, Ser-109, Ser-155, Thr-159, Ser-268, Ser-280, and Ser-291). Interestingly, mutating four of them to alanines (Vgll4-4A, S58A/S155A/T159A/S280A) completely abolished 32P incorporation on Vgll4 in an *in vitro* kinase assay, suggesting that these four sites are the main phosphorylation sites for CDK1 (Fig. 2-2B). Database analysis revealed that all four sites had been identified as mitotic phosphorylation sites by previous phospho-proteomic studies [34].

We have generated phospho-specific antibodies against Ser-58, Ser-155/Thr-159, and Ser-280. *In vitro* kinase assays confirmed that CDK1 robustly phosphorylates Vgll4 at

all these sites (Fig. 2-2C). As expected, the addition of RO3306 or mutating the sites to alanines abolished the phosphorylation (Fig. 2-2C). These data suggest that CDK1 phosphorylates Vgll4 at Ser-58, Ser-155/Thr-159, and Ser-280 *in vitro*. Next, we explored whether mitotic phosphorylation of Vgll4 occurs in cells. Nocodazole treatment significantly increased the phosphorylation of Ser-58 on transfected Vgll4 (Fig. 2-3A). Phosphopeptide, but not the regular non-phosphopeptide, incubation completely blocked the phospho-signal, suggesting that this antibody detects the phosphorylated form of Vgll4 (Fig. 2-3A). Similar results were observed for phospho-antibodies against Ser-155/Thr-159 and Ser-280 (Fig. 2-3, B and C). The signal was abolished by mutating the relevant site to alanine (Fig. 2-3, D–F), confirming the specificity of these phospho-antibodies. Using kinase inhibitors, we further demonstrated that phosphorylation of Vgll4 is CDK1 kinase-dependent (Fig. 2-3G, fourth and seventh lanes). In line with the *in vitro* data (Fig. 2-2B), the mobility upshift of Vgll4 induced by nocodazole treatment was also largely inhibited when these sites were mutated to alanines (Fig. 2-3H). Taken together, these observations indicate that Vgll4 is phosphorylated at Ser-58, Ser-155/Thr-159, and Ser-280 by CDK1 in cells during antimitotic drug-induced G2/M arrest.

2.4.5. CDK1 mediated Vgll4 phosphorylation in mitotically arrested cells

We next performed immunofluorescence microscopy with these phospho-specific antibodies to examine the phospho-status of endogenous Vgll4. The antibodies against Ser-155/Thr-159 detected strong signals in nocodazole-arrested prometaphase cells (Fig. 2-4A, white arrows). The signal was very low or not detectable in interphase cells (Fig. 2-4A, yellow arrows). Again, phosphopeptide, but not control non-phosphopeptide, incubation completely blocked the signal, suggesting that these antibodies specifically detect Vgll4 only when it is phosphorylated (Fig. 2-4A). The addition of RO3306 (CDK1 inhibitor) largely diminished the signals detected by p-Vgll4 Ser-155/Thr-159 antibodies in

mitotically arrested cells, further indicating that the phosphorylation is CDK1-dependent (Fig. 2-4A, low panels). Moreover, siRNA-mediated knockdown of Vgll4 also significantly reduced the phospho-signal (Fig. 2-4B), confirming the antibody's specificity. Similar results were observed when the phospho-Ser-280 antibody was used (Fig. 2-4, C and D).

2.4.6. Vgll4 phosphorylation occurred during normal mitosis

Taxol or nocodazole was used to arrest cells in the G2/M phase in all of the above experiments. We wanted to determine whether phosphorylation of Vgll4 occurs during normal mitosis. We performed immunofluorescence staining on cells collected from a double thymidine block and release [35]. Consistent with the results in Fig. 2-4, very weak signals were detected in interphase or telophase/cytokinesis cells (Fig. 2-5, A–C). The phospho-signal increased in prometaphase and peaked in metaphase cells (Fig. 2-5, A–C). These results indicate that Vgll4 phosphorylation occurs dynamically during normal mitosis.

2.4.7. Mitotic phosphorylation of Vgll4 inhibited its tumor-suppressing activity *in vitro*

Vgll4 suppresses tumor growth in colorectal, lung, and gastric cancer cells and functions as a potential tumor suppressor in pancreatic cancer as well [24, 36-40]. Next, we utilized pancreatic cancer cell lines as a model system to determine the biological significance of mitotic phosphorylation of Vgll4. First, we examined Vgll4 protein levels in HPNE (an immortalized pancreatic epithelial cell line) and various pancreatic cancer cell lines. Vgll4 expression was very low or not detectable in half of the cancer cell lines and was high in HPNE cells (Fig. 2-6*A*). We stably re-expressed wild-type Vgll4 or Vgll4-4A (non-phosphorylatable mutant) or Vgll4-4D (phospho-mimetic mutant) in S2.013 (Fig. 2-6*B*). Not surprisingly, ectopic expression of wildtype Vgll4 suppressed migration and proliferation in S2.013 cells (Figs. 2-6,*C*–*F*, and data not shown). Interestingly, cells

expressing Vgll4-4A showed greater inhibition in migration (Figs. 2-6, *C*–*F*). In contrast, Vgll4-4D-expressing cells migrated similarly to Vgll4-expressing or vector-expressing cells (Figs. 2-6, *C*–*F*). Using a doxycycline-inducible system (Fig. 2-6*G*), we further showed that BxPC3 cells expressing Vgll4-4A possess stronger inhibitory activity in migration when compared with wild-type Vgll4-expressing cells (Fig. 2-6, *H*–*I*). Without doxycycline induction, these BxPC3 cell lines express similar levels of Vgll4 proteins (Fig. 2-6*G*, *left four lanes*), and no migration and proliferation differences were detected among these cells (data not shown). These findings suggest that mitotic phosphorylation of Vgll4 inhibits its tumor-suppressive function.

2.4.8. Mitotic phosphorylation of Vgll4 inhibits its tumor-suppressing activity *in vivo*

We next evaluated the influence of mitotic phosphorylation of Vgll4 on tumor growth in animals. BxPC3 cells expressing wild-type Vgll4 or Vgll4-4A were subcutaneously inoculated into immuno-deficient mice. Interestingly, tumors from mice harboring Vgll4-4A-expressing cells were significantly smaller when compared with those from mice injected with wild-type Vgll4-expressing cells (Figs. 2-7, *A* and *B*). Histopathological examination revealed that tumor cells expressing Vgll4-4A were smaller and in higher density when compared with wildtype Vgll4 tumor cells (Fig. 2-7*C* and data not shown). Immunohistochemistry staining with cleaved caspase-3 (an apoptosis marker) showed that expression of Vgll4-4A significantly promoted tumor cell death (Fig. 2-7*C*). Similarly, we found that S2.013 cells expressing Vgll4-4A proliferate at a significantly lower rate and form smaller tumors than cells expressing Vgll4-WT (Figs. 2-7, *D*–*F*). These results support the hypothesis that mitotic phosphorylation inhibits Vgll4's tumor suppressive activity *in vivo*.

2.4.9. Mitotic phosphorylation of Vgll4 affected YAP and β-catenin activity

Vgll4 competes with YAP to associate with TEADs [19]. The association between Vgll4 and TEAD1 was confirmed with transfected proteins (Figs. 2-8, A and B). Interestingly, the nonphosphorylatable (Vgll4-4A) mutant had greater binding affinity with TEAD1 compared with wild-type Vgll4 (Figs. 2-8, A and B), suggesting that Vgll4 phosphorylation inhibits its association with TEAD1. These observations are consistent with our results from functional assays shown in Fig. 2-6 and Fig. 2-7 and support the notion that Vgll4-4A suppresses tumor growth by regulating TEAD1 transcriptional activity. Indeed, the mRNA level for CTGF (a well known YAP-TEAD target) was significantly reduced in Vgll4-4A-expressing cells (Fig. 2-8C). TEAD-luciferase reporter assays further confirmed that Vgll4-4A has higher suppressing activity than wild-type Vgll4 (Fig. 2-8D). Interestingly, total YAP protein levels, as well as YAP phosphorylation at Ser-127 and Ser-397, were significantly reduced in Vgll4- or to a greater extent in Vgll4-4A-expressing cells (Fig. 2-8E). In addition to repressing the YAP-TEAD activity, a recent report showed that Vgll4 also suppresses the TCF4-TEAD transcription complex in the Wnt/-catenin pathway [5]. In line with this previous study, the expression of -catenin/TCF4 target LEF1 was significantly inhibited by Vgll4 or Vgll4-4A expression in S2.013 cells (Fig. 2-8F). Vgll4 expression also decreased the levels of the -catenin protein and the activating phosphorylation at Ser-675, probably through increasing the inhibitory phosphorylation at Ser-33/Ser-37/Thr-41 (Fig. 2-8G). Again, expression of the Vgll4-4A mutant tended to have stronger inhibitory activity compared with wild-type Vgll4 (Figs. 2-8, F and G). These results suggest that mitotic phosphorylation of Vgll4 affects both YAP and -catenin activity in pancreatic cancer cells.

We further determined whether Vgll4 and its mitotic phosphorylation affects cell cycle regulators. Interestingly, the levels of budding uninhibited by benzimidazole 1-related protein kinase (BubR1), mitotic arrest deficiency 2 (MAD2), cyclin A2, and CDC25C

declined upon Vgll4/Vgll4-4A expression in S2.013 cells (Fig. 2-8H). However, both Vgll4 and Vgll4-4A decreased these proteins to similar levels (Fig. 2-8H), suggesting that these regulators are unlikely involved in mediating the effects of Vgll4-4A in suppressing tumor growth.

2.5. Discussion

Dysregulation of the Hippo-YAP signaling pathway has been associated with the development of various cancers. Oncoprotein YAP functions together with transcriptional factors TEAD1–4 to regulate downstream target gene expression [41]. Like YAP, Vgll4 does not contain a DNA-binding domain, and it functions as a transcriptional repressor via Tondu domains binding with TEADs [19]. Therefore, Vgll4 suppresses cell growth by directly competing with YAP via binding with TEADs. The Tondu region of Vgll4 is sufficient for inhibiting YAP activity, and a peptide mimicking Vgll4 could function as a YAP antagonist and potently inhibit gastric and colorectal tumor growth [5, 24]. Low expression of Vgll4 is correlated with poor prognosis and survival in several cancers [5, 20, 24, 36]. However, although its tumor-suppressive activity has been well documented, little attention has been directed at the possible regulation for Vgll4 in cancer development. This study identified novel mitotic phosphorylation of Vgll4 and demonstrated that this mitotic phosphorylation controls Vgll4's tumor-suppressing activity. Compared with wild-type Vgll4, the phospho-deficient Vgll4-4A mutant has a higher affinity pairing with TEAD1 and shows stronger tumor-suppressive activity. These observations suggest that in addition to its expression levels, the phosphorylation status of Vgll4 is also critical for its tumor-suppressive function. Thus, our study revealed another layer of regulation for Vgll4 activity during tumorigenesis.

In the current study, we found that CDK1 phosphorylates Vgll4 *in vitro* and *in vivo* at Ser-58, Ser-155/Thr-159, and Ser- 280 during mitosis (Figs. 2-2 – 2-5). Recently, we reported that CDK1-mediated phosphorylation of YAP promotes mitotic defects, including centrosome amplification and chromosome missegregation, and potentiates oncogenic functions of YAP [28, 42]. Considering that CDK1 phosphorylates both YAP and Vgll4 during mitosis and these proteins function together in regulating tumorigenesis, one question is whether these phosphorylation events affect each other during mitosis. Mechanistic elucidation of this unanswered question will help us further understand the regulation and role of Vgll4 in normal and cancer cells. Many Hippo-YAP pathway members, including YAP, have been shown previously to be associated with the mitotic machinery and cause mitotic defects when dysregulated. Therefore, future studies are required to define the role of Vgll4 and its phosphorylation in cell cycle progression, especially in mitosis-related events. Another interesting finding from this study is that Vgll4 is a phospho-protein (multiple bands were observed on Phos-tag gels) (Fig. 2-1B-D). There is basal level phosphorylation of Vgll4 that is not regulated by mitotic arrest and is CDK1-independent (Figs. 2-1, B–D, and 2-3H), suggesting that in addition to CDK1-mediated mitotic phosphorylation, Vgll4 is phosphorylated by other unknown kinases (s). We are currently investigating this phosphorylation.

Our current study indicates that Vgll4 could down-regulate YAP, BubR1, and MAD2 (Fig. 2-8, E and H). We previously showed that mitotic phosphorylation of YAP positively regulates MAD2 and BubR1 levels [42]. Therefore, it is possible that Vgll4 will control BubR1/MAD2 levels through YAP. It is also interesting that Vgll4 inhibits YAP protein levels in pancreatic cancer cells, an activity that has not been shown in other cancer cell types. The underlying mechanisms of this down-regulation are not known. However, it is unlikely due to YAP's inhibitory phosphorylation at Ser-127 or Ser-397 as their

phosphorylation is also reduced in Vgll4-expressing cells (Fig. 2-8E). Our future studies will explore how Vgll4 regulates YAP as well as -catenin. Addressing these questions will help understand the biological significance of these proteins in mitosis and provide insights into their underlying mechanisms in cancer development.

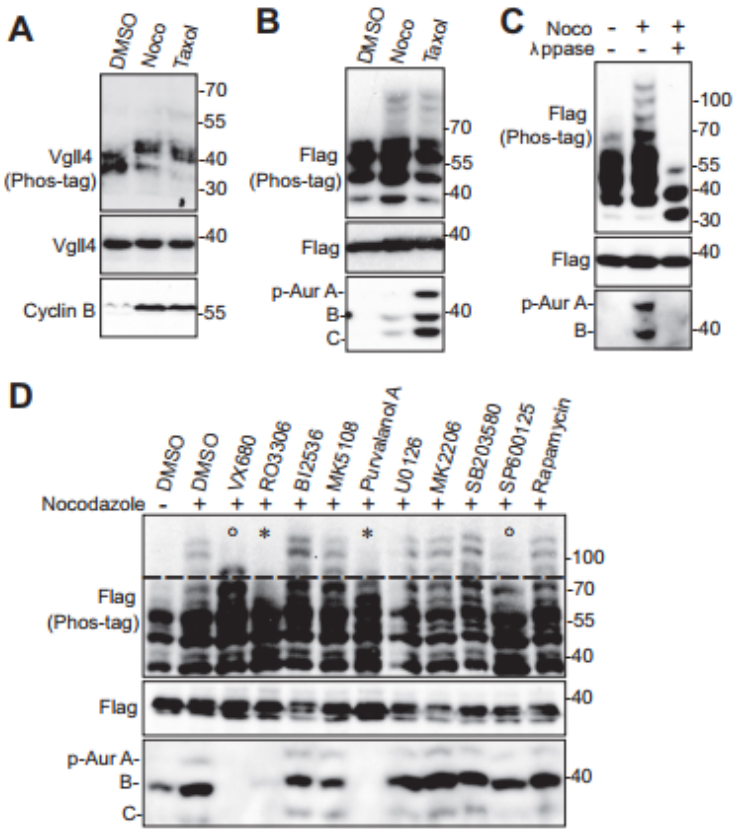
A
DMSO
Noco
Taxol
Vgll4
(Phos-tag)
Vgll4
Cyclin B
70
55
40
30
40
55
B
DMSO
Noco
Taxol
Flag
(Phos-tag)
Flag
p-Aur A-
B-
C-
70
55
40
40
40
C
Noco - + +
λppase - - +
Flag
(Phos-tag)
Flag
p-Aur A-
B-
100
70
55
40
30
40
40
D
Nocodazole
DMSO
DMSO
VX680
RO3306
BI2536
MK5108
Purvalanol A
U0126
MK2206
SB203580
SP600125
Rapamycin
- + + + + + + + + + + +
Flag
(Phos-tag)
Flag
p-Aur A-
B-
C-
100
70
55
40
40
40

Figure 2-1. CDK1-dependent phosphorylation of Vgll4 during G2/M arrest.

(A) HeLa cells were treated with DMSO, taxol (100 nM for 16 h), or nocodazole (Noco, 100 ng/ml for 16 h). Total cell lysates were probed with the indicated antibodies on Phos-tag or regular SDS-polyacrylamide gels. Increased cyclin B levels served as a mitotic marker. (B) HEK293T cells were transfected with FLAG-tagged Vgll4 and treated as indicated in A. Total cell lysates were used for Western blotting analysis as described in A. p-Aur, Phospho-Aurora. (C) HEK293T was transfected and treated as in B. The transfected cell lysates were further treated with (+) or without (-) λ-phosphatase (ppase). (D) HEK293T cells were transfected and treated with nocodazole together with or without various kinase inhibitors as indicated. VX680 (2 M), MK5108 (10 M), BI2536 (100 nM), RO3306 (5 M), U0126 (20 M), MK2206 (1 M), SB203580 (10 M), SP600125 (20 M), rapamycin (100 nM), and purvalanol A (10 M) were used. Inhibitors were added (with MG132 to prevent cyclin B from degradation and cells from exiting from mitosis) 2 h before harvesting the cells. Total cell lysates were subjected to Western blotting with the indicated antibodies. O and * mark the modest and significant inhibition of mobility upshift, respectively. Phospho-Aurora levels (in panels B–D) served as a mitotic marker and indicate the inhibitory effects mediated by kinase inhibitors (in panel D).

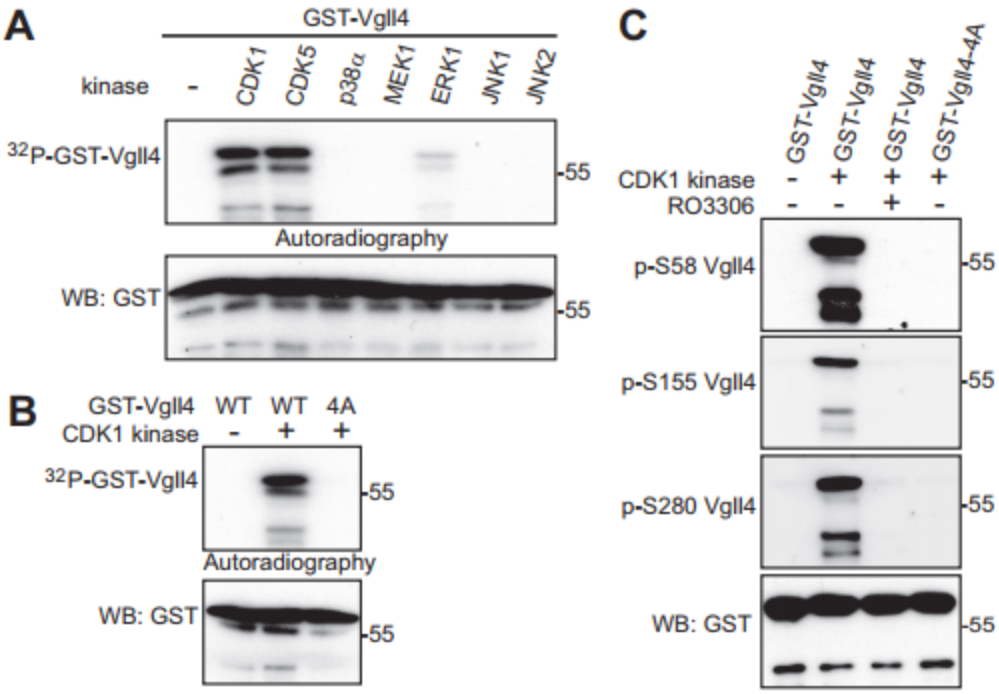

Figure 2-2.Vgll4 is phosphorylated by CDK1 *in vitro*.

(A) GST-taggedVgll4proteinswere used for *in vitro* kinase assays with purified kinases. (B) GST-taggedVgll4 or Vgll4-4A (S58A/S155A/T159A/S280A) proteins were used for *in vitro* kinase assays with purified CDK1– cyclin B kinase complex. WB, Western blotting. (C) *in vitro* kinase assays were done as in B, except anti-phospho-Vgll4 antibodies were used. RO3306 (5 M) was used to inhibit CDK1 kinase activity. The phosphoVgll4 Ser-155/Thr-159 antibody was labeled as p-S155 Vgll4.

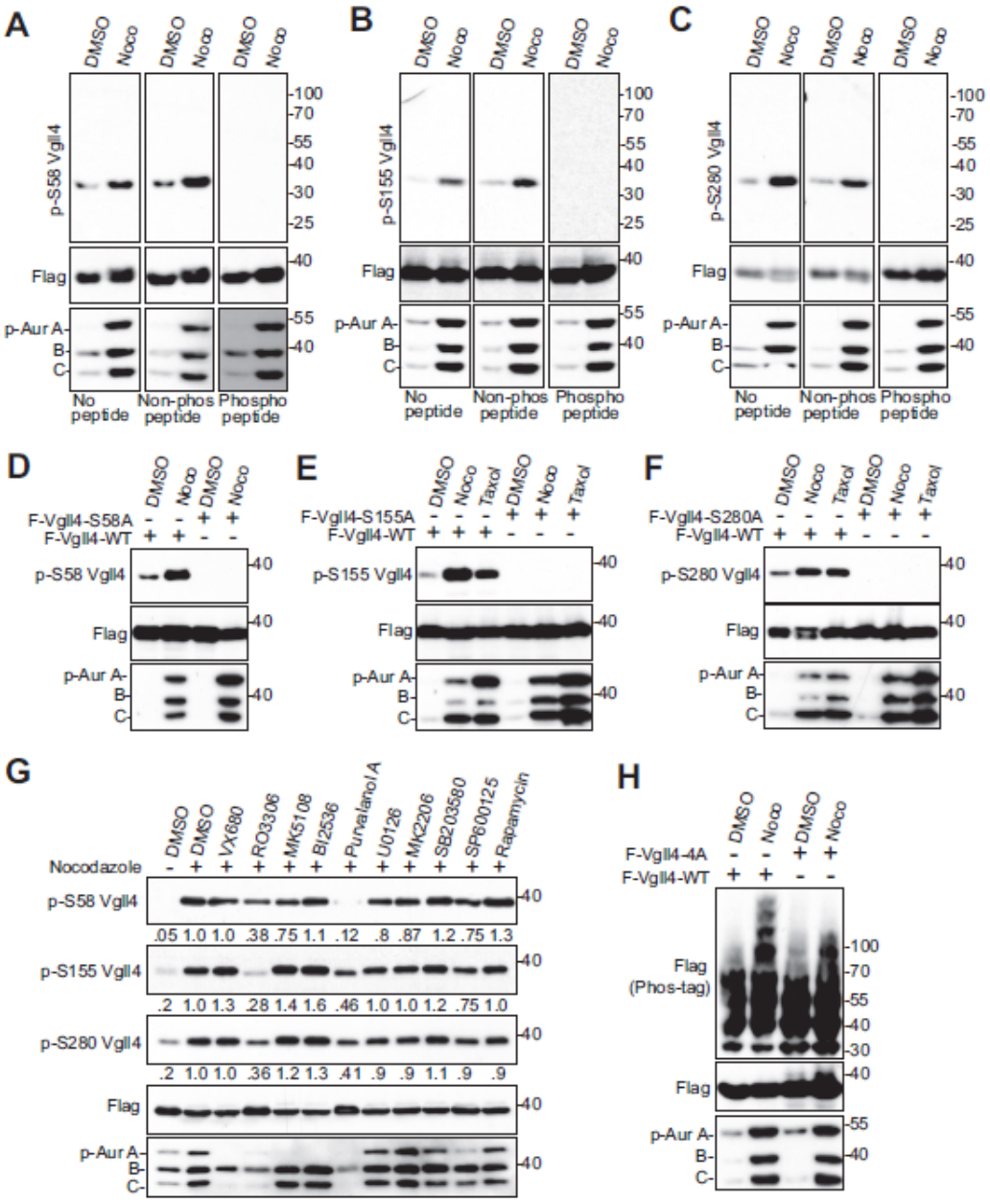
A
B
C
DMSO
Noco
p-S58 Vgll4
p-S155 Vgll4
p-S280 Vgll4
Flag
p-Aur A
B
C
No peptide
Non-phos peptide
Phospho peptide
D
E
F
F-Vgll4-S58A
F-Vgll4-WT
F-Vgll4-S155A
F-Vgll4-S280A
Taxol
G
Nocodazole
VX680
RO3306
MK5108
BI2536
Purvalanol A
U0126
MK2206
SB203580
SP600125
Rapamycin
H
F-Vgll4-4A
Flag (Phos-tag)

Figure 2-3. Vgll4 is phosphorylated by CDK1 in cells.

(A–C) HEK293T cells were transfected with FLAG-Vgll4. At 32 h post-transfection, the cells were treated with nocodazole (Noco) for 16 h. Total cell lysates were subjected to Western blotting with the indicated antibodies. No peptide, Western blotting without any peptide (regular Western blotting); Non-phospho peptide, Western blotting in the presence of control (not phosphorylated) peptide; phosphopeptide, Western blotting in the presence of corresponding phosphorylated peptide (used for antibody generation). See “Materials and Methods.” p-Aur, PhosphoAurora. (D–F) HEK293T cells were transfected with FLAG-Vgll4 or FLAG-Vgll4 mutants as indicated. At 32 h post-transfection, the cells were treated with nocodazole or taxol for 16 h. Total cell lysates were subjected to Western blotting with the indicated antibodies. (G) HEK293T cells were transfected and treated with nocodazole together with or without various kinase inhibitors as indicated. Inhibitors were added (with MG132 to prevent cyclin B from degradation and cells from exiting from mitosis) 1.5 h before harvesting the cells. Total cell lysates were subjected to Western blotting with the indicated antibodies. The phospho-Vgll4 Ser-155/Thr-159 antibody was labeled as p-S155 Vgll4. The relative phosphorylation levels are quantified from three blots by ImageJ. H, HEK293T cells were transfected with FLAG-Vgll4 or FLAG-Vgll4-4A and treated as indicated. Total cell lysates were subjected to Western blotting with the indicated antibodies. Phospho-Aurora levels (in panels A–F and H) served as a mitotic marker and indicate the inhibitory effects mediated by kinase inhibitors (in panel G).

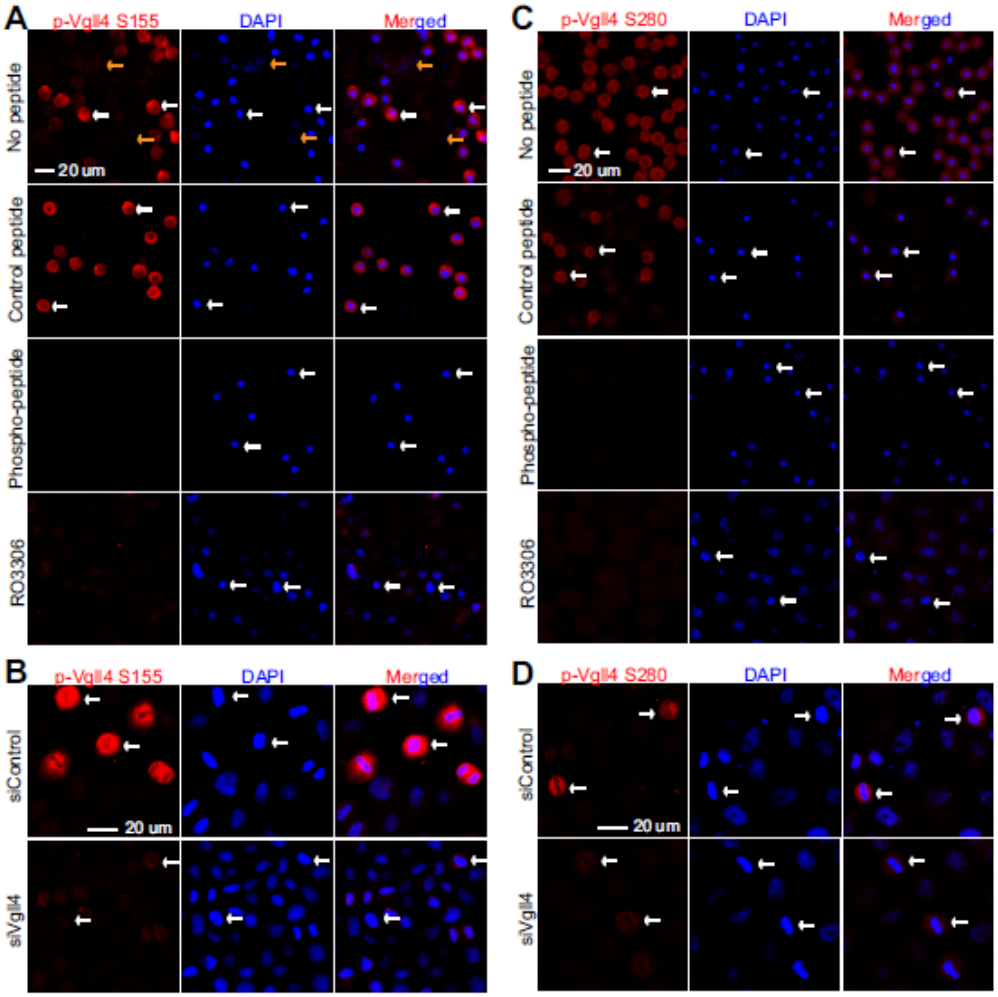
A
p-Vgll4 S155
DAPI
Merged
No peptide
Control peptide
Phospho-peptide
RO3306
20 um
C
p-Vgll4 S280
DAPI
Merged
No peptide
Control peptide
Phospho-peptide
RO3306
20 um
B
p-Vgll4 S155
DAPI
Merged
siControl
siVgll4
20 um
D
p-Vgll4 S280
DAPI
Merged
siControl
siVgll4
20 um

Figure 2-4. CDK1 phosphorylated Vgll4 during G2/M-phase arrest.

(A) HeLa cells were treated with nocodazole and then fixed. Before the cells were stained with phospho-specific antibody against Ser-155/Thr-159 of Vgll4 (p-Vgll4 S155), they were preincubated with PBS (no peptide control) or non-phosphorylated (control) peptide or the phosphorylated peptide used for immunizing rabbits. CDK1 inhibitors RO3306 (5 M) together with MG132 (25 M) were added 2 h before the cells were fixed. (B) HeLa cells were transfected with scramble siRNA or siRNAs targeting Vgll4. At 48 h post-transfection, cells were treated with nocodazole and then fixed for staining with phospho-Vgll4 Ser-155/Thr-159 (p-Vgll4 S155) antibodies. (C,D) Experiments were done similarly as in A and B with phospho-specific antibody against Ser-280 of Vgll4. White and yellow arrows mark some of the prometaphase cells and the interphase cells, respectively.

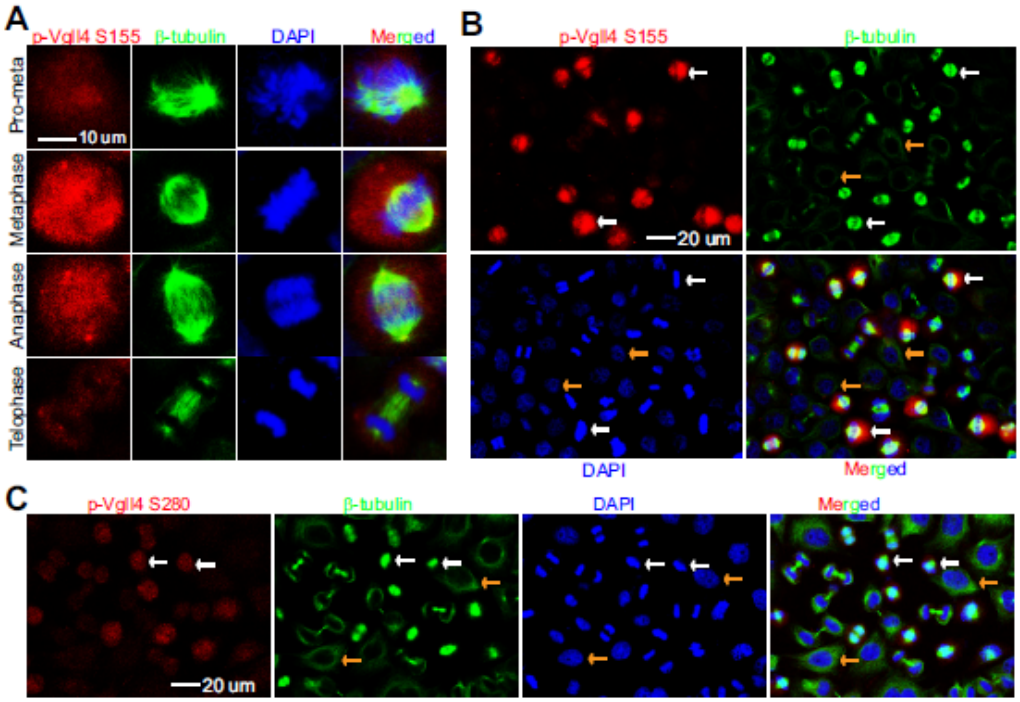

Figure 2-5. Vgll4 is phosphorylated during unperturbed mitosis.

(A, B) HeLa cells were synchronized by a double thymidine block and release method. Cells were stained with antibodies against p-Vgll4 Ser-155/Thr-159 (labeled as p-Vgll4 S155) or -tubulin or with DAPI. A low-power (40X objective) lens was used to view various phases of the cells in a field (B). (C) Experiments were done similarly as in B with p-Vgll4 Ser-280 antibodies. White and yellow arrows (in panels B and C) mark the metaphase and interphase cells, respectively.

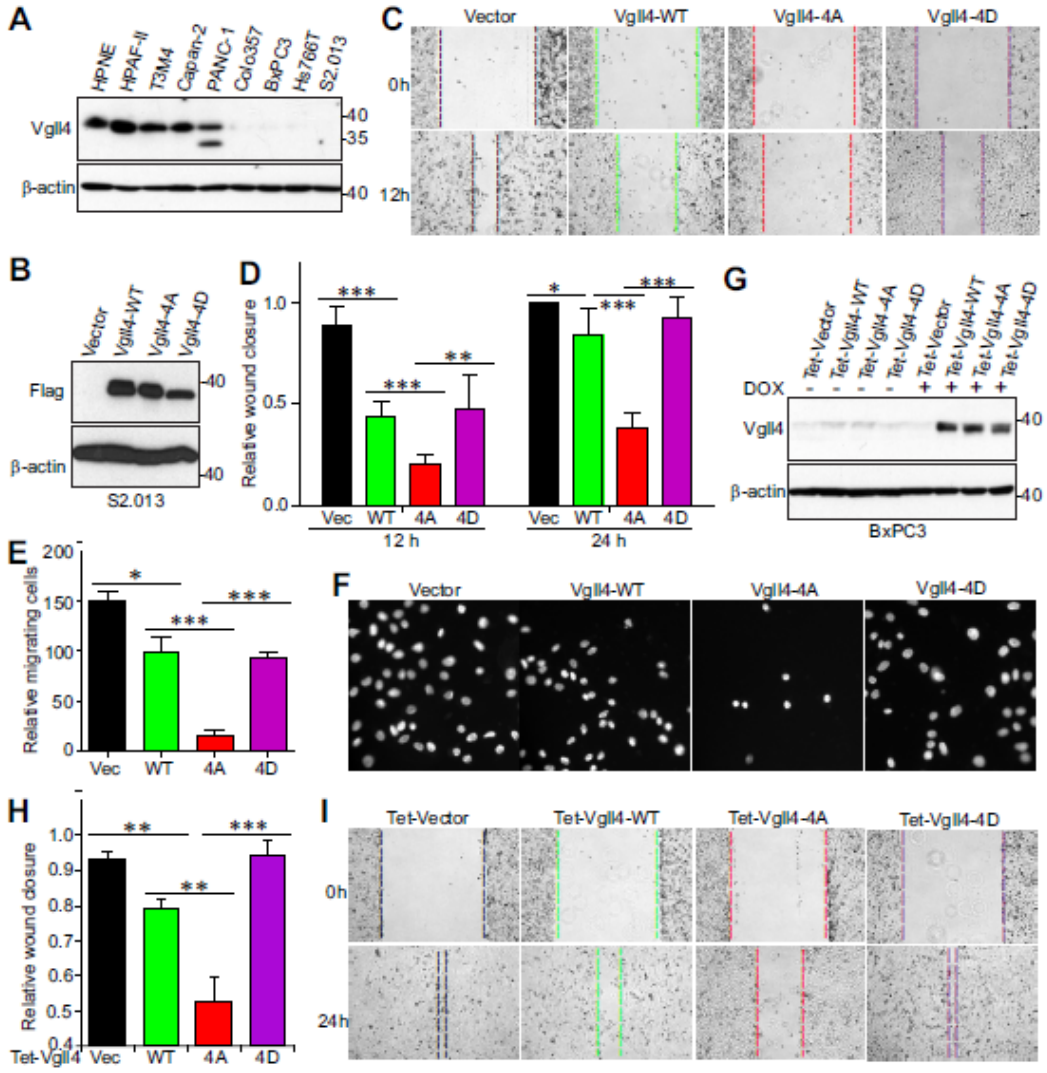
A
HPNE
HPAF-II
T3M4
Capan-2
PANC-1
Colo357
BxPC3
Hs766T
S2.013
Vgll4
β-actin
40
35
40
B
Vector
Vgll4-WT
Vgll4-4A
Vgll4-4D
Flag
β-actin
40
40
S2.013
C
Vector
Vgll4-WT
Vgll4-4A
Vgll4-4D
0h
12h
D
Relative wound closure
1.0
0.5
0.0
***
***
**
*
***
***
Vec
WT
4A
4D
12 h
24 h
E
Relative migrating cells
200
150
100
50
0
*
***
***
Vec
WT
4A
4D
F
Vector
Vgll4-WT
Vgll4-4A
Vgll4-4D
G
Tet-Vector
Tet-Vgll4-WT
Tet-Vgll4-4A
Tet-Vgll4-4D
DOX
Vgll4
β-actin
40
40
BxPC3
H
Relative wound closure
1.0
0.9
0.8
0.7
0.6
0.5
0.4
**
**
***
Tet-Vgll4
Vec
WT
4A
4D
I
Tet-Vector
Tet-Vgll4-WT
Tet-Vgll4-4A
Tet-Vgll4-4D
0h
24h

Figure 2-6. Mitotic phosphorylation of Vgll4 inhibited its tumor-suppressing activity in pancreatic cancer cells.

(A) Vgll4 expression in pancreatic non-cancer (HPNE) and cancer cells. (B) Establishment of S2.013 cell lines stably expressing vector (Vec), wild-type Vgll4, Vgll4-4A, or Vgll4-4D (all are FLAG-tagged). 4A, S58A/S155A/T159A/S280A; 4D, S58D/S155D/T159D/S280D. (C, D) Cell migration (wound healing) assays with cell lines established in B. Data are expressed as the mean ±S.D. of at least three independent experiments. ***, $p < 0.001$; **, $p < 0.01$; *, $p < 0.05$ (t-test). (E, F) cell migration (Transwell) assays with cell lines established in B. Data are expressed as the mean ±S.D. of three independent experiments. ***, $p < 0.001$; *, $p < 0.05$ (t-test). (G) Establishment of Tet-On-inducible cell lines expressing wild-type Vgll4 or Vgll4-4A or Vgll4-4D in BxPC3 pancreatic cancer cells. Cells were kept on Tet-approved FBS, and doxycycline was added (1 <g/ml) to the cells 2 days before the experiments. (H, I) Cell migration (wound healing) assays with cell lines established in G. Data are expressed as the mean ±S.D. of three independent experiments. ***, $p < 0.001$; **, $p < 0.01$ (t-test).

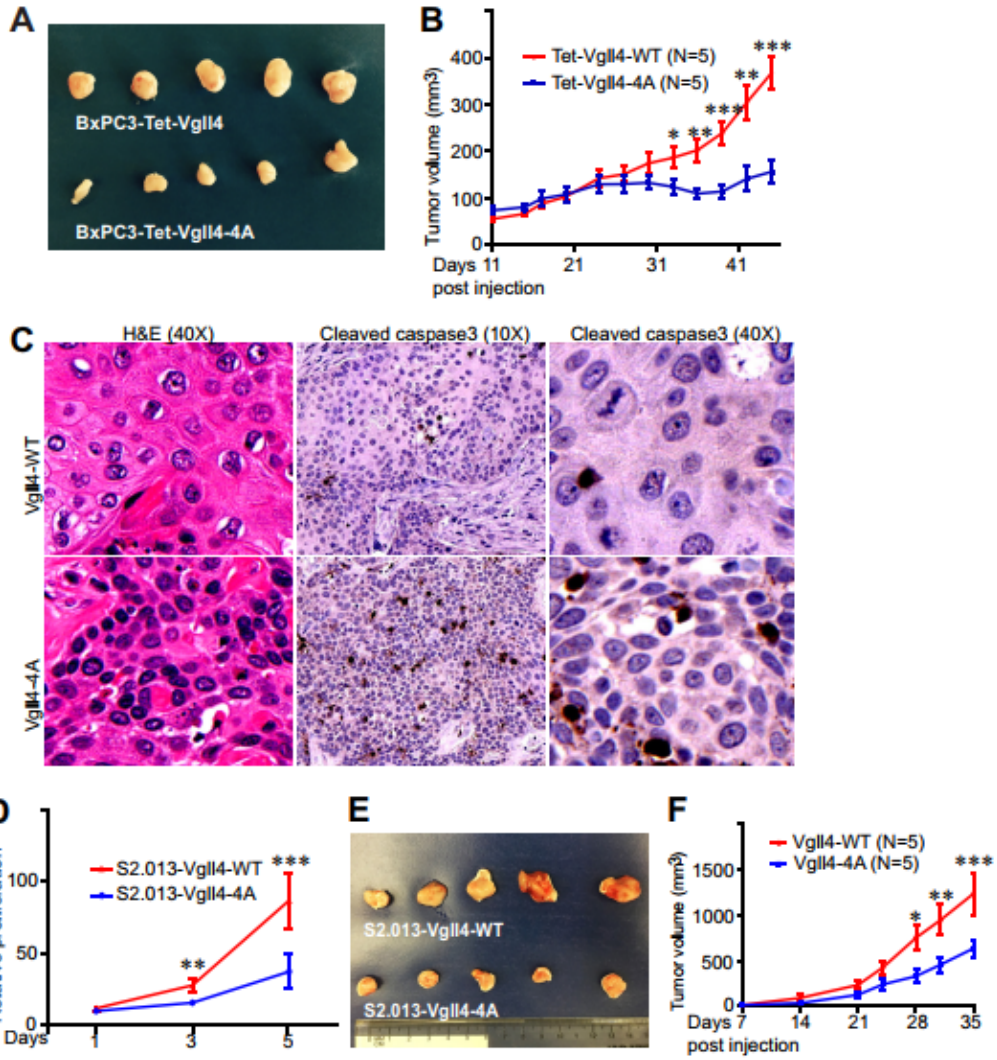
A
BxPC3-Tet-Vgll4
BxPC3-Tet-Vgll4-4A
B
Tet-Vgll4-WT (N=5)
Tet-Vgll4-4A (N=5)
Tumor volume (mm3)
Days post injection
C
H&E (40X)
Cleaved caspase3 (10X)
Cleaved caspase3 (40X)
Vgll4-WT
Vgll4-4A
D
S2.013-Vgll4-WT
S2.013-Vgll4-4A
Relative proliferation
Days
E
S2.013-Vgll4-WT
S2.013-Vgll4-4A
F
Vgll4-WT (N=5)
Vgll4-4A (N=5)
Tumor volume (mm3)
Days post injection

Figure 2-7.Non-phosphorylatedVgll4 suppressed tumorigenesis in mice.

(A) Representative five tumors in each group were excised and photographed at the end point. (B) Tumor growth curve with BxPC3 cells. BxPC3 cells expressing wild-type Vgll4 or Vgll4-4A (Tet-On-inducible) were subcutaneously inoculated into athymic nude mice on both flanks, and the mice were kept on doxycycline (0.5 mg/ml) in their drinking water throughout the experiment. The tumor volume shown at each point was the average from 8 tumors (two injections on two mice in each group did not form visible tumors and were excluded from the analysis). ***, $p<0.001$; **, $p<0.01$; *, $p<0.05$ (t-test). (C) Hematoxylin and eosin and cleaved caspase-3 staining in tumors shown in A. Three tumors from each group were analyzed. (D) Cell proliferation curve with S2.103 cells expressing Vgll4-WT or Vgll4-4A. ***, $p< 0.001$; **, $p<0.01$(t-test). E and F, similar experiments were done as in (A and B) with S2.013 cell lines. ***, $p<0.001$; **, $p<0.01$; *, $p<0.05$ (t-test).

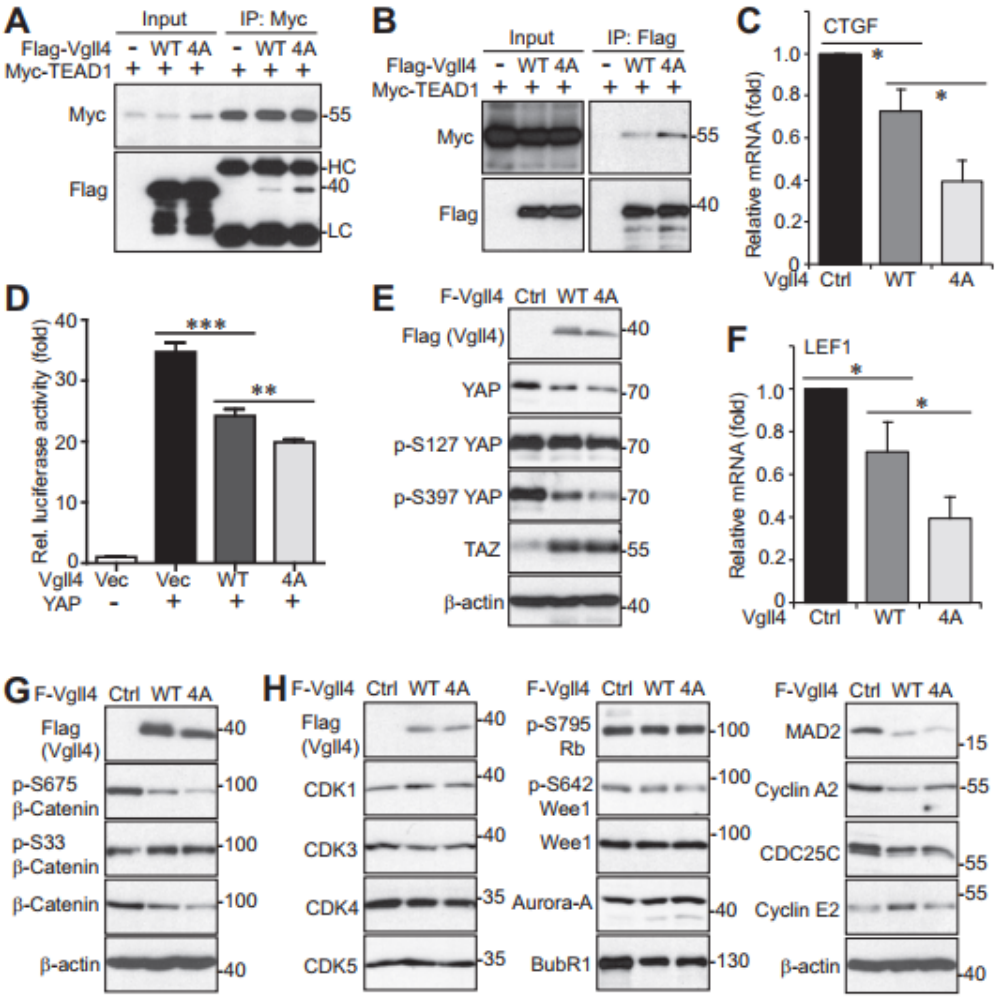
A
Input
IP: Myc
Flag-Vgll4 - WT 4A - WT 4A
Myc-TEAD1 + + + + + +
Myc
Flag
55
HC
40
LC
B
Input
IP: Flag
Flag-Vgll4 - WT 4A - WT 4A
Myc-TEAD1 + + + + + +
Myc
Flag
55
40
C
CTGF
Relative mRNA (fold)
1.0
0.8
0.6
0.4
0.2
0
Vgll4 Ctrl WT 4A
D
Rel. luciferase activity (fold)
40
30
20
10
0
***
**
Vgll4 Vec Vec WT 4A
YAP - + + +
E
F-Vgll4 Ctrl WT 4A
Flag (Vgll4)
YAP
p-S127 YAP
p-S397 YAP
TAZ
β-actin
40
70
70
70
55
40
F
LEF1
Relative mRNA (fold)
1.0
0.8
0.6
0.4
0.2
0
Vgll4 Ctrl WT 4A
G
F-Vgll4 Ctrl WT 4A
Flag (Vgll4)
p-S675 β-Catenin
p-S33 β-Catenin
β-Catenin
β-actin
40
100
100
100
40
H
F-Vgll4 Ctrl WT 4A
Flag (Vgll4)
CDK1
CDK3
CDK4
CDK5
40
40
40
35
35
F-Vgll4 Ctrl WT 4A
p-S795 Rb
p-S642 Wee1
Wee1
Aurora-A
BubR1
100
100
100
40
130
F-Vgll4 Ctrl WT 4A
MAD2
Cyclin A2
CDC25C
Cyclin E2
β-actin
15
55
55
55
40

Figure 2-8. Mitotic phosphorylation of Vgll4 affected YAP and β-catenin activity and regulated the expression of cell cycle regulators.

(A, B) HEK293T cells were transfected with various DNA plasmids as indicated. The immunoprecipitates (IP, with FLAG or Myc antibodies) were probed with the indicated antibodies. Total cell lysates before immunoprecipitation were also included (input). (C) Quantitative RT-PCR for CTGF in S2.013 cell lines expressing vector, wild-type Vgll4, or Vgll4-4A. *, $p<0.05$ (t-test). (D) Luciferase reporter assays in HEK293T cells. **, $p<0.01$; ***, $p<0.001$ (t-test). (E) Total cell lysates from S2.013 cell lines expressing vector, wild-type Vgll4, or Vgll4-4A were probed with the indicated antibodies (YAP-related). (F) Quantitative RT-PCR for LEF1 in S2.013 cell lines expressing vector, wild-type Vgll4, or Vgll4-4A. *, $p<0.05$ (t-test). (G) Total cell lysates from S2.013 cell lines expressing vector, wild-type Vgll4, or Vgll4-4A were probed with the indicated antibodies (β-catenin-related). (H) Total cell lysates were harvested from S2.013 cell lines expressing vector, wild-type Vgll4, or Vgll4-4A and were subjected to Western-blotting analysis with various cell cycle regulators.

CHAPTER 3 A PHOS-TAG-BASED SCREEN IDENTIFIES THE MARK2-HDAC AXIS AS A DRUGGABLE TARGET FOR OVERCOMING CHEMORESISTANCE IN PANCREATIC CANCER

3.1. Abstract

Paclitaxel is one of the anti-tubulin drugs and has been widely used in ovarian, breast, non-small cell lung cancers, and recently pancreatic cancer. Despite their wide use in cancer treatment, the patient response rate is still low, and drug resistance is a major clinical obstacle. Through a Phos-tag-based kinome-wide screens, we identified microtubule affinity-regulating kinase 2 (MARK2) as a critical regulator for Paclitaxel chemosensitivity in pancreatic ductal adenocarcinoma (PDAC). We show that MARK2 is phosphorylated by cyclin-dependent kinase 1 (CDK1) in response to anti-tubulin chemotherapeutics and in unperturbed mitosis in a kinase activity-independent manner. Phosphorylation is essential for MARK2 in regulating mitotic progression and Paclitaxel cytotoxicity in PDAC cells. Mechanistically, our findings also suggest that MARK2 controls Paclitaxel chemosensitivity by regulating class IIa histone deacetylase (HDACs). MARK2 directly phosphorylates HDAC4 specifically during anti-tubulin treatment. Phosphorylated HDAC4 promotes Yes-associated protein (YAP, the transcriptional coactivator of the Hippo pathway) activation and controls expression of YAP target genes induced by Paclitaxel. Importantly, a combination of HDAC inhibition (by knockdown or Vorinostat) and Paclitaxel overcomes chemoresistance in preclinical PDAC animal models. Furthermore, the expression levels of MARK2, class IIa HDACs, and YAP are upregulated and positively correlated in PDAC patients. Inhibition of MARK2 or class IIa HDACs potentiates Paclitaxel cytotoxicity by inducing mitotic abnormalities in PDAC cells. Together, our findings identify the MARK2-HDAC axis as a druggable target for overcoming chemoresistance in PDAC.

3.2. Introduction

Microtubule affinity-regulating kinase proteins (MARK1-4) are critical for microtubule dynamics by modulating MAPs (microtubule-associated proteins) such as Tau [43, 44]. They are members of the AMPK/Snf1 family and control cell polarity and asymmetric cell division [44, 45]. Deregulation of MARKs has also been associated with pathological conditions such as cancer and Alzheimer's disease [45]. For example, MARK1 is involved in cervical tumor cell migration [46], and MARK1-mediated phosphorylation is critical for DIXDC1's tumor-suppressive function in lung cancer [47]. MARK2 is an oncogene in non-small cell lung cancer associating with cisplatin resistance and DNA damage response [48]. MARK4 is upregulated in glioblastomas and implicated in prostate cancer, breast cancer, hepatocarcinoma, and leukemia [49-54]. Several recent studies showed that MARK family members are important regulators of Hippo-YAP signaling [53, 55-57], which is critical in cancer development, drug resistance, and stem cell biology [2, 3, 58-60]. However, how MARKs are regulated and their biological significance in response to antimitotic agents have not been defined.

MARKs regulate class IIa histone deacetylases (HDAC4/5/7/9) by direct phosphorylation [61]. Since HDACs reverse the acetylation of nucleosomal histones by histone acetyltransferases and promote chromatin condensation and transcriptional repression, MARK phosphorylation promotes HDACs cytoplasmic retention. It inhibits their deacetylation/transcription repression activity [61-63]. HDACs regulate cellular processes critical in tumorigenesis, including gene transcription, cell cycle progression, cell survival, DNA repair, protein trafficking, protein degradation, and cell migration [64]. The HDAC inhibitor Vorinostat (SAHA) has been approved by the US FDA for cutaneous T-cell lymphoma patients. While HDAC inhibitor monotherapy showed clinical activity in hematological malignancies, results have been largely disappointing in most solid tumors,

including PDAC [65]. Thus, a major effort for the HDAC inhibitors' clinical application is focusing on combinations with other chemotherapeutic agents [66]. Despite the important function of HDACs in tumorigenesis, how they sense the stress signal to antimitotic drugs (e.g., Paclitaxel) is very unclear.

Identifying regulators and/or signaling involved in the mitotic cell cycle may lead to the addition of druggable targets and the development of novel chemotherapeutics for combatting cancer.To understand how the kinome is involved in regulating anti-tubulin chemotherapeutics, we conducted kinome-wide screens using a Phos-tag-based approach. Our screens have a twofold purpose: 1) identifying novel mitotic kinases, as anti-tubulin agents arrest cells at G2/M; 2) identifying novel kinases that determine anti-tubulin drug sensitivity. These screens identified MARK2 as a phospho-protein during mitosis and a critical determinant of Paclitaxel cytotoxicity in PDAC cells. We further showed that MARK2 controls Paclitaxel chemosensitivity in PDAC by phosphorylating class IIa HDACs. MARK2-HDAC controls a unique transcriptional program in response to anti-tubulin agents in a YAP-dependent manner. Our findings reveal the MARK2-HDAC-YAP axis as a druggable target for overcoming the resistance to chemotherapy in PDAC.

3.3. Materials and Methods

3.2.1. Cell culture and transfection

The immortalized human pancreatic nestin-expressing (HPNE) cell line was provided by Dr. Michel Ouellette (University of Nebraska Medical Center), who originally established the cell line and deposited it at the American Type Culture Collection (ATCC) [21]. Dr. Michael (Tony) Hollingsworth (University of Nebraska Medical Center) kindly provided the T3M4, S2.013, and Colo-357 pancreatic cancer cell lines. HEK293T, HeLa, HPAF-II, Capan-2, PANC-1, BxPC-3, and Hs776T cell lines were purchased from ATCC and cultured as ATCC instructed. The cell lines were authenticated at ATCC and were used at low (<30) passages. The mouse PDAC cell lines UN-KC-6141, UN-KPC-960, and UN-KPC-961, have been described [67]. Attractene (Qiagen) was used for transient overexpression of proteins in HEK293T and HEK293GP cells following the manufacturer's instructions. HiPerFect (Qiagen) was used for siRNA transfections. siRNA duplex for MARK2 was obtained from Sigma-Aldrich. Nocodazole (100 ng/ml for 20 h) and Taxol (100 nM for 20 h) (Selleck Chemicals) were used to arrest cells in mitosis unless otherwise indicated. VX680, ZM447439, BI2536, Purvalanol A, SP600125, Rapamycin, and MK2206 were purchased from Selleck Chemicals. RO3306 and Roscovitine were from ENZO Life Sciences. U0126, SB203580, and LY294002 were from LC Laboratory. MK5108 (Aurora-A inhibitor) was from Merck. All other chemicals were from either Sigma-Aldrich or Thermo Fisher.

3.2.2. Expression constructs

The following plasmids were purchased from Addgene: pBa-eGFP-MARK2-WT (#66706), pEGFP-HDAC4-WT (#45636), and pEGFP-HDAC4-3SA (#45637), pLKO.1-H2B-RFP (#26001), pLenti PGK V5-LUC Puro (#19360), and GFP-Cyclin B1-R42A

(#61849). Expression constructs GFP-YAP, Myc-WW45, Flag-MST1, Flag-MST2, Myc-LATS2 have been described previously [10]. To make MARK2 or HDAC4 expression constructs, the full-length cDNA was cloned into the pSIN4-Flag-IRES-puro vector, respectively [68]. Point mutations were generated by the QuikChange Site-directed PCR Mutagenesis Kit (Stratagene) and verified by Sanger sequencing.

3.2.3. shRNA-mediated knockdown and CRISPR/Cas9-mediated knockout

Downregulation of MARK2, HDAC4, or HDAC7 in HeLa, S2.013, Capan2, PANC-1, and UN-KC-6141 cells was achieved by lentivirus-mediated corresponding shRNA expression [69]. All MISSION shRNA constructs were purchased from Sigma-Aldrich, and targeting sequences were listed in Table 1. The shRNA construct targeting 3'-UTR of human MARK2 was also used to knock down mouse Mark2 in KC6141 cells. Ectopic expression of MARK2, MAR2-3A, MARK2-KD, HDAC4, or HDAC4-3A was also achieved by a lentivirus-mediated approach [69]. The HeLa cell line expressing TetOn-shCDK1 has been described [70].

To construct the EGFP-expressing all-in-one CRISPR/Cas9n plasmid targeting human MARK2, the sense and antisense oligonucleotides from Table 2 were synthesized, annealed, and Golden Gate-assembled into the pX330A_D10A-1×2-EGFP and pX330S-2 vectors as described previously [68]. The final construct was transfected into U2OS cells, and GFP-positive clones were selected by flow cytometry-based cell sorting.

3.2.4. Recombinant protein purification and *in vitro* kinase assay

GST-tagged MARK2, MARK2-3A (amino acids 388-788), HDAC4, HDAC4-3A (amino acids 200-680), and MST2-KD (kinase-dead) proteins were bacterially expressed and purified on GSTrap FF affinity columns (GE Healthcare) following the manufacturer's instructions. The GST-MARK2 proteins (0.5-1 μg) were incubated with recombinant 100

ng of CDK1–Cyclin B1 (SignalChem) in kinase buffer (New England BioLabs) in the presence of 10 µCi of [γ-^{32}P]ATP (3000 Ci/mmol, Perkin Elmer Life Sciences). GST-MST2-KD and GST-HDAC4 proteins (1 µg) were also used as substrates for MARK2 (150 ng) phosphorylation. Active MARK2, CDK5–p25, MEK1, ERK1, JNK1, JNK2, and p38α kinases were purchased from SignalChem. Phosphorylation (^{32}P incorporation) was visualized by autoradiography followed by Western blotting or detected by phospho-specific antibodies.

3.2.5. Western blotting, immunoprecipitation, and Phos-tag analysis

Cell lysate preparation, Western blotting analysis, immunoprecipitation, and lambda phosphatase treatment were done as previously described [23]. Phos-tag was obtained from Wako Pure Chemical Industries, Ltd. (catalog no. 304-93521) and used at concentrations of 10-25 µM (with 100 µM $MnCl_2$) in 6-8% SDS-acrylamide gels.

3.2.6. Immunofluorescence (IF) staining, confocal microscopy, and immunohistochemistry (IHC) staining

Fluorescence staining was done as described [35]. The stained cells were mounted with Fluoromount (Vector Laboratories) and visualized on an LSM800 Zeiss fluorescence microscope (Carl Zeiss). The ZEN 2.3 (blue edition) software (Carl Zeiss) was used to analyze and process all IF images. YAP cellular localization was visualized by YAP IF staining with an Alexa Fluor 647-conjugated YAP antibody (1:100, Cell Signaling Technology) following the manufacturer's instructions. The p-HDAC4 S246 antibody (1:100, Cell Signaling Technology) was also used for IF staining**.** IHC staining with cleaved caspase 3 (1:100, Cell Signaling Technology) in tumor tissues was performed according to a previously described protocol [71].

3.2.7. Antibodies

Rabbit polyclonal phospho-specific antibodies against MARK2 S456, S569, S619, and MST2 S15 were generated and purified by AbMart, Inc. The peptides used for immunizing rabbits were AKVPA-pS-PLPGL (MAR2 S456), RVPVA-pS-PSAHN (MARK2 S569), GVTPA-pS-PSGHS (MARK2 S619), and KLKKL-pS-EDSLT (MST2 S15). The corresponding non-phosphorylated peptides were also used for antibody purification and blocking assays. Anti-MARK2, Cyclin B1, β-actin were purchased from Santa Cruz Biotechnology. Anti-MARK1, MARK3, MARK4, p-MARK T208 (activation loop), HDAC1, HDAC2, HDAC4, HDAC5, HDAC6, HDAC7, p-HDAC4/5/7(S246/S259/S155), p-HDAC4/5/7(S632/S661/S486), cleaved-PARP (human-specific), cleaved-PARP (rodent specific), cleaved-caspase 3, Erk1/2, Zyxin, Survivin, p-YAP S127, YAP, and p-Aurora-A/B/C were from Cell Signaling Technology. Anti-GST and LATS2 antibodies were from Bethyl Laboratories. Anti-Aurora-A and Flag antibodies were from Sigma. The anti-α-tubulin antibody was from Abcam Inc. All other antibodies used in this study were listed in Table 3.

3.2.8. qRT-PCR

The Direct-zol RNA Kit (ZYMO Research) was used for total RNA isolation. RNA reverse transcription and qRT-PCR were done as we have described[10].

3.2.9. Live-cell imaging

Cells were plated on black 96-well optical bottom plates (Thermo Fisher). Live-cell imaging was performed in a Cellomics Arrayscan VTI HCS Reader with 37°C, 5% CO2 incubation using FluroBrite DMEM (Thermo Fisher). Cells were monitored for 24 h and

pictures were taken every 5 min using an RFP filter. Measurements of cell cycle durations were done using the time-lapse sequences.

3.2.10. Luciferase reporter assays

Luciferase reporter assays were done as we previously described [10].

3.2.11. Caspase-Glo 3/7 assay

Control and MARK2-KD cells were plated in white-walled 96-well plates (NUNC, 136101, Thermo Fisher) for 24 hours and treated with Paclitaxel for an additional 16 hours. Apoptosis was measured by Caspase-Glo 3/7 Assay Kit (Promega, G8090) according to the manufacturer's instructions and quantified on a luminometer.

3.2.12. Clonogenic assay

Cells (2,000) were seeded at low density in six-well plates and incubated overnight. The cells were then treated with paclitaxel for 24 hours and were replaced with a fresh medium without a drug. After 14 days of incubation, colonies were fixed with 4% paraformaldehyde for 15 minutes at room temperature and were stained with 0.5% crystal violet for 30 minutes. Quantification was achieved by ImageJ software (ImageJ 1.53e, Wayne Rasband and contributors, National Institutes of Health, USA).

3.2.13. Animal studies

For *in vivo* xenograft studies, mouse PDAC cells (5.0×10^6) were subcutaneously injected into both flanks of six to eight-week-old male or female immunocompetent C57BL/6 mice (Charles River Laboratories, Wilmington, MA, USA). Cells were suspended in phosphate-buffered saline (PBS). Tumor sizes were measured twice a week using an

electronic caliper ten days post-injection. Tumor volume (V) was calculated by the formula: $V = 0.5 \times length \times width^2$.

For orthotopic studies, UN-KC-6141 cells expressing luciferase (5000 cells/50 µl Hanks' Balanced Salt Solution each mouse) were injected into the head of the pancreas of six to eight-week-old C57BL/6 mice (Charles River Laboratories). The orthotopic injection was performed as previously described[72]. Approximately 10 min prior to imaging, mice were intraperitoneally injected with D-luciferin (150 mg/kg). Tumor burdens (primary and metastasis) were monitored by measuring bioluminescence emission using an IVIS imaging system (Perkin Elmer) once a week seven days post-injection. Gemcitabine was purchased from SAGENT Pharmaceuticals (NDC 25021-234-10). Paclitaxel was purchased from Hospira, Inc. (NDC 61703-342-22). Vorinostat/SAHA was purchased from Selleck Chem and was dissolved in 2% DMSO, 30% PEG300, 5% Tween 80, and ddH_2O and was used every other day at 25 mg/kg via intraperitoneal injection. Mice were euthanized by CO_2 inhalation at the end of the experiment, and the tumors were excised for subsequent analysis. All animals were housed in pathogen-free facilities. Animal experiments were approved by the University of Nebraska Medical Center Institutional Animal Care and Use Committee.

3.2.14. Statistical analysis

Statistical significance was analyzed using a two-tailed, unpaired Student's t-test, a one-way ANOVA with a post-hoc Tukey HSD (Honestly Significant Difference) test, or a Chi-Square test for multiple comparisons. A P value of <0.05 was considered to indicate statistical significance.

3.4. Results

3.3.1. A Phos-tag-based kinome screen for regulators of anti-tubulin drug response

To identify new kinases that are triggered by anti-tubulin agents, we used two approaches. We systematically investigated individual kinase's response (expression level) to anti-tubulin drugs (Paclitaxel and Nocodazole) by Western blotting. Second, using a Phos-tag method, we determined each kinase's phospho-regulation (phosphorylation-status) in response to anti-tubulin drugs. The Phos-tag specifically binds phosphate ions and selectively separates phosphorylated proteins on SDS-PAGE gels [27]. The human kinome has 518 protein kinases [73], including 90 protein tyrosine kinases [74]. We screened 115 kinases (79 protein tyrosine kinases and 36 serine/threonine protein kinases) using primary antibodies obtained from Cell Signaling Technology, Bethyl Laboratories, and Santa Cruz Biotechnology (Table 3) (Fig. 3-1A; 3-2 and data not shown) [32, 68, 75, 76].

Previous studies showed that ABL1[77], AMPK[76], FAK[78], EGFR [79], SRC[80], and YES [75] are phosphorylated during mitotic arrest. We confirmed their mobility upshift (phosphorylation) during drug-induced mitotic arrest (Fig. 3-2), which validated our screen's robustness. We also identified numerous novel alterations of protein kinases in response to anti-tubulin drugs, including ABL2 (ARG), ACK, EphA2, EphA3/4/5, EphB4, FGFR2, JAK1, MER, MET, PYK2, ROR2, AMPK, CHK1, IKKβ, MARK2/3, PKN1/2/3, PKR, and TAOK1. These kinases were upshifted (phosphorylated) during Taxol or Nocodazole treatment, suggesting a role of these proteins in response to anti-tubulin drugs (Fig. 3-1A and 3-2). Another significant change we noted was a marked reduction of protein levels of FGFR4, TNK1, and AXL during anti-tubulin treatment (Fig. 3-1A and 3-2). This study

characterizes the increased phosphorylation of MARK2 and its role in mitotic progression and anti-tubulin chemotherapeutics.

3.3.2. CDK1 phosphorylates MARK2 *in vitro*

We further confirmed that the mobility upshift of MARK2 occurred in other cancer cells, including PDAC cells (Fig. 3-1B and data not shown). The MARK2 kinase activity (revealed by the autophosphorylation at the activation loop site T208) was not altered during antimitotic drug-induced mitosis (Fig. 3-1C), suggesting the existence of phosphorylation site(s) other than T208 in MARK2.

Lambda phosphatase treatment largely converted MARK2 mobility upshifted bands to fast-migrating bands, confirming MARK2 was phosphorylated during G2/M arrest induced by antimitotic agents (Fig. 3-1D).

We used various kinase inhibitors to identify the candidate kinase for MARK2 phosphorylation. Treatments with RO3306 (a CDK1 inhibitor) or purvalanol A (a CDK1/2/5 inhibitor) almost completely inhibited the mobility shift (Fig. 3-3E, lanes 4 and 6). These data suggested that CDK1 is likely the relevant kinase for MARK2 phosphorylation induced during paclitaxel or nocodazole treatment.

To determine whether CDK1 kinase can directly phosphorylate MARK2, we performed *in vitro* kinase assays with GST-tagged MARK2 proteins as substrates. Figure 3-1F shows that purified CDK1–Cyclin B1 kinase complex phosphorylated GST-MARK2 proteins *in vitro*. CDK2 and CDK5 were also able to phosphorylate MARK2 to a lesser extent (Fig. 3-1F). We also included MAPK-p38α, MEK1, ERK1, and JNK1/2 kinases in these assays as these kinases recognize the same phosphorylation sequence consensus as CDK1 (Fig. 3-1F). Little MARK2 phosphorylation was detected in the presence of these kinases (Fig. 3-1F).

CDK1 phosphorylates substrates at a minimal proline-directed consensus sequence [33]. Database analysis (https://www.phosphosite.org) identified three SPs (S456, S569, and S619) in MARK2 as possible CDK1 phosphorylation sites during mitosis. RO3306 treatment or mutating all these three sites to alanines completely blocked ^{32}P incorporation *in vitro* (Fig. 3-1G), suggesting that these sites are the main phosphorylation sites for CDK1. We next generated phospho-specific antibodies against these sites. CDK1-Cyclin B1 complex significantly increased phosphorylation of S456, S569, and S619 of GST-MARK2 *in vitro,* and the signals were abolished when the non-phosphorylatable mutant (3A: S456A/S569A/S619A) was used (Fig. 3-1H). Together, these data indicate that CDK1 phosphorylates MARK2 at S456, S569, and S619 *in vitro*.

3.3.3. CDK1 phosphorylates MARK2 in cells during mitosis

After confirming MARK2 phosphorylation by CDK1 *in vitro*, we next examined this phosphorylation in cells. Nocodazole or Taxol treatment significantly increased the phosphorylation of S569 and S619 of endogenous MARK2 (Fig. 3-3A, B). The signal was abolished by siRNA-mediated knockdown (Fig. 3-3B). Phosphopeptide-, but not regular non-phosphopeptide-, incubation completely blocked the phospho-signal of transfected MARK2, suggesting that these antibodies detect the phosphorylated form of MARK2 (Fig. 3-3C, D). Mutating all three serines to alanine also greatly diminished the phosphorylation of MARK2 (Fig. 3-3E), confirming the specificity of these phospho-antibodies.

Treatment with RO3306 or Purvalanoal A blocked MARK2 phosphorylation at S569 and S619 induced by taxol, suggesting that phosphorylation of MARK2 is CDK1 kinase-dependent in cells (Fig. 3-3F, lanes 3 and 4). Furthermore, knockdown CDK1 inhibited MARK2 phosphorylation in cells (Fig. 3-3G), and enhanced expression of hyperactive CDK1 or Cyclin B1 greatly increased MARK2 phosphorylation (Fig. 3-3H). The kinase

activity of MARK2 is not required for its mitotic phosphorylation since MARK2-KD (kinase-dead) was also phosphorylated at S569 and S619 during mitotic arrest (Fig. 3-3I). The non-phosphorylatable mutant (MARK2-3A) possesses similar kinase activity (measured by T208 autophosphorylation) when compared with wild type MARK2, suggesting that mitotic phosphorylation of MARK2 does not impact on its kinase activity (Fig. 3-3J). Together, these observations indicate that MARK2 is phosphorylated at S569 and S619 in cells during anti-tubulin drug treatment.

3.3.4. MARK2 regulates mitotic progression in a CDK1 phosphorylation-dependent manner

We next explored the possible role of MARK2 in regulating mitotic processes. Deletion of MARK2 (MARK2-KO) in U2OS cells did not affect other MARK family members' expression levels (Fig. 3-4A). We monitored mitotic progression in parental and MARK2-KO cells stably expressing RFP-H2B by utilizing fluorescence live-cell imaging. The parental U2OS cells condensed their chromatin and aligned their chromosomes in a tightly packed metaphase plate within 20 min after the nuclear envelope breaks down (NEBD). Anaphase onset occurred at approximately 52 min, following with telophase, measured by chromatin decondensation, occurring at 60 min post-NEBD (Fig. 3-5A). In contrast, MARK2-KO cells showed a dramatic delay in chromosome alignment at metaphase for approximately 100 min (Fig. 3-5B, C). Accordingly, the mitotic length was significantly increased in MARK2-KO cells compared with parental cells (Fig. 3-4B). These data suggest that MARK2 is required for metaphase-anaphase transition. Similar findings were observed in HeLa cells with MARK2 knockdown (Fig. 3-4C;3-5D).

The necessity of MARK2 for proper prophase-to-anaphase progression prompted us to explore the role of CDK1-mediated MARK2 phosphorylation events. We generated

stable cell lines expressing either MARK2-WT or MARK2-3A in the MARK2-KO U2OS or MARK2 knockdown HeLa cells (Fig. 3-5E). Inhibition of MARK2 significantly altered U2OS cells into fibroblast-like morphology (Fig. 3-5F) and resulted in mitotic defects, including chromosome misalignment and missegregation (Fig. 3-5G, H). A significantly higher percentage of cells with MARK2 knockdown contain multiple nuclei (Fig. 3-5G). Importantly, the addback of wild type MARK2 completely rescued the mitotic abnormality and morphology seen in MARK2-KO and knockdown cells (Fig. 3-3F, I). However, the non-phosphorylatable mutant MARK2 (MARK2-3A) re-expression failed to restore the defects (Fig. 3-5F, I). Accordingly, MARK2, but not the MARK2-3A mutant, addback largely restored the mitotic delay to normal (Fig. 3-5J, K). These observations suggest that CDK1-mediated phosphorylation of MARK2 is critical for proper mitotic progression.

3.3.5. MARK2 regulates chemosensitivity in PDAC

To determine the biological significance of MARK2, we analyzed MARK2 expression in different types of cancer in public datasets, and the most significant change (cancer vs. normal) of MARK2 signaling was found in PDAC (Fig. 3-4D and 3-6A). Importantly, high expression of MARK2 strongly correlates with poor survival in PDAC patients (Fig. 3-6B). MARK2 protein levels were also overexpressed in most pancreatic cancer cell lines compared with the non-cancerous HPNE (immortalized human pancreatic nestin-expressing) cells (Fig. 3-6C).

To directly examine the role of MARK2 in PDAC cells, we knocked down MARK2 (MARK2-KD) in various cell lines (Fig. 3-6D). Knockdown of MARK2 did not induce apoptosis and had little effect on tumor growth under normal culture conditions (data not shown). Significant changes were observed when cells were exposed to the anti-tubulin agent Taxol, which has been used together with Gemcitabine as first-line chemotherapy for metastatic pancreatic cancer. PDAC cells (PANC-1, Capan-2, and S2.013) are

relatively resistant to Taxol treatment (Fig. 3-6D). MARK2 knockdown greatly sensitized PDAC cells to Taxol-induced cell death (revealed by cleaved PARP) compared to control cells (Fig. 3-6D). We further performed clonogenic assays to examine the effect of MARK2 in survival rate in response to Taxol treatment. As shown in Figure 3-6E and Figure 3-6F, knockdown of MARK2 significantly impaired cell survival after Taxol treatment compared with control cells.

We next determined whether anti-tubulin drug-induced phosphorylation is involved in regulating Taxol cytotoxicity in PDAC cells. Re-expression of MARK2, but not MARK2-3A mutant, completely blocked cell death induced by Taxol in MARK2-knockdown cells, suggesting that CDK1 phosphorylation is essential for MARK2-driven Taxol chemosensitivity (Fig. 3-6 H).

In addition, knockdown of Mark2 in mouse PDAC cells (KC6141) also enhanced Taxol cytotoxicity (Fig. 3-6I, J). In the clinic, Gemcitabine is used along with Nab-Taxol. Interestingly, knockdown of MARK2/Mark2 synergistically induced cell death with Gemcitabine in both human and mouse PDAC cells (Fig. 3-6 K, L). Next, control and Mark2-KD KC6141 cells were subcutaneously inoculated into immune-competent C57BL/6 mice and treated with DMSO, Taxol, or Gemcitabine. No significant difference was observed in the sizes of tumors from control and MARK2-KD cells (Fig. 3-6 M-O). Paclitaxel or Gemcitabine treatment in control cells did not suppress tumor growth under the doses we used (Fig. 3-6 M-O). Consistent with our observations from *in vitro* models (Fig. 3-6 J, L), Mark2-KD cells formed significantly smaller tumors than the control cells under Taxol or Gemcitabine treatments, suggesting that inhibition of Mark2 sensitizes PDAC cells to Taxol or Gemcitabine cytotoxicity (Fig. 3-6 M-O). Together, our studies elucidated a novel regulatory mechanism and function of MARK2 in response to anti-

tubulin drugs and indicate that MARK2 is a potent and novel regulator in chemoresistance in PDAC cells.

3.3.6. MARK2 phosphorylates MST2 and positively regulates YAP activity

Having established the role and regulation of MARK2 in Taxol chemotherapy, we next explored the downstream effector and mechanism of MARK2 in response to Taxol treatment. The Hippo (MST1/2-LATS1/2) kinase cascade phosphorylates primarily on the S127 site and inactivates YAP by sequestering it in the cytoplasm [10, 81]. The transcriptional co-activator YAP binds to and functions through TEAD (TEA-domain containing proteins) transcription factors to regulate downstream targets, including *CTGF* (connective tissue growth factor), *Cyr61*, *LATS2*, and *Survivin* [4, 10]. YAP, Survivin, CTGF, LATS2, and Cyr61 are also critical regulators for anti-tubulin chemosensitivity [70, 82-84]. Consistent with previous studies in *Drosophila* [57], we found that MARK2 deletion greatly increased YAP cytoplasmic localization and p-S127 YAP levels (Fig. 3-7 A-C), suggesting that MARK2 is a positive regulator of YAP. We and others showed that some of the YAP targets (*Survivin, Zyxin, LATS2*) were induced during anti-tubulin treatment [71, 83, 84]. Importantly, we showed that Taxol-induced Survivin, LATS2, and Zyxin were largely blocked upon MARK2 deletion (Fig. 3-7 D).

MARK2 interacts with MST1/2 and WW45 and inhibits their inhibitory effects towards YAP activity [53, 57]. The precise mechanism, including the phosphorylation sites on MST1/2/WW45 has not been defined. We found that MARK2 enhanced the mobility upshift of MST2 on a Phos-tag gel, suggesting that MST2 (not MST1) is phosphorylated upon MARK2 activation (Fig. 3-7E, F). CDK1 phosphorylation of MARK2 is not required for promoting MST2 shift/phosphorylation (Fig. 3-7E). Our *in vitro* kinase assay revealed MARK2 indeed phosphorylated MST2 (Fig. 3-7G). Sequence analysis identified a highly conserved site S15 on MST2 (not on MST1) as the MARK2 site. We generated a phospho-

specific antibody against S15 and confirmed that MARK2 phosphorylated MST2 S15 *in vitro* (Fig. 3-7H). Enhanced the expression of MARK2 stimulated S15 phosphorylation in cells in a mitotic phosphorylation-independent manner (Fig. 3-7I). Interestingly, increased phosphorylation at S15 was negatively correlated with reduced MST2 kinase activity (measured by the p-T180 (autophosphorylation) (Fig. 3-7I). In line with this observation, the non-phosphorylatable mutant MST2-S15A possess enhanced kinase activity compared with wild-type MST2 (Fig. 3-7J). Neither MST2 kinase activity (p-T180) or S15 was induced by anti-tubulin agents (Fig. 3-7J) [32]. These observations suggest that MARK2 promotes YAP activation by phosphorylating MST2 at S15 and inactivating it. However, this mechanism is unlikely regulated by anti-tubulin drugs or in mitosis.

3.3.7. MARK2 phosphorylates HDAC4 in response to anti-tubulin treatment and in mitosis

Our study suggests that MARK2 regulates YAP activity in response to anti-tubulin drugs/mitosis in a Hippo kinase/MST-independent manner. In addition to MST/WW45, MARK family proteins also phosphorylate MAP2/4 [44], HDACs [61], CLASP1/2, APC, and DIXDC1 [47]. MARK2 phosphorylates class IIa HDACs (HDAC4/5/7/9) at S246, S467, and S632 (numbering in HDAC4), and phosphorylation promotes HDACs cytoplasmic retention and inhibits its deacetylation/transcription repression activity [61-63]. Interestingly, p-S246 levels were greatly increased during anti-tubulin treatment and these increases were largely blocked upon MARK2 deletion or knockdown in various cell lines (Fig. 3-8A, B). Increased phosphorylation at HDAC4 S246 is also evident in normal mitotic cells (Fig. 3-8C). MARK2 directly phosphorylates HDAC4 at S246 and S632 *in vitro* (Fig. 3-8D). Enhanced expression of MARK2 increased phosphorylation at S246, and the non-phosphorylatable MARK2-3A mutant was less active in promoting HDAC4 phosphorylation (Fig. 3-8E). Knockdown of HDAC4, like MARK2 inhibition, significantly

delayed metaphase to anaphase transition and prolonged mitosis (Fig. 3-8F-H). It is important to re-express wild-type HDAC4, but not the non-phosphorylatable mutant HDAC4-3A (S246A/S467A/S619A), restored the mitotic defects in the knockdown cells (Fig. 3-8G, H). Together these studies identified class IIa HDACs as mitotic substrates for MARK2, and MARK2-meditated phosphorylation plays a vital role in mitotic progression.

3.3.8. HDAC4 promotes YAP activity in a mitotic phosphorylation-dependent manner

Given the connection between MARK2 and YAP/HDAC4, we hypothesize that HDAC4 also regulates YAP activity. Interestingly, exogenous HDAC4 significantly suppressed YAP S127 phosphorylation, and enhanced expression of HDAC4-3A did not affect S127 phosphorylation, suggesting that HDAC4 promotes YAP activity in a mitotic phosphorylation-dependent manner (Fig. 3-8I). In contrast, YAP S397 (mediates YAP protein degradation) levels were not altered (Fig. 3-8I). Consistent with these observations, HDAC4, but not the HDAC4-3A mutant, stimulated YAP/TEAD transcription activity (Fig. 3-8J). Importantly, HDAC inhibitor SAHA greatly inhibited the expression (both mRNA and protein levels) of YAP targets *Survivin*, *LATS2*, and *Zyxin* induced by Taxol treatment in PDAC cells (Fig. 3-8K-N). Knockdown of HDAC4 in S2.013 cells was sufficient to block the expression of LATS2, Survivin, and Zyxin induced by Taxol treatment (Fig. 3-8O). These data identified class IIa HDACs as positive regulators for YAP and suggest that HDAC-YAP controls a unique transcriptional program specific to the response to anti-tubulin treatment in PDAC cells.

We further explored the underlying mechanism through which HDAC4 regulates YAP. Consistent with the findings in Figure 3-8I, J, we found that HDAC4-3A nutant had increased binding affinity with LATS2 when compared with wild-type HDAC4 (Fig. 3-8P).

In contrast, non-phosphorylatable HDAC4 (HDAC4-3A) reduced its association with YAP (Fig. 3-8Q). These observations suggest that HDAC4 promotes YAP activity by modulating the LATS2/YAP complex.

3.3.9. MARK2 regulates Taxol chemosensitivity by phosphorylating HDAC4 in PDAC cells

Alterations of HDAC4 have been implicated in several disease conditions, including cancer [85-87]. HDAC inhibitors have been shown to be promising in clinical and preclinical models in treating cancer [85, 88]. However, the functional significance, especially in Taxol chemosensitivity, of class IIa HDACs (HDAC4/5/7/9) in PDAC is largely unclear. Class IIa HDACs (mRNA) are all overexpressed in PDAC compared with normal pancreatic tissue (Fig. 3-9A). Furthermore, HDAC4 and HDAC7 protein levels were also increased in most PDAC lines compared with the non-cancerous human pancreatic cells (HPNE) (Fig. 3-10A). HDAC5 and HDAC9 protein expression were extremely low in most cell lines. Another class HDACs (HDAC1/2/6) expression was not significantly upregulated in PDAC cell lines (Fig. 3-10A). Furthermore, HDAC4 and HDAC7 expressions are positively correlated with MARK2 and YAP in PDAC patients (Fig. 3-10B, C). Knockdown HDAC4 or HDAC7 in PANC-1 and S2.013 cells did not impair cell proliferation nor caused cell apoptosis (Fig. 3-10D). Interestingly, knockdown of HDAC4 or HDAC7 greatly sensitized these cells to Taxol-induced cytotoxicity as revealed by cleaved PARP (Fig. 3-10E, F). Consistent with these studies, combined Vorinostat (SAHA) or Panobinostat (LBH-589) (pan-HDAC inhibitors) with Taxol treatment greatly induced cell death while single-agent treatment failed to promote significant apoptosis (Fig. 3-10G). Clonogenic assays confirmed that HDAC4 or HDAC7 knockdown significantly impaired cell survival after Taxol treatment compared with control cells (Fig. 3-10H, I). These observations

suggest that HDAC4/7, like MARK2, are critical determinants for Taxol chemosensitivity in PDAC cells.

To examine the role of MARK2-mediated phosphorylation of HDAC4, we reexpressed HDAC4-WT or -3A in HDAC4 knockdown cells (Fig. 3-10J). As expected, the addback of HDAC4-WT completely blocked the cell death induced by Taxol, and reexpression of HDAC4-3A failed to do so (Fig. 3-10K), suggesting that MARK2 phosphorylation of HDAC4 promotes Taxol chemoresistance. Interestingly, knockdown of HDAC4 or HDAC7 also potentiated Gemcitabine cytotoxicity (Figs. 3-10L, M). To further explore functional and genetic interactions between MARK2 and HDAC4, we ectopically expressed HDAC4-WT or -3A in MARK2 knockdown cells (Fig. 3-10O). MARK2 knockdown synergized cell apoptosis with Taxol as expected, and expression of HDAC4-WT, but not HDAC4-3A, largely blocked apoptosis in these cells (Fig. 3-10P), suggesting that MARK2 regulates Taxol chemosensitivity through phosphorylating HDAC4.

3.3.10. HDAC inhibition synergizes Taxol chemotherapy in PDAC *in vivo*

We found that HDAC7, but not HDAC1, HDAC2, HDAC4, and HDAC6, is upregulated in mouse KPC (concomitant expression of K-Ras^{G12D} p53^{R172H})/KC cells compared with normal mouse pancreas (Fig. 3-11A). These mouse PDAC cell lines mimic the genetic compendium of human PDAC and, importantly, form both subcutaneous and orthotopic tumors in mice with the intact immune system [67]. In line with the observations in human PDAC cells (Fig. 3-10), knockdown of mouse HDAC7 was sufficient to significantly sensitize mouse PDAC cells (KC6141) to Taxol or Gemcitabine-induced apoptosis (Fig. 3-11B, C). To further confirm whether knockdown HDAC7 is sufficient to potentiate Taxol and Gemcitabine efficacy *in vivo*, KC6141 (shControl and shHDAC7) were subcutaneously inoculated on immune-competent mice followed by PBS, Taxol, or

Gemcitabine treatment. Knockdown of HDAC7, Taxol, or Gemcitabine treatment alone did not affect tumor growth in KC6141 cells (Figs. 3-11 D, E). However, knockdown of HDAC7 greatly inhibited tumor growth with Taxol or Gemcitabine treatment (Figs. 3-11 D, E). Next, we implanted KPC961 and KC6141 cells in mice, followed by PBS, Taxol, SAHA, or Taxol combined with SAHA treatment. No significant differences were detected for the tumor sizes among PBS, Taxol, and SAHA treatment groups in both cell lines (Figs. 3-11 F-I). Paclitaxel and SAHA combination treatment significantly suppressed tumor growth compared with the rest groups (Figs. 3-11 F-I). We also labeled KC6141 cells with luciferase for orthotopic implantation in animals. Again, SAHA+Taxol treatment substantially inhibited tumor growth (Figs. 3-11 J-L). We observed metastasis in 4 of 6 control mice and no metastasis in all drug-treated mice (Fig. 3-11M). As expected, massive apoptosis was detected in SAHA/Taxol treated tumors (Fig. 3-11N). No overall toxicity was observed in animals (which had normal body weight and foodintake), suggesting that these drugs were well tolerated in these animals. Furthermore, SAHA and paclitaxel treatment synergistically suppressed PDAC organoids growth (Figs. 3-11 O, P). These observations suggest that HDAC inhibition overcomes Taxol chemoresistance in immune-intact animals.

3.3.11. MARK2-HDAC inhibition induces mitotic defects to potentiate Taxol cytotoxicity in PDAC cells

Previous studies showed that in patient tumors, the mitotic index and the actual taxol concentration are much lower than those in cell culture [89, 90]. Low concentrations of Taxol are sufficient to induce cell death due to chromosome missegregation on multipolar spindles [89]. We wanted to explore whether inhibition of the MARK2-HDAC axis is sufficient to cause mitotic abnormality and subsequent cell death under the low concentrations of Taxol treatment. To test this hypothesis, we treated PDAC cells with

knockdown of MARK2 or HDAC4 or HDAC7 with 5 nM Taxol and monitored mitotic abnormality by visualizing microtubule and chromosome. Treatment with 5 nM Taxol or MARK2/HDAC4 knockdown induced modest mitotic defects, including lagging chromosomes at metaphase and chromosome misalignment in PANC-1 cells (Figs. 3-12 A-E). Importantly, a significant higher percentage of cells with mitotic defects (chromosome missegregation and multipolar spindles) were observed in MARK2, HDAC4, or HDAC7 knockdown PANC-1 cells with Taxol treatment (Figs. 3-12 A-F). Consistent with these observations, combined treatment of HDAC inhibitor (SAHA or LBH589) with Taxol also resulted in significant mitotic defects (Figs. 3-12 A-F). Similar findings were observed in S2.013 cells (Figs. 3-9 B-E and 3-12G). In line with these findings, we further confirmed that inhibition of MARK2, HDAC4, or HDAC7 induced cell death even under low concentrations of Taxol treatment (Figs. 3-12 H-J). Together, our data suggest a link between Taxol cytotoxicity and mitotic defects induced by MARK2-HDAC inhibition in PDAC cells.

3.5. Discussion

MARK family proteins are less studied protein kinases, and their biological function, especially in cancer, is somewhat unclear. Emerging evidence showed that they control cell growth through the Hippo-YAP signaling,, although it remains controversial. For example, MARK1/3/4, but not MARK2, have been identified as negative regulators of YAP oncogenic activity by promoting SCRIB association with MST1/2 and LATS1/2 [55]. This observation is consistent with the fact that MARKs are phosphorylated and activated by tumor suppressor LKB1. In line with these studies, MARK1/4 has been shown to phosphorylate DIXDC1 to suppress cell invasion and metastasis [47]. In contrast, several other studies showed that MARK1/4 and MARK3 promote YAP activation by inhibiting the Hippo kinase signaling [53, 56, 57]. Our data support a positive role of MARK2 in the regulation of YAP activity, likely through phosphorylating and inactivating MST2 (Fig. 3-7). Furthermore, MARK2 is overexpressed in human PDAC and negatively correlates with PDAC patients' prognosis, and its expression is positively correlated with YAP (Figs. 3-6A, B; 3-10B), supporting a protumorigenic function of MARK2 in PDAC. Upstream kinases can activate mARKs via phosphorylation of the catalytic kinase domain and numerous studies identified many activation regulators of the MARK family, including MARKK/TAO-1, LKB1, CAMK1, GSK-3β, and αPKC [43]. The current study identifies CDK1 as an upstream kinase that phosphorylates MARK2 specifically in mitosis, adding a new layer of regulation for MARK2. Differing from other kinase-mediated phosphorylation, mitotic phosphorylation does not influence its kinase activity (Fig. 3-3I, J) and yet still plays a critical role (Figs. 3-5, 3-6). Thus, future studies are needed to investigate how CDK1-mediated phosphorylation of MARK2 regulates its role in mitotic progression and chemosensitivity. Interestingly, we found that in addition to MARK2, MARK3 is also up-shifted upon Taxol or Nocodazole treatment (Fig. 3-1A). We are

currently investigating how MARK3 is regulated and whether MARK3 also plays a role in regulating mitosis and anti-tubulin chemosensitivity similar to MARK2.

The poor prognosis of pancreatic cancer patients is mainly due to drug resistance. This study identifies class IIa HDACs as mitotic substrates for MARK2. MARK2 directly phosphorylates class IIa HDACs in response to anti-tubulin chemotherapy, and MARK2-HDAC controls a YAP-dependent transcriptional program induced by Paclitaxel treatment (Fig. 3-8). These observations added class IIa HDACs as new positive regulators of YAP. Given that MARK2-HDAC controls chemosensitivity in PDAC (Figs. 3-6, 3-10, 3-11), these findings provided new options for targeting MARK2-HDAC activity in reversing chemoresistance in PDAC. FDA approves Pan-HDAC inhibitors as anticancer agents and several studies showed that HDAC inhibitors reverse Paclitaxel resistance in non-small cell lung cancer, papillary serous endometrial cancer, and ovarian cancer [91-93]. HDAC inhibitors induced synergistic cytotoxicity with Paclitaxel via regulation of HDAC class I members HDAC1 and HDAC6, stabilization of microtubules, and inhibition of Paclitaxel-induced Survivin accumulation [91-93]. Though we could not exclude the possibility of the involvement of other HDACs in Paclitaxel chemosensitivity in PDAC cells, our current data support the role of class IIa HDAC (i. e. HDAC4/7) in regulating Paclitaxol cytotoxicity downstream MARK2. Therefore, targeting class IIa HDACs seems to be a more feasible way to overcome chemoresistance in PDAC. A common limitation of HDAC inhibitors in the clinic is dose-limiting toxicity, which has necessitated dose reductions or changes in dose scheduling [94]. A strategy to maximize efficacy, reducing toxicity, and resistance by administering lower drug doses are combining anticancer drugs with other chemotherapeutic agents with synergistic or additive antitumor effects [66, 95]. When relatively low doses of pan-HDAC inhibitor were used in our animal models, it was still sufficient together with Paclitaxel or Gemcitabine to suppress PDAC tumor growth without

significant toxicity observed (Fig. 3-11). These results indicate that the combination treatment may help pancreatic cancer patients tolerate the drug (SAHA) by lowering the drug dose. Furthermore, the development of more selective inhibitors targeting a subset of HDACs can reduce toxicity while retaining their antitumor activity. Thus, it will be interesting to develop HDAC4 or HDAC7 selective inhibitors and test them in animals in our case.

Many studies have shown that multidrug resistance expression, alterations in microtubule dynamics, and altered metabolism contribute to anti-tubulin drug resistance [96]. However, attempts in reversing resistance by targeting these mechanisms have not successfully translated to the clinic. Thus, identification of new regulators and/or signaling pathways that a-ntitubulin agents trigger may shed light on resistance mechanisms and lead to the development of novel prognostic or therapeutic approaches related to anti-tubulin chemotherapeutics. In the present study, we aimed to probe kinases, as a quarter of all drug discovery spending is used to target kinases, using a Phos-tag-based approach. In addition to MARK2/3, our screens identified many novel kinases such as FGFR2/4, EPHA family, JAK1, MER, PKR, and TNK1 that are regulated during anti-tubulin treatment (Figs. 3-1A and 3-2).

Interestingly, most of these kinases are heavily involved in cancer cell growth and tumorigenesis. However, their regulation and function in response to anti-tubulin agents have not been defined. Therefore, elucidation of the roles of these molecules may provide additional targets for reversing anti-tubulin chemoresistance. Large-scale phospho-proteomic studies have identified an array of phosphorylation events, including MARK2 and PKR phosphorylation, in response to anti-tubulin agents [34]. However, hits from our studies, such as phosphorylation for FGFR2/4, EPHA family kinases, JAK1, and MER, were not identified in these proteomic studies. Thus, our current study reveals Phos-tag-

based Western blotting analysis as an alternative tool for identifying regulators in response to antitubulin agents and can be applied in other systems.

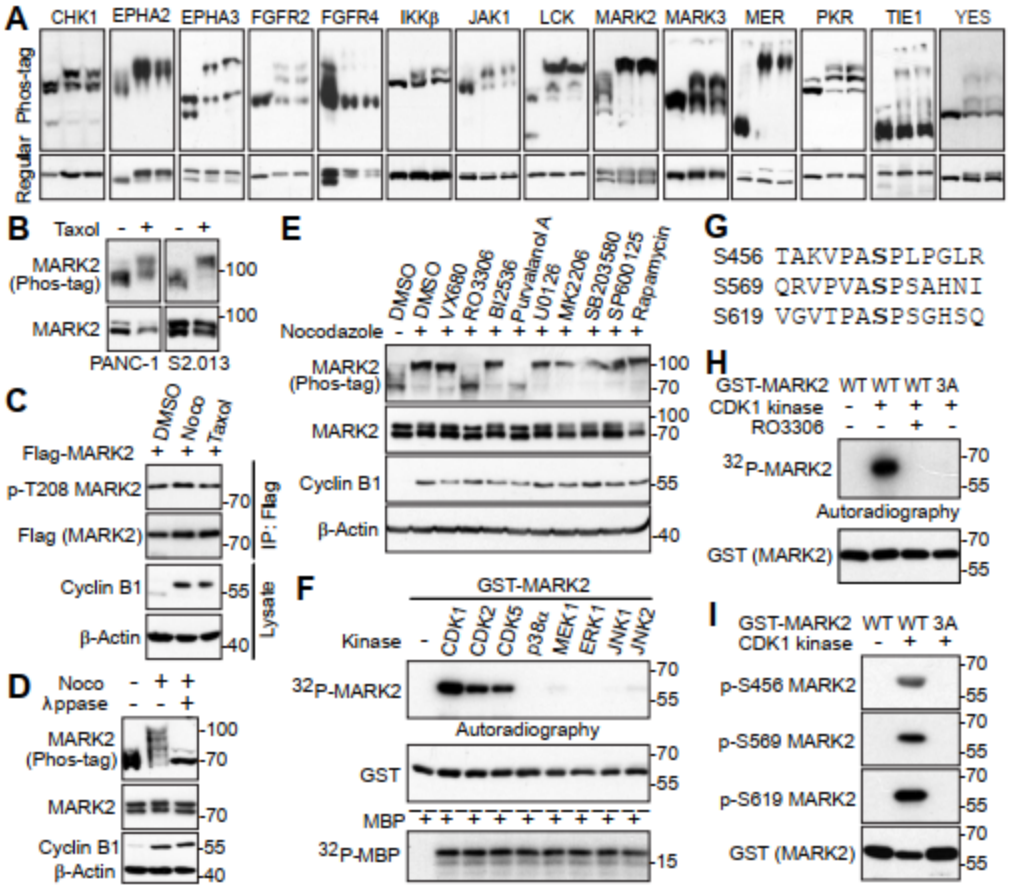
A
CHK1
EPHA2
EPHA3
FGFR2
FGFR4
IKKβ
JAK1
LCK
MARK2
MARK3
MER
PKR
TIE1
YES
Phos-tag
Regular
B
Taxol - + - +
MARK2 (Phos-tag)
MARK2
100
100
PANC-1 S2.013
C
DMSO
Noco
Taxol
Flag-MARK2 + + +
p-T208 MARK2
Flag (MARK2)
Cyclin B1
β-Actin
70
70
55
40
IP: Flag
Lysate
D
Noco - + +
λppase - - +
MARK2 (Phos-tag)
MARK2
Cyclin B1
β-Actin
100
70
70
55
40
E
DMSO
DMSO
VX680
RO3306
BI2536
Purvalanol A
U0126
MK2206
SB203580
SP600125
Rapamycin
Nocodazole - + + + + + + + + + +
MARK2 (Phos-tag)
MARK2
Cyclin B1
β-Actin
100
70
100
70
55
40
F
GST-MARK2
Kinase - CDK1 CDK2 CDK5 p38α MEK1 ERK1 JNK1 JNK2
32P-MARK2
Autoradiography
GST
MBP + + + + + + + + +
32P-MBP
70
55
70
55
15
G
S456 TAKVPASPLPGLR
S569 QRVPVASPSAHNI
S619 VGVTPASPSGHSQ
H
GST-MARK2 WT WT WT 3A
CDK1 kinase - + + +
RO3306 - - + -
32P-MARK2
Autoradiography
GST (MARK2)
70
55
70
55
I
GST-MARK2 WT WT 3A
CDK1 kinase - + +
p-S456 MARK2
p-S569 MARK2
p-S619 MARK2
GST (MARK2)
70
55
70
55
70
55
70
55

Figure 3-1. A Phos-tag-based kinome wide screen identifies MARK2 as a phospho-kinase by CDK1 during anti-tubulin agent-induced mitotic arrest

(A) HeLa cells were treated with DMSO, Nocodazole (Noco, 100 ng/ml for 20 h, or Taxol (100 nM for 20 h). Total cell lysates were probed with the indicated antibodies on Phos-tag or regular SDS-polyacrylamide gels with the indicated antibodies. (B) Human PDAC cells were treated with or without Taxol (100 nM for 24 h), and MARK2 was probed on Phos-tag or regular gels.(C) HEK293T cells were transfected with Flag-MARK2 and treated with DMSO, Taxol (100 nM for 16 h), or Nocodazole (Noco, 100 ng/ml for 16 h). MARK2 was immunoprecipitated by anti-Flag antibody and was subjected to Western blotting with the indicated antibodies.(D) HeLa cells were treated with Nocodazole as indicated and cell lysates were further treated with (+) or without (−) λ-phosphatase (ppase). Total cell lysates were probed with the indicated antibodies.(E) HeLa cells were treated with Nocodazole, with or without various kinase inhibitors as indicated. VX680 (2 μM), RO3306 (5 μM), BI2536 (100 nM), Purvalanol A (10 μM), U0126 (20 μM), MK-2206 (10 μM), SB203580 (10 μM), SP600125 (20 μM), and Rapamycin (100 nM) were used. Inhibitors were added (with MG132 to prevent Cyclin B1 from degradation and cells from exiting from mitosis) 2 h before harvesting the cells.(F) GST-tagged MARK2 (amino acids 388-788) proteins were used for *in vitro* kinase assays with various purified kinases. MBPs (myelin basic protein) (Sigma) were included as positive controls, confirming the kinases are active. (G) Identification of phosphorylation sites in MARK2.(H) GST-tagged MARK2 or MARK2-3A (S456A/S569A/S619A) proteins were used for *in vitro* kinase assays with purified CDK1-Cyclin B1 kinase complex. RO3306 (5 μM) was used to inhibit CDK1 kinase activity. (I) *In vitro* kinase assays with purified CDK1-Cyclin B1 complex and recombinant GST-MARK2 or GST-MARK2-3A and probed with phospho-antibodies.

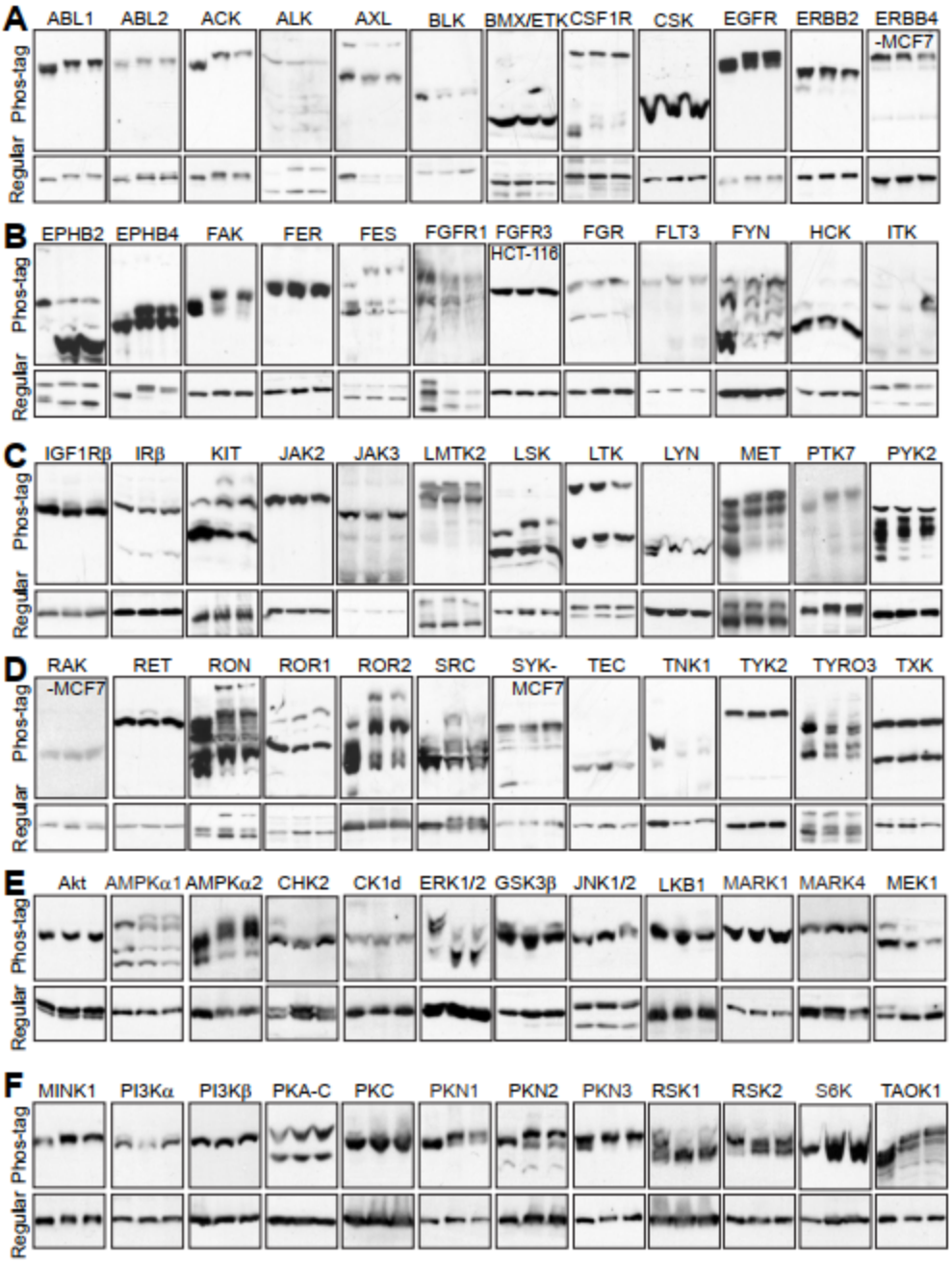
A
ABL1
ABL2
ACK
ALK
AXL
BLK
BMX/ETK
CSF1R
CSK
EGFR
ERBB2
ERBB4
-MCF7
Phos-tag
Regular
B
EPHB2
EPHB4
FAK
FER
FES
FGFR1
FGFR3
HCT-116
FGR
FLT3
FYN
HCK
ITK
Phos-tag
Regular
C
IGF1Rβ
IRβ
KIT
JAK2
JAK3
LMTK2
LSK
LTK
LYN
MET
PTK7
PYK2
Phos-tag
Regular
D
RAK
-MCF7
RET
RON
ROR1
ROR2
SRC
SYK-
MCF7
TEC
TNK1
TYK2
TYRO3
TXK
Phos-tag
Regular
E
Akt
AMPKα1
AMPKα2
CHK2
CK1d
ERK1/2
GSK3β
JNK1/2
LKB1
MARK1
MARK4
MEK1
Phos-tag
Regular
F
MINK1
PI3Kα
PI3Kβ
PKA-C
PKC
PKN1
PKN2
PKN3
RSK1
RSK2
S6K
TAOK1
Phos-tag
Regular

Figure 3-2. A Phos-tag-based sub-kinome-wide screen for kinases in response to anti-tubulin agents

(A-F) HeLa (unless otherwise indicated) cells were treated with DMSO, Taxol (100 nM for 20 h) or Nocodazole (100 ng/mL for 20 h) (lanes 1, 2, 3, respectively in each blot). Total cell lysates were electrophoresed on regular or Phos-tag SDS-polyacrylamide gels and systematically probed with individual antibodies. Total 115 kinases were screened, and 18 of them were not detected or with high/non-specific background (data not shown).

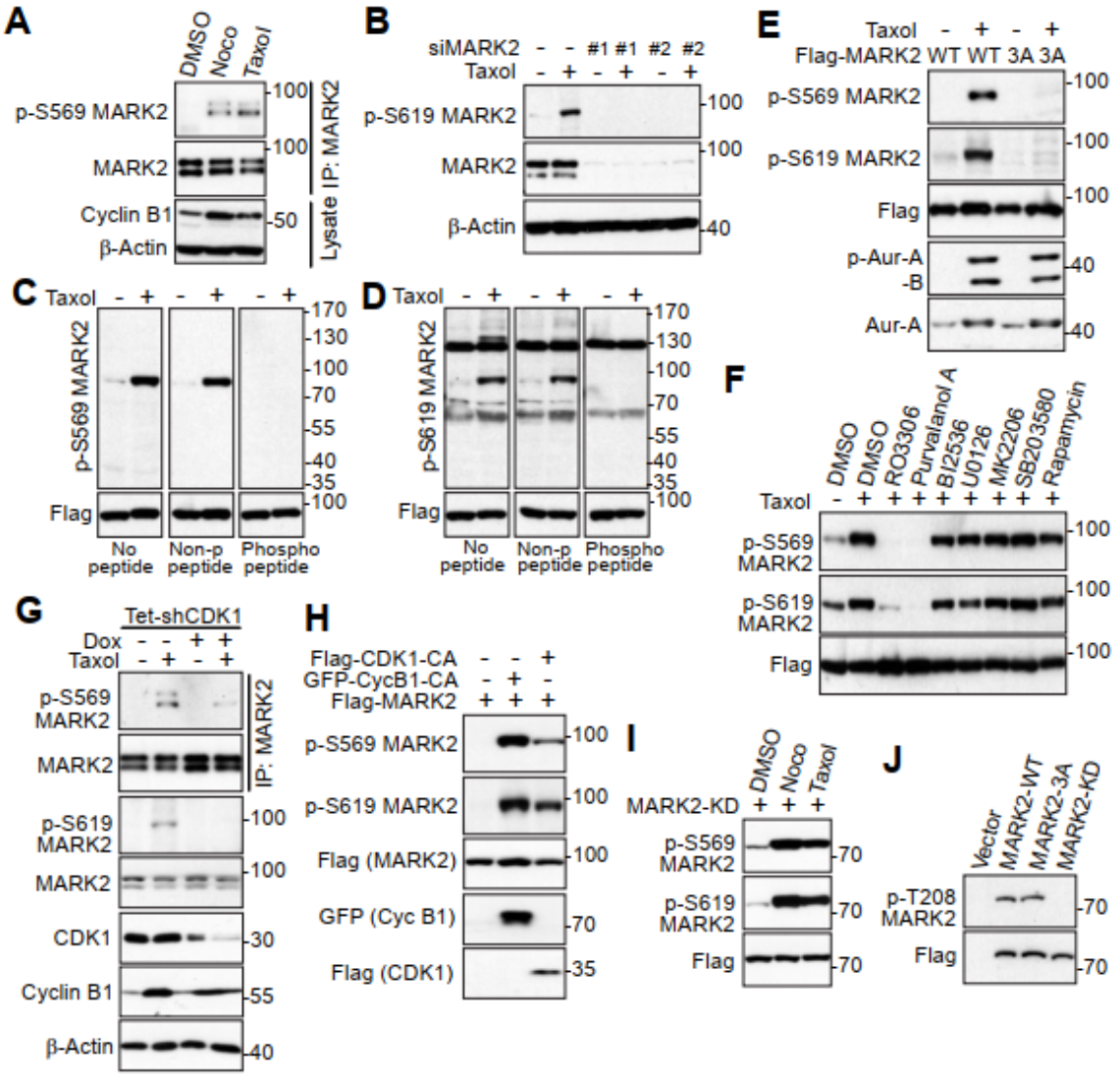
A
DMSO
Noco
Taxol
p-S569 MARK2
MARK2
Cyclin B1
β-Actin
Lysate IP: MARK2
B
siMARK2 - - #1 #1 #2 #2
Taxol - + - + - +
p-S619 MARK2
MARK2
β-Actin
C
Taxol - + - + - +
p-S569 MARK2
Flag
No peptide
Non-p peptide
Phospho peptide
D
Taxol - + - + - +
p-S619 MARK2
Flag
No peptide
Non-p peptide
Phospho peptide
E
Taxol - + - +
Flag-MARK2 WT WT 3A 3A
p-S569 MARK2
p-S619 MARK2
Flag
p-Aur-A -B
Aur-A
F
DMSO
DMSO
RO3306
Purvalanol A
BI2536
U0126
MK2206
SB203580
Rapamycin
Taxol - + + + + + + + +
p-S569 MARK2
p-S619 MARK2
Flag
G
Tet-shCDK1
Dox - - + +
Taxol - + - +
p-S569 MARK2
MARK2
IP: MARK2
p-S619 MARK2
MARK2
CDK1
Cyclin B1
β-Actin
H
Flag-CDK1-CA - - +
GFP-CycB1-CA - + -
Flag-MARK2 + + +
p-S569 MARK2
p-S619 MARK2
Flag (MARK2)
GFP (Cyc B1)
Flag (CDK1)
I
DMSO
Noco
Taxol
MARK2-KD + + +
p-S569 MARK2
p-S619 MARK2
Flag
J
Vector
MARK2-WT
MARK2-3A
MARK2-KD
p-T208 MARK2
Flag

Figure 3-3. MARK2 is phosphorylated by CDK1 during antitubulin agent-induced mitotic arrest

(A) Endogenous MARK2 was immunoprecipitated from HeLa cells treated with Nocodazole or Taxol and probed with the MARK2 p-S569 antibody.(B) HeLa cells were transfected with 40 nM scramble (control) or siRNA against MARK2 for 48 h and were further treated with Taxol as indicated. Total lysates were probed with the MARK2 p-S619 antibody.(C, D) HEK293T cells were transfected with Flag-MARK2. At 32 h post-transfection, the cells were treated with Taxol. Total cell lysates were subjected to Western blotting with the indicated antibodies. Non-p peptide: Western blotting in the presence of control (not phosphorylated) peptide; phospho-peptide: Western blotting in the presence of phosphorylated peptide (used for antibody generation).(E) HEK293T cells were transfected with Flag-MARK2 or Flag-MARK2-3A (S456A/S569A/S619A) mutant. At 32 h post-transfection, the cells were treated with Taxol. Increased phospho-Aurora (p-Aur) marks cells in mitosis.(F) HEK293T cells were transfected and treated with Taxol together with or without various kinase inhibitors as indicated. (G) CDK1 knockdown inhibited MARK2 phosphorylation. TetOn-inducible shRNA targeting CDK1 was expressed in HeLa cells. The cells were treated with or without doxycycline (Dox) for 2 days and were further treated with Taxol for an additional 20 h. Immunoprecipitated MARK2 and total cell lysates were subjected to Western blotting with the indicated antibodies. (H) HEK293T cells were transfected as indicated. At 48 h post-transfection, total cell lysates were subjected to Western blotting with the indicated antibodies. Flag-CDK1-CA indicates the constitutively active form of CDK1 (T14 and Y15 sites were mutated to non-phosphorylatable Alanine and Phenylalanine). GFP-CycB1-CA: constitutive active of Cyclin B1 (R42A non-degradable mutant).(I) Kinase activity is not required for MARK2 phosphorylation. HEK293T cells were transfected with Flag-MARK2 kinase-dead mutant (KD: kinase-dead, T208A/S212A). At 32 h post-transfection, the cells were treated with Nocodazole or Taxol.

(J) Mitotic phosphorylation does not affect MARK2 kinase activity. HEK293T cells were transfected with Flag-MARK2, -MARK2-3A (S456A/S569A/S619A) or -MARK2-KD. Total cell lysates were probed with the indicated antibodies.

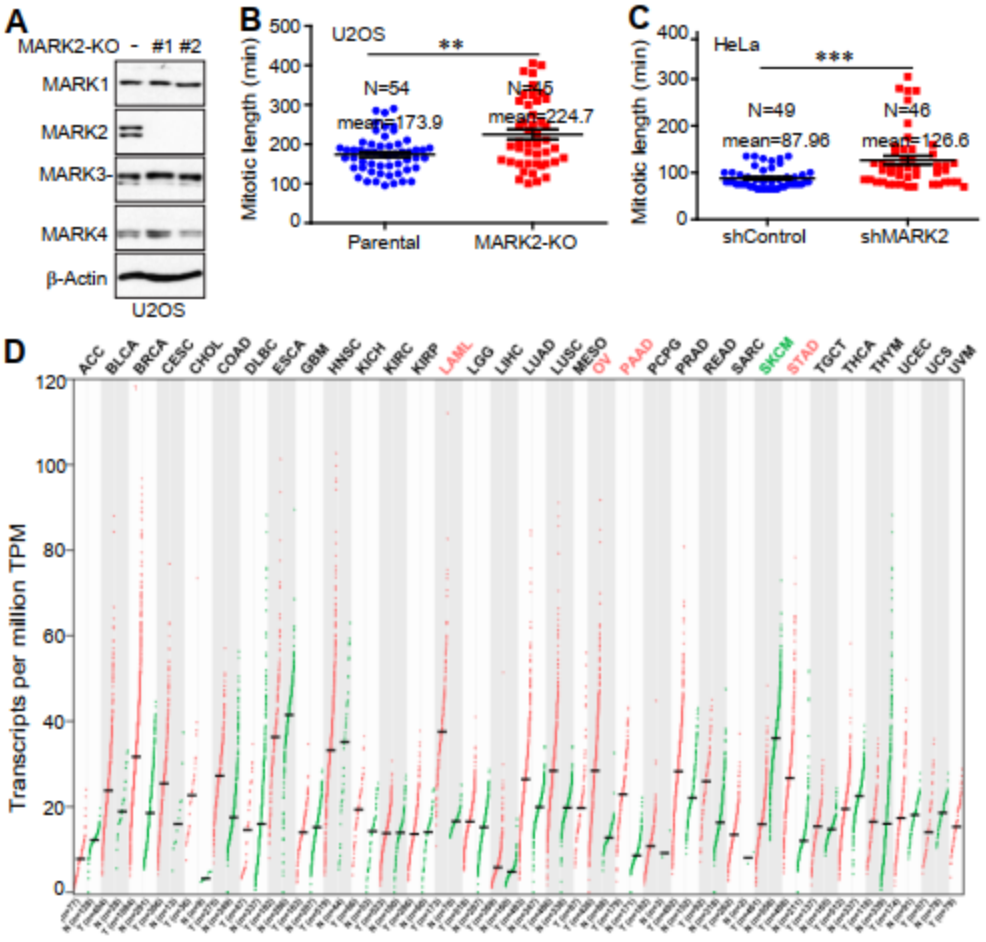
A
MARK2-KO - #1 #2
MARK1
MARK2
MARK3
MARK4
β-Actin
U2OS
B
U2OS
**
N=54
mean=173.9
N=46
mean=224.7
Mitotic length (min)
Parental
MARK2-KO
C
HeLa
***
N=49
mean=87.96
N=46
mean=126.6
Mitotic length (min)
shControl
shMARK2
D
Transcripts per million TPM
ACC BLCA BRCA CESC CHOL COAD DLBC ESCA GBM HNSC KICH KIRC KIRP LAML LGG LIHC LUAD LUSC MESO OV PAAD PCPG PRAD READ SARC SKCM STAD TGCT THCA THYM UCEC UCS UVM

Figure 3-4. MARK2 regulates mitotic length and is highly correlated with PDAC

(A) Establishment of U2OS MARK2-knockout cells by utilizing the CRISPR system. Total cell lysates were probed with the indicated antibodies on regular SDS-polyacrylamide gels with the indicated antibodies. (B, C) Inhibition of MARK2 prolongs mitotic length in U2OS (B) and HeLa cells (C). . ***: $p<0.001$, **: $p<0.01$ (Student's t-test). (D) MARK2 expression (mRNA) levels normal and tumor tissue. Data were generated at gepia2.cancer-pku.cn using the TCGA database.

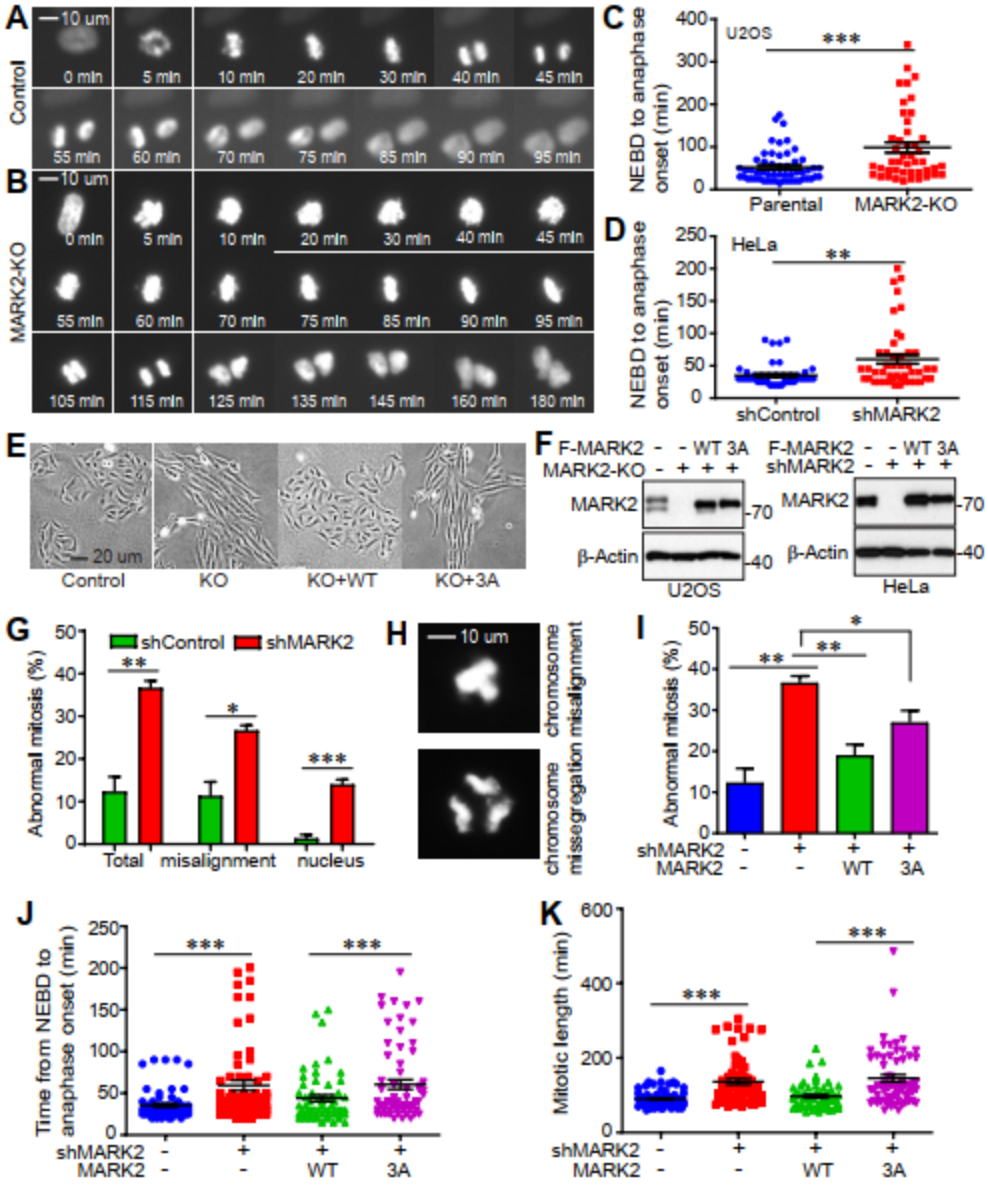
A
Control
10 um
0 min
5 min
10 min
20 min
30 min
40 min
45 min
55 min
60 min
70 min
75 min
85 min
90 min
95 min
B
MARK2-KO
105 min
115 min
125 min
135 min
145 min
160 min
180 min
C
U2OS
***
NEBD to anaphase onset (min)
Parental
MARK2-KO
D
HeLa
**
shControl
shMARK2
E
20 um
Control
KO
KO+WT
KO+3A
F
F-MARK2
MARK2-KO
WT
3A
shMARK2
MARK2
β-Actin
-70
-40
U2OS
HeLa
G
shControl
shMARK2
Abnormal mitosis (%)
Total
misalignment
nucleus
H
chromosome misalignment
chromosome missegregation
I
shMARK2
MARK2
J
Time from NEBD to anaphase onset (min)
K
Mitotic length (min)

Figure 3-5. Phosphorylation of MARK2 is essential for precise mitosis

(A, B) Inhibition of MARK2 delays mitotic progression. Live-cell images of U2OS-RFP-H2B or U2OS-RFP-H2B-MARK2-KO (knockout) cells entering and exiting mitosis.(C, D) Quantification of mitotic length in HeLa and U2OS cells. Data were based on 54 (U2OS) or 49 (HeLa) mitotic cells for control and 45 (U2OS) or 46 (HeLa) for MARK2 knockout or knockdown cells. **: $p<0.01$, ***: $p<0.001$ (Student's t-test). (E) Morphology change in MARK2-KO U2OS cells. Representative light microscopy images were shown.(F) Establishment of U2OS MARK2-KO or HeLa MARK2-KD cells expressing Flag-MARK2-WT or Flag-MARK2-3A (S456A/S569A/S619A).(G, H) Inhibition of MARK2 causes mitotic defects. Quantification of abnormal mitosis from live-cell imaging of HeLa cells expressing RFP-H2B. Data were expressed as mean ± SEM from three independent experiments (**G**). *: $p=0.02$, **: $p<0.003$, ***: $p=0.001$ (Student's t-test). Representative images of chromosome misalignment and chromosome missegregation in MARK2-KD cells (**H**). (I) Phosphorylation of MARK2 is required for normal mitosis. Quantification of mitotic defects from the indicated cell lines expressing RFP-H2B. Data were expressed as mean ± SEM from three independent experiments. Total cell counted: 37, 110, 57, 71 for control, KD, KD+WT, KD+3A, respectively. *: $p=0.03$, **: $p=0.003$ (knockdown vs control); $p=0.005$ (addback of WT vs knockdown) (Student's t-test).(J, K) Phosphorylation of MARK2 is essential for mitotic progression. Quantification of mitotic length in RFP-H2B-expressing HeLa cells. NEBD: nuclear envelope breakdown. ***: $p=0.0003$ or 0.0001 (J); $p=0.0001$ (K) (Student's t-test). Total cell counted: 63, 61, 57, 63 for control, KD, KD+WT, KD+3A, respectively.

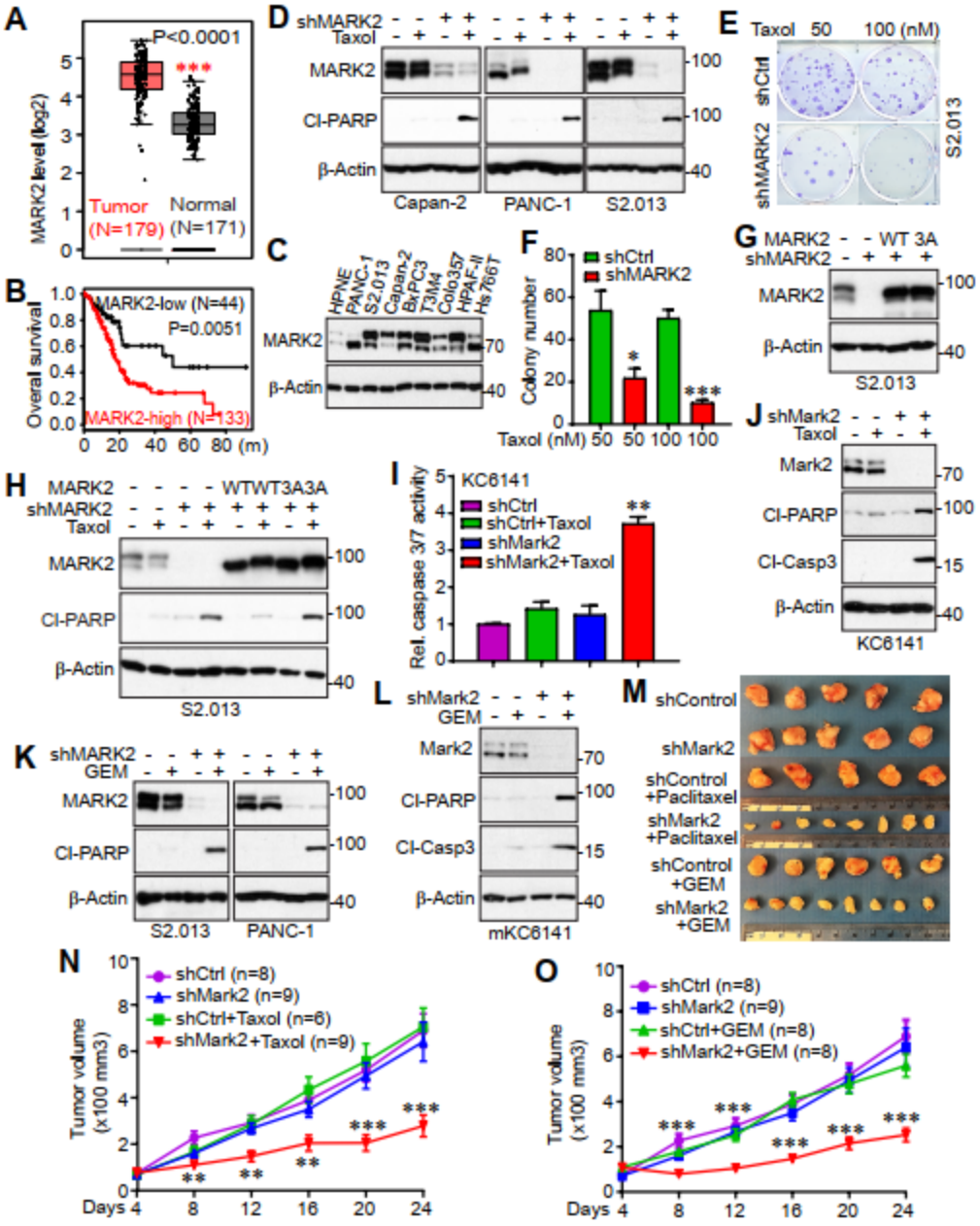
A
P<0.0001
***
MARK2 level (log2)
Tumor (N=179)
Normal (N=171)
B
MARK2-low (N=44)
P=0.0051
MARK2-high (N=133)
Overal survival
(m)
C
HPNE
PANC.1
S2.013
Capan-2
BxPC3
T3M4
Colo357
HPAF-II
Hs766T
MARK2
β-Actin
D
shMARK2
Taxol
MARK2
Cl-PARP
β-Actin
Capan-2
PANC-1
S2.013
E
Taxol 50 100 (nM)
shCtrl
shMARK2
S2.013
F
shCtrl
shMARK2
Colony number
Taxol (nM) 50 50 100 100
G
MARK2 - - WT 3A
shMARK2 - + + +
MARK2
β-Actin
S2.013
H
MARK2 - - - - WTWT3A3A
shMARK2 - - + + + + + +
Taxol - + - + - + - +
MARK2
Cl-PARP
β-Actin
S2.013
I
KC6141
shCtrl
shCtrl+Taxol
shMark2
shMark2+Taxol
Rel. caspase 3/7 activity
J
shMark2 - - + +
Taxol - + - +
Mark2
Cl-PARP
Cl-Casp3
β-Actin
KC6141
K
shMARK2 - - + + - - + +
GEM - + - + - + - +
MARK2
Cl-PARP
β-Actin
S2.013
PANC-1
L
shMark2 - - + +
GEM - + - +
Mark2
Cl-PARP
Cl-Casp3
β-Actin
mKC6141
M
shControl
shMark2
shControl +Paclitaxel
shMark2 +Paclitaxel
shControl +GEM
shMark2 +GEM
N
shCtrl (n=8)
shMark2 (n=9)
shCtrl+Taxol (n=6)
shMark2+Taxol (n=9)
Tumor volume (x100 mm3)
Days
O
shCtrl (n=8)
shMark2 (n=9)
shCtrl+GEM (n=8)
shMark2+GEM (n=8)
Tumor volume (x100 mm3)
Days

Figure 3-6. MARK2 inhibition promotes chemosensitivity in human and mouse PDAC cells

(A, B) Clinical relevance of MARK2 in PDAC. MARK2 expression levels (mRNA) are upregulated in PDAC patients compared with normal tissue (A). MARK2 expression is positively correlated with the overall survival rate in pancreatic cancer patients (p=0.0051) (B). Data were generated by an online software using TCGA datasets (gepia2.cancer-pku.cn).

(C) MARK2 protein expression in HPNE (non-cancerous) and human pancreatic cancer cell lines. (D) Knockdown of MARK2 increased Taxol-induced apoptosis. Cells were treated with DMSO or Taxol (1 μM for 24 h). Total cell lysates were probed with the indicated antibodies. Cl-PARP: Cleaved PARP. (E, F) MARK2 promoted cell survival under Taxol treatment in clonogenic assays. Cells were treated with Taxol for 24 h as indicated, and colonies were quantified after 14 days. Data were from three independent experiments. *: p=0.034, ***: p=0.006 (Student's t-test). (G, H) Phosphorylation is required for MARK2-driven resistance to Taxol in PDAC cells. Establishment of MARK2-KO cells expressing Flag-MARK2 or Flag-MARK2-3A (S456A/S569A/S619A) (**E**). Cells from (E) were treated with DMSO or Taxol (1 μM for 24 h). (I, J) Knockdown of MARK2 increased Taxol-induced apoptosis in mouse PDAC cells. Caspase 3/7 assay from mouse KC6141 cells treated with Taxol (10 nM for 16 h) (n=3) (I). **: p=0.007 (Student's t-test). (K, L) MARK2 inhibition enhanced Gemcitabine cytotoxicity in human (K) and mouse (L) PDAC cells. Control and MAKR2-knockdown cell lines were treated with DMSO or Gemcitabine (500 nM for 48 h for S2.013, 10 μM for 72 h for PANC-1, and 50 nM for 16 h for KC6141). Total cell lysates were probed with the indicated antibodies. Cl-Casp3: Cleaved caspase 3.(M-O) MARK2 inhibition sensitized PDAC cells to chemotherapy. KC6141-shControl and –shMark2 cells were subcutaneously inoculated into C57BL/6 mice (both left and right

sides). Drug treatment started at day 4 post-injection. Paclitaxel (12 mg/kg) and Gemcitabine (50 mg/kg) were used at every other day via intraperitoneal injection. The representative tumors in each group were excised and photographed at the endpoint (M). The shCtrl and shMark2 groups are identical in panels (N) and (O). The P values are 0.002 (day 8), 0.001 (day 12), 0.001 (day 16), 0.0001 (day 20), 0.0001 (day 24) (N). ***: p=0.0001 (O).

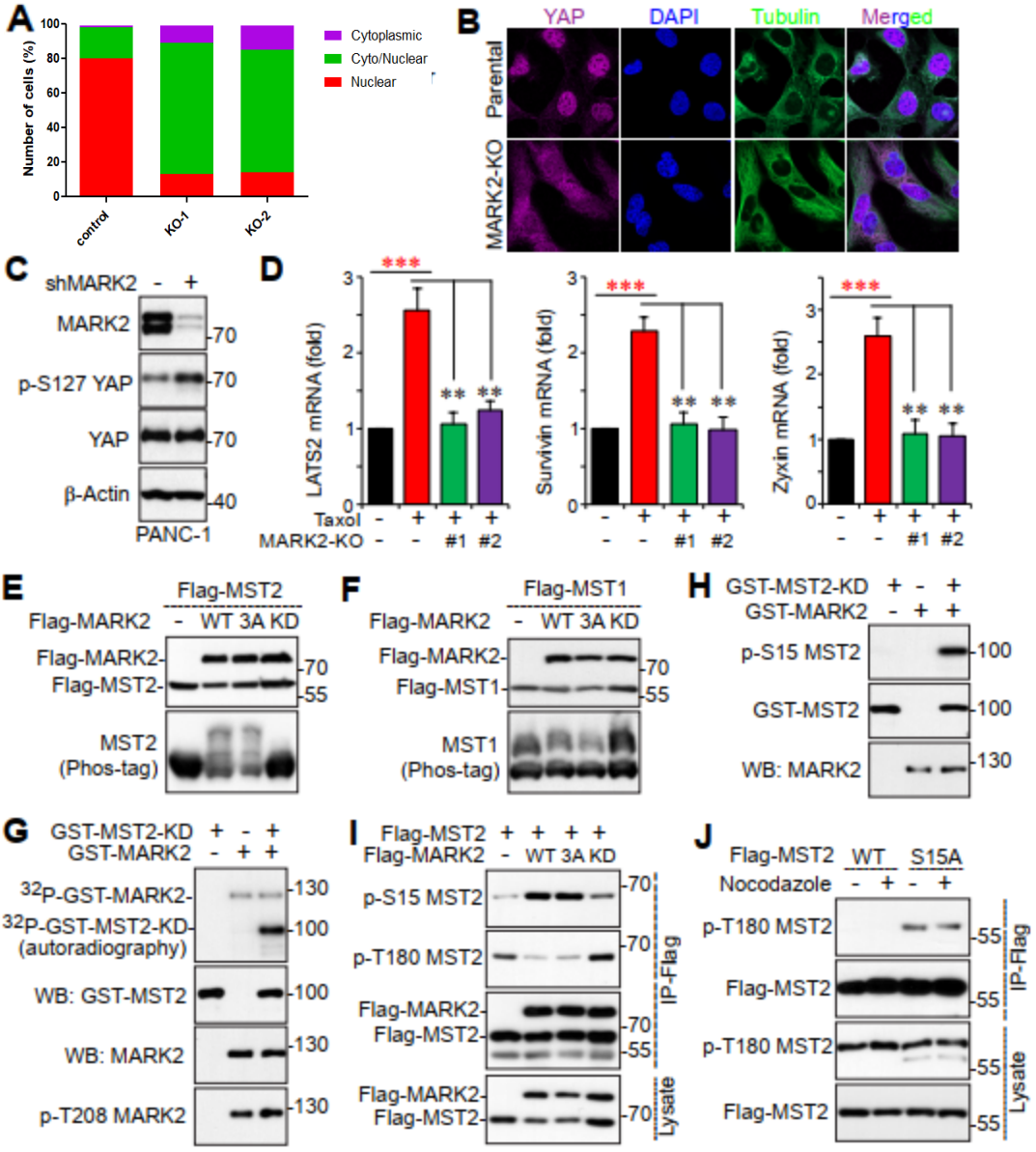
A
Number of cells (%)
Cytoplasmic
Cyto/Nuclear
Nuclear
control
KO-1
KO-2
B
YAP
DAPI
Tubulin
Merged
Parental
MARK2-KO
C
shMARK2
MARK2
p-S127 YAP
YAP
β-Actin
PANC-1
D
LATS2 mRNA (fold)
Survivin mRNA (fold)
Zyxin mRNA (fold)
Taxol
MARK2-KO
E
Flag-MST2
Flag-MARK2
WT 3A KD
Flag-MARK2
Flag-MST2
MST2
(Phos-tag)
F
Flag-MST1
Flag-MARK2
WT 3A KD
Flag-MARK2
Flag-MST1
MST1
(Phos-tag)
H
GST-MST2-KD
GST-MARK2
p-S15 MST2
GST-MST2
WB: MARK2
G
GST-MST2-KD
GST-MARK2
32P-GST-MARK2
32P-GST-MST2-KD
(autoradiography)
WB: GST-MST2
WB: MARK2
p-T208 MARK2
I
Flag-MST2
Flag-MARK2
WT 3A KD
p-S15 MST2
p-T180 MST2
Flag-MARK2
Flag-MST2
IP-Flag
Flag-MARK2
Flag-MST2
Lysate
J
Flag-MST2
WT
S15A
Nocodazole
p-T180 MST2
Flag-MST2
IP-Flag
p-T180 MST2
Flag-MST2
Lysate

Figure 3-7. MARK2 promotes YAP activation and phosphorylates MST2

(A, B) MARK2 deletion causes YAP cytoplasmic localization (inactivation) in U2OS cells. ***: $p<0.001$ (Chi-Square tests). (C) MARK2 knockdown increases YAP S127 phosphorylation PANC-1 cells. (D) MARK2 deletion blocks YAP targets induced by Taxol treatment in U2OS cells. Quantitative RT-PCR for LATS2, Survivin, and Zyxin in cells treated with Taxol (100 nM for 24 h). ***: $p<0.001$, **: $p<0.01$ (Student's t-test). (E, F) MARK2 promotes MST2 phosphorylation. HEK293T cells were transfected with various DNA plasmids as indicated. Total cell lysates were probed with the indicated antibodies on Phos-tag or regular SDS-polyacrylamide gels with the indicated antibodies. (G, H) MARK2 phosphorylates MST2 *in vitro*. *In vitro* kinase assays with purified MARK2 kinase using GST-tagged MST2-KD proteins as substrates. Autophosphorylation of MARK2 was also indicated by the p-T208 antibody. (I, J) MARK2 phosphorylates and inactivates MST2. HEK293T cells were transfected as indicated, and immunoprecipitated samples were probed with p-S15 MST2 and p-T180 MST2 (measuring its kinase activity) antibodies.

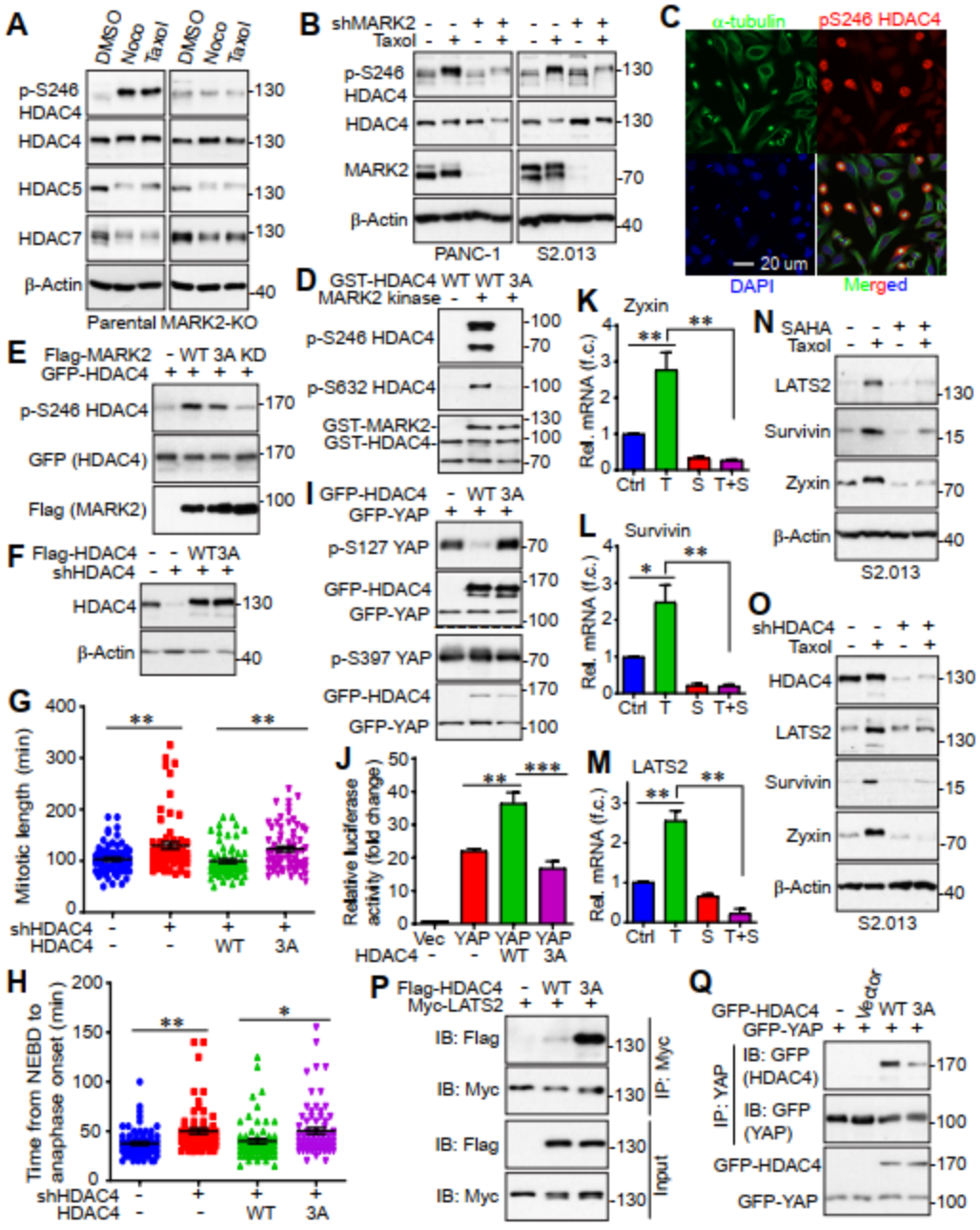
A
DMSO
Noco
Taxol
p-S246 HDAC4
HDAC4
HDAC5
HDAC7
β-Actin
Parental MARK2-KO
B
shMARK2
Taxol
p-S246 HDAC4
HDAC4
MARK2
β-Actin
PANC-1
S2.013
C
α-tubulin
pS246 HDAC4
20 um
DAPI
Merged
D
GST-HDAC4 WT WT 3A
MARK2 kinase
p-S246 HDAC4
p-S632 HDAC4
GST-MARK2-
GST-HDAC4-
E
Flag-MARK2 - WT 3A KD
GFP-HDAC4
p-S246 HDAC4
GFP (HDAC4)
Flag (MARK2)
F
Flag-HDAC4 - - WT3A
shHDAC4
HDAC4
β-Actin
G
Mitotic length (min)
shHDAC4
HDAC4
WT
3A
H
Time from NEBD to anaphase onset (min)
I
GFP-HDAC4 - WT 3A
GFP-YAP
p-S127 YAP
p-S397 YAP
J
Relative luciferase activity (fold change)
Vec
YAP WT
YAP 3A
K
Zyxin
Rel. mRNA (f.c.)
Ctrl
T
S
T+S
L
Survivin
M
LATS2
N
SAHA
Taxol
LATS2
Survivin
Zyxin
β-Actin
S2.013
O
shHDAC4
Taxol
HDAC4
LATS2
Survivin
Zyxin
β-Actin
S2.013
P
Flag-HDAC4 - WT 3A
Myc-LATS2
IB: Flag
IB: Myc
IP: Myc
Input
Q
GFP-HDAC4 - Vector WT 3A
GFP-YAP
IP: YAP
IB: GFP (HDAC4)
IB: GFP (YAP)
GFP-HDAC4
GFP-YAP

Figure 3-8. MARK2 promotes YAP activity by phosphorylating class IIa HDACs

(A, B) Class IIa HDACs are phosphorylated during mitosis in a MARK2-dependent manner. HeLa cells (shCtrl and shMARK2) were treated with DMSO, Nocodazole (Noco), or Taxol, and total cell lysates were probed with the indicated antibodies (A). Phosphorylation of HDAC4 S246 is blocked upon MARK2 knockdown in human PDAC cells (B). (C) Phosphorylation of HDAC4 S246 occurs during unperturbed mitosis. HeLa cells were synchronized by a double thymidine (DT) block and release method. Cells were stained with antibodies against p-HDAC4 S246 (red) together with α-tubulin (microtubule) and DAPI (DNA). A 20× objective lens was used to view various phases of the cells in a field. (D) MARK2 directly phosphorylates HDAC4 at S246 and S632. GST-tagged HDAC4 or HDAC4-3A (S246A/S467A/S632A) (amino acids 200-680) proteins were used for *in vitro* kinase assays with purified GST-MARK2 kinase (SignalChem). (E) HEK293T cells were transfected as indicated. At 48 h post-transfection, total cell lysates were subjected to Western blotting with the indicated antibodies. 3A: S456A/S569A/S619A. KD: kinase-dead (T208A/S212A). (F-H) Phosphorylation of HDAC4 is essential for mitotic progression. Quantification of mitotic length in RFP-H2B-expressing HeLa cells. NEBD: nuclear envelope breakdown. **: p=0.002 or 0.005 (G); **: p=0.006 (H); *: p=0.03 (H) (Student's t-test). Total cell counted: 68, 64, 64, 70 for control, KD, KD+WT, KD+3A, respectively. (I, J) HDAC4 promotes YAP activation in a phosphorylation-dependent manner. (I) HEK293T cells were transfected as indicated. At 48 h post-transfection, total cell lysates were subjected to Western blotting with the indicated antibodies. 3A: S246A/S467A/S632A. (J) Luciferase reporter assays in HEK293T cells (n=3). **: p=0.004; ***: p=0.0009 (Student's t-test). (K-O) HDAC inhibition blocks YAP target expression induced by Taxol. HeLa cells were treated as indicated. T: Taxol (100 nM for 16 h); S: SAHA (HDAC inhibitor, 500 nM for 48h). qRT-PCRs were performed to measure Zyxin, Survivin, and LATS2 mRNA levels (K-M). Data were expressed as the mean ± SEM of

three independent experiments. **: p=0.009 and p=0.006 (K); *: p=0.011 and **: p=0.009 (**L**); **: p=0.003 and p=0.004 (M); (Student's t-test). Knockdown of HDAC4 or inhibition of HDACs inhibits Zyxin, Survivin, and LATS2 protein expression in PDAC cells (N, O). (P, Q) HEK293T cells were transfected as indicated. LATS2 or YAP proteins were immunoprecipitated, and the samples were probed with the indicated antibodies.

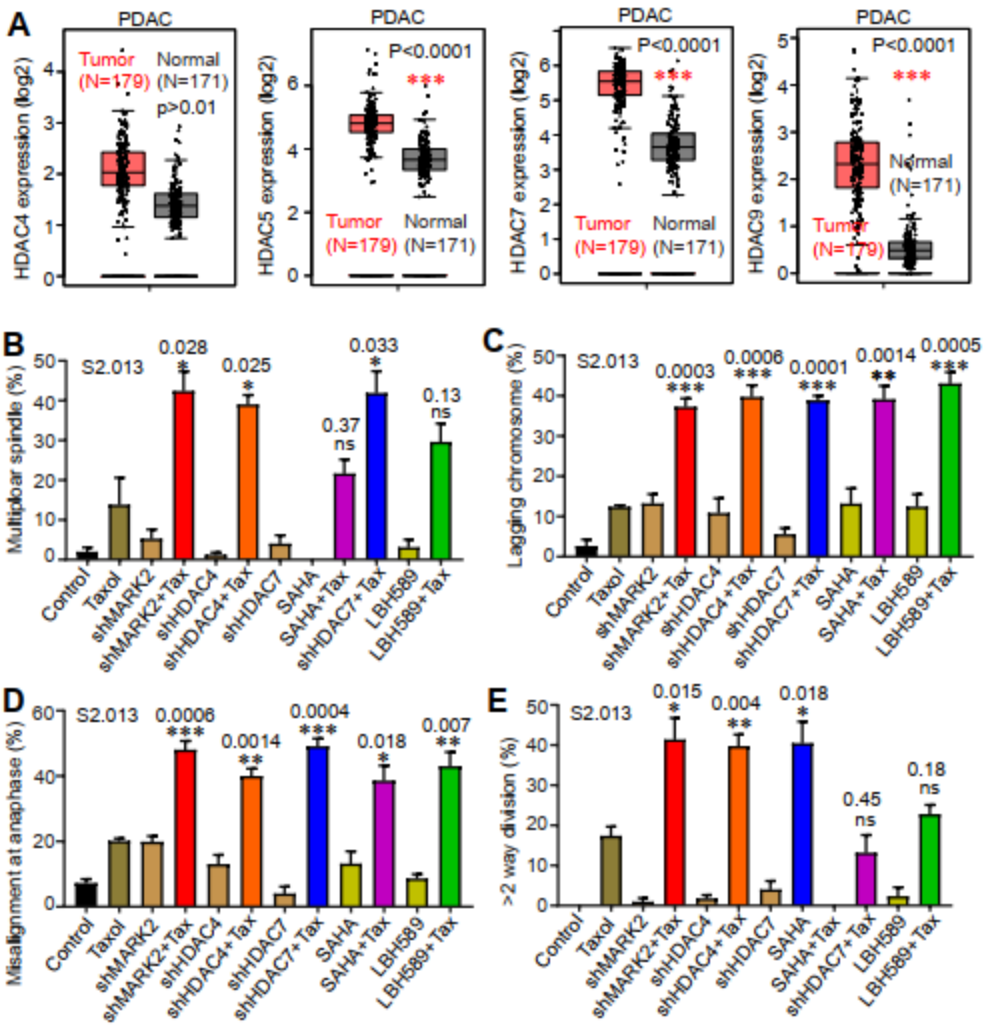
A
PDAC
HDAC4 expression (log2)
Tumor (N=179)
Normal (N=171)
p>0.01
HDAC5 expression (log2)
P<0.0001
***
HDAC7 expression (log2)
HDAC9 expression (log2)
B
Multiploar spindle (%)
S2.013
0.028
0.025
0.37 ns
0.033
0.13 ns
C
Lagging chromosome (%)
0.0003
0.0006
0.0001
0.0014
0.0005
D
Misalignment at anaphase (%)
0.0006
0.0014
0.0004
0.018
0.007
E
>2 way division (%)
0.015
0.004
0.018
0.45 ns
0.18 ns
Control
Taxol
shMARK2
shMARK2+Tax
shHDAC4
shHDAC4+Tax
shHDAC7
shHDAC7+Tax
SAHA
SAHA+Tax
LBH589
LBH589+Tax

Figure 3-9. MARK2-HDAC inhibition synergizes with Taxol treatment to induce mitotic defects in S2.013 cells

(A) Clinical relevance of class IIa HDACs in PDAC. HDAC4/5/7/9 expression levels (mRNA) are upregulated in PDAC patients compared with normal tissue. Data were generated by an online software using TCGA datasets (gepia2.cancer-pku.cn). (B-E) Mitotic defects were quantified in S2.013 cells under various treatments. Low concentrations of Taxol (5 nM) were used in all experiments. Under this condition, cells proliferate without arrest. SAHA and LBH589 were used at 5 μM and 0.2 μM, respectively. Experiments were done at 24 h post-treatment. N=3 from 40-60 mitotic cells of each condition. P values are shown for comparing with Taxol-treated cells (Student's t-test).

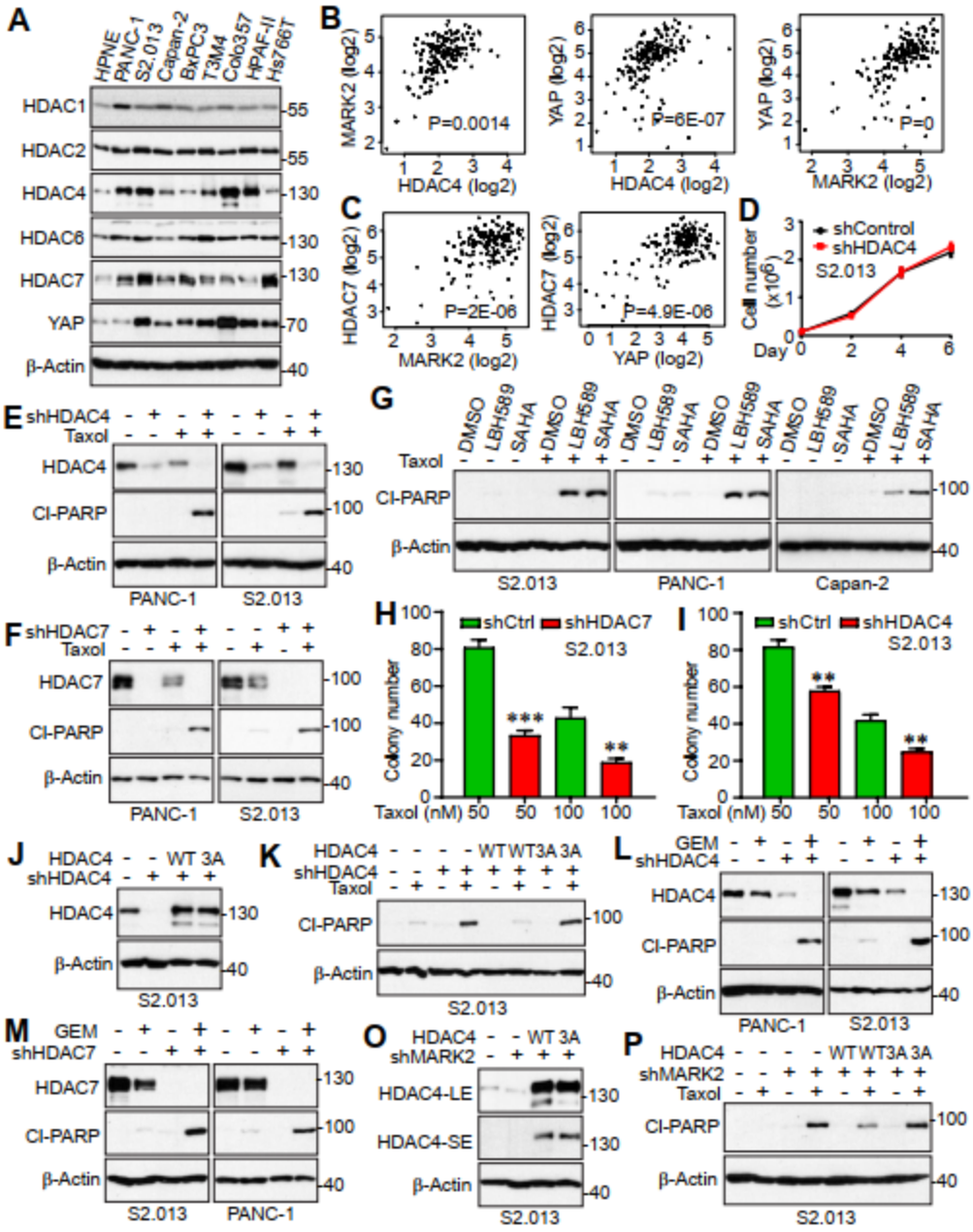
A
HPNE
PANC-1
S2.013
Capan-2
BxPC3
T3M4
Colo357
HPAF-II
Hs766T
HDAC1
HDAC2
HDAC4
HDAC6
HDAC7
YAP
β-Actin
B
MARK2 (log2)
HDAC4 (log2)
P=0.0014
YAP (log2)
P=6E-07
P=0
C
HDAC7 (log2)
P=2E-06
P=4.9E-06
D
shControl
shHDAC4
S2.013
Cell number (x10^6)
Day
E
shHDAC4
Taxol
HDAC4
Cl-PARP
β-Actin
PANC-1
S2.013
F
shHDAC7
HDAC7
G
DMSO
LBH589
SAHA
Capan-2
H
shCtrl
shHDAC7
Colony number
Taxol (nM)
I
shHDAC4
J
WT
3A
K
L
GEM
M
O
shMARK2
HDAC4-LE
HDAC4-SE
P

Figure 3-10. HDAC4/7 control chemosensitivity in human and mouse PDAC cells

(A) Protein expression of HDACs and YAP HPNE (immortalized human pancreatic cells) and human pancreatic cancer cell lines. HDAC1/2, HDAC4/7, HDAC6 are class I, IIa, IIb HDACs, respectively. Class IIa HDAC5 and HDAC9 proteins were not detectable in most cell lines.(B, C) MARK2, HDAC4/7, and YAP expressions are positively correlated in PDAC patients. Data were generated from an online analysis tool (gepia2.cancer-pku.cn) using TCGA database.(D) Knockdown of HDAC4 did not affect cell proliferation rate in S2.013 cells.(E, F) Human PDAC cell lines with or without HDAC4 knockdown were treated with or without Taxol (1 μM for 24 h). Total cell lysates were probed with the indicated antibodies. Cl-PARP: cleaved PARP.(G) Human PDAC cell lines were treated with Taxol in the presence/absence of pan-HDAC inhibitors for 24 h. LBH589 was used at 300 nM for S2.013, 200 nM for PANC-1, and 10 nM for Capan-2. SAHA was used at 3 μM for S2.013, 5 μM for PANC-1, and 2.5 μM for Capan-2. (H, I) Knockdown of HDAC4 or HDAC7 impairs survival in clonogenic assays. Cells were treated with Taxol (50 nM, 100 nM for 24 h) and colonies were quantified from three independent experiments. ***: $p<0.001$, **: $p=0.001$ (Student's t-test) (H). **: $p=0.003$, **: $p=0.006$ (Student's t-test) (I). (J, K) Phosphorylation is required for HDAC4-driven resistance to Taxol in PDAC cells. Establishment of HDAC4-knockdown cells expressing wild type HDAC4 or HDAC-3A (S246/S467A/S632A) (J). Cells from J were treated with DMSO or Taxol (1 μM for 24 h). (L, M) HDAC4/7 knockdown enhanced Gemcitabine cytotoxicity in human PDAC cells. Control and HDAC4- or HDAC7-knockdown cell lines were treated with DMSO or Gemcitabine (GEM, 500 nM for 48 h in S2.013 and 10 μM for 72 h in PANC-1).**O, P.** MARK2 regulates Taxol chemosensitivity through HDAC4. Establishment of MARK2-knockdown cells expressing HDAC4 or HDAC4-3A. LE: long exposure; SE: short exposure (O). Cells were treated with DMSO or Taxol (1 μM for 24 h). Total cell lysates were probed with the indicated antibodies.

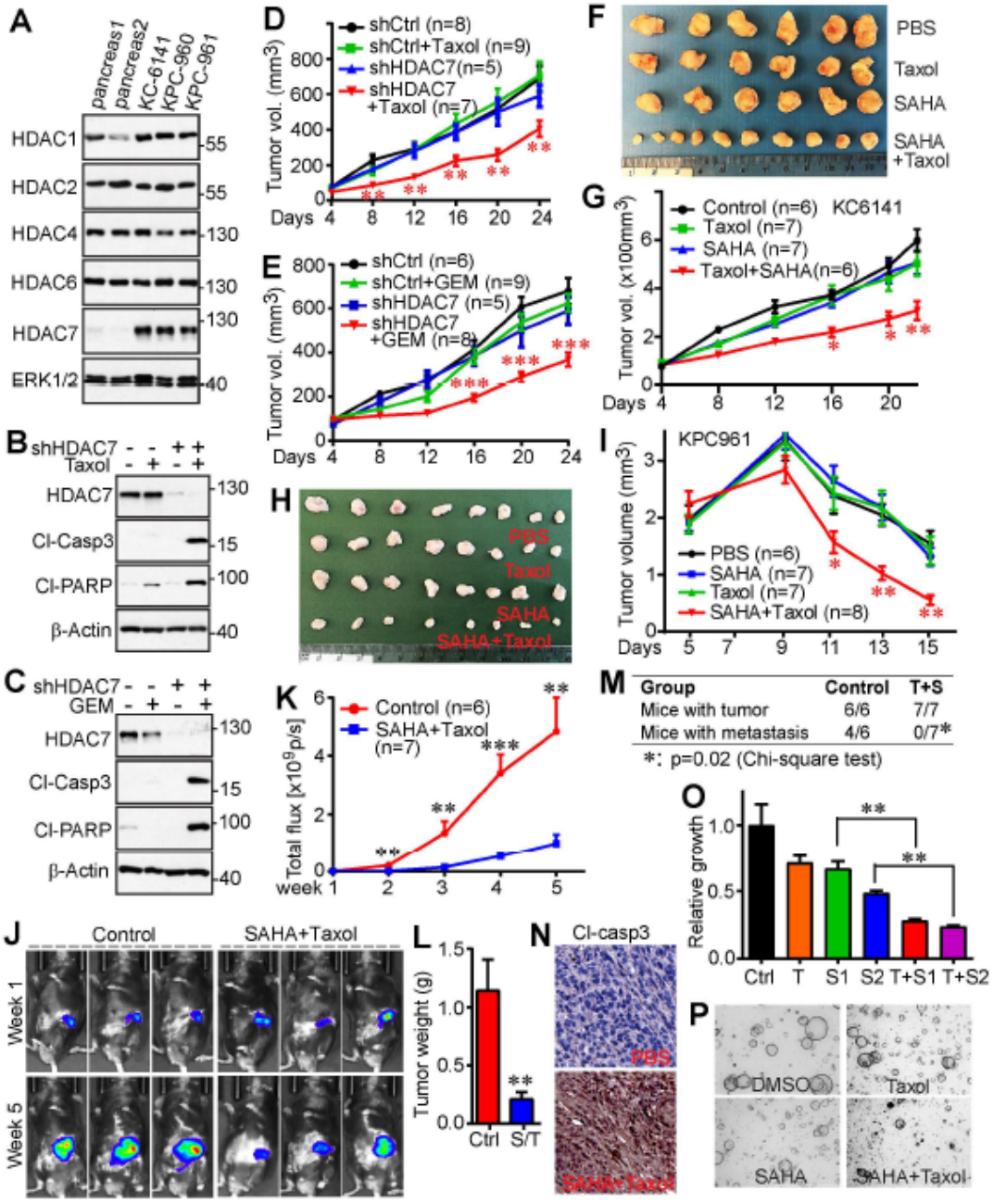
A
pancreas1
pancreas2
KC-6141
KPC-960
KPC-961
HDAC1
HDAC2
HDAC4
HDAC6
HDAC7
ERK1/2
55
55
130
130
130
40
B
shHDAC7 - - + +
Taxol - + - +
HDAC7
Cl-Casp3
Cl-PARP
β-Actin
130
15
100
40
C
shHDAC7 - - + +
GEM - + - +
HDAC7
Cl-Casp3
Cl-PARP
β-Actin
130
15
100
40
D
shCtrl (n=8)
shCtrl+Taxol (n=9)
shHDAC7(n=5)
shHDAC7 +Taxol (n=7)
Tumor vol. (mm3)
Days
E
shCtrl (n=6)
shCtrl+GEM (n=9)
shHDAC7 (n=5)
shHDAC7 +GEM (n=8)
Tumor vol. (mm3)
Days
F
PBS
Taxol
SAHA
SAHA +Taxol
G
Control (n=6) KC6141
Taxol (n=7)
SAHA (n=7)
Taxol+SAHA(n=6)
Tumor vol. (x100mm3)
Days
H
PBS
Taxol
SAHA
SAHA+Taxol
I
KPC961
PBS (n=6)
SAHA (n=7)
Taxol (n=7)
SAHA+Taxol (n=8)
Tumor volume (mm3)
Days
K
Control (n=6)
SAHA+Taxol (n=7)
Total flux [x10^9 p/s]
week
M
Group | Control | T+S
Mice with tumor | 6/6 | 7/7
Mice with metastasis | 4/6 | 0/7*
*: p=0.02 (Chi-square test)
O
Relative growth
Ctrl T S1 S2 T+S1 T+S2
J
Control
SAHA+Taxol
Week 1
Week 5
L
Tumor weight (g)
Ctrl S/T
N
Cl-casp3
PBS
SAHA+Taxol
P
DMSO
Taxol
SAHA
SAHA+Taxol

Figure 3-11. Inhibition of HDAC promotes chemosensitivity *in vivo*

(A) Protein expression of HDACs in normal mouse pancreas and mouse pancreatic cancer cell lines. HDAC1/2, HDAC4/7, HDAC6 are class I, IIa, IIb HDACs, respectively. Class IIa HDAC5 and HDAC9 protein levels were extremely low/not detectable in mouse pancreatic tissue and cell lines. (B-E) Knockdown of HDAC7 enhances Taxol and Gemcitabine cytotoxicity in mouse pancreatic cancer cell line KC6141. Cell lines were treated with DMSO, Taxol (10 nM for 16h) or Gemcitabine (GEM, 50 nM for 16h). Cl-Casp3: cleaved caspase 3; Cl-PARP: cleaved PARP (B, C). Knockdown of HDAC7 synergizes with Taxol (D) or Gemcitabine (E) chemotherapy *in vivo.* KC6141 cells were subcutaneously inoculated into C57BL/6 mice. Drug treatment started at day 4 post-injection. Paclitaxel (8 mg/kg) and Gemcitabine (50 mg/kg) were used at every other day via intraperitoneal injection. The P values are 0.01 (day 8), 0.002 (day 12), 0.004 (day 16), 0.002 (day 20), 0.005 (day 24) (D); 0.0004 (day 16), 0.0003 (day 20), 0.0004 (day 24) (E). The P values are shown for comparing shCtrl+Taxol with shHDAC7+Taxol or shCtrl+GEM with shHDAC7+GEM groups using one-way ANOVA, Tukey's test. (F-I**)** Pan-HDAC inhibitor SAHA synergizes with Taxol treatment *in vivo*. KPC961 (F, G) and KC6141 (H, I) cells were subcutaneously inoculated into C57BL/6 mice. Animals were randomized (4 or 5 days post-injection) and treated with PBS, Paclitaxel (8 mg/kg), SAHA (25 mg/kg) or the combination. The P values are 0.02 (day 11), 0.002 (day 13), 0.004 (day 15) (**G**); 0.02 (day 16), 0.01 (day 20), 0.001 (day 22) (**I**). The P values are shown for comparing SAHA with SAHA+Taxol groups using one-way ANOVA, Tukey's test.(J-M) Pan-HDAC inhibitor SAHA synergizes with Taxol treatment *in vivo* (orthotopic model) (J, K). KC6141-luciferase cells were implanted to the head of the mouse pancreas, and treatment was initiated 7 days post-injection. The representative animals in each group at week 1 and week 5 were shown (J). At the end of week 5, tumors (primary and metastatic) were removed and weighed (L). SAHA+Taxol treatment-induced apoptosis (M). The P values are 0.003

(week 2), 0.009 (week 3), 0.0006 (week 4), 0.005 (week 5) (K); **: p=0.004 (L) (Student's t-test).

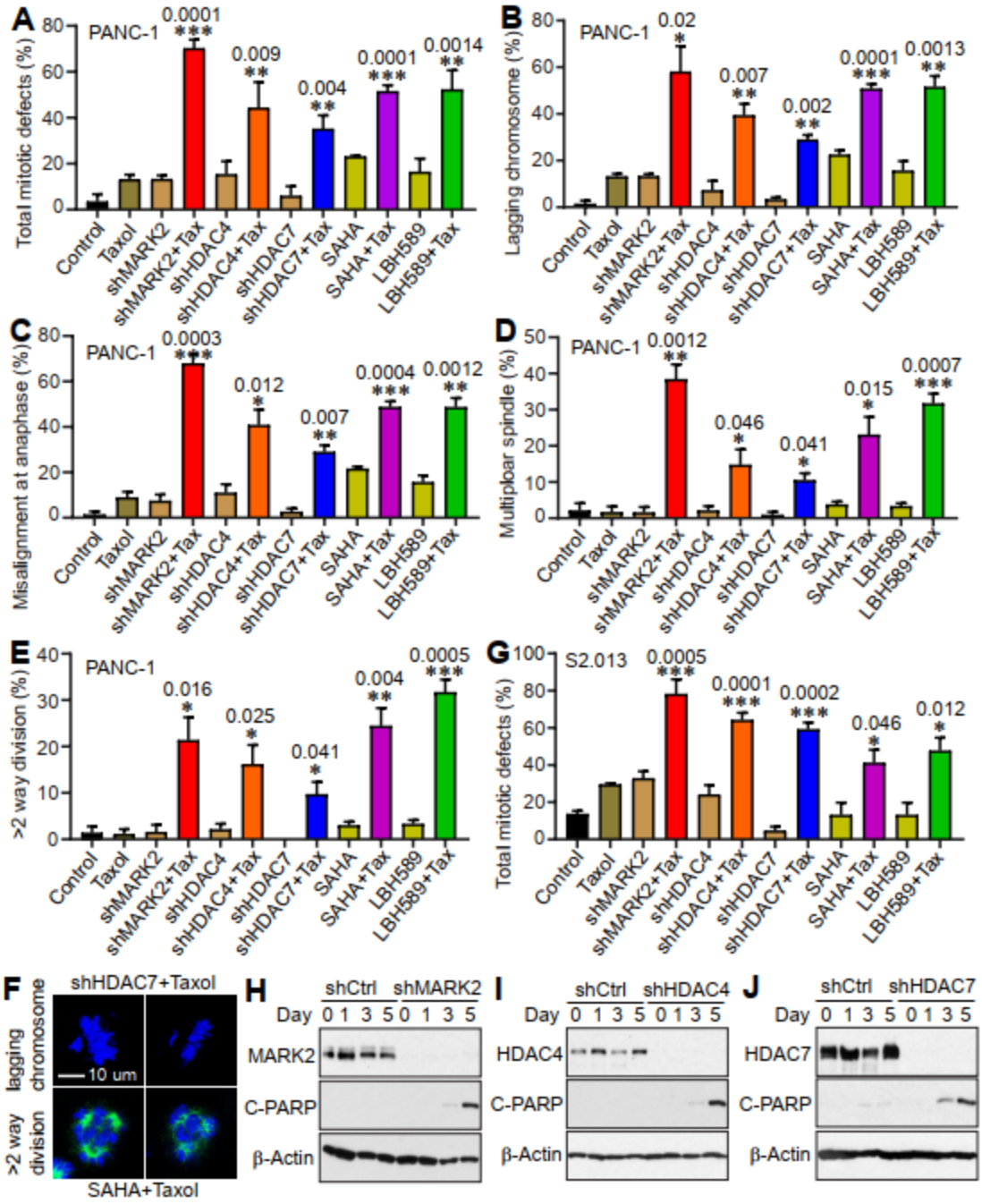
A
PANC-1
Total mitotic defects (%)
0.0001
0.009
0.004
0.0001
0.0014
B
PANC-1
Lagging chromosome (%)
0.02
0.007
0.002
0.0001
0.0013
C
PANC-1
Misalignment at anaphase (%)
0.0003
0.012
0.007
0.0004
0.0012
D
PANC-1
Multiploar spindle (%)
0.0012
0.046
0.041
0.015
0.0007
E
PANC-1
>2 way division (%)
0.016
0.025
0.041
0.004
0.0005
G
S2.013
Total mitotic defects (%)
0.0005
0.0001
0.0002
0.046
0.012
Control
Taxol
shMARK2
shMARK2+Tax
shHDAC4
shHDAC4+Tax
shHDAC7
shHDAC7+Tax
SAHA
SAHA+Tax
LBH589
LBH589+Tax
F
shHDAC7+Taxol
lagging chromosome
>2 way division
10 um
SAHA+Taxol
H
shCtrl
shMARK2
Day 0 1 3 5 0 1 3 5
MARK2
C-PARP
β-Actin
I
shCtrl
shHDAC4
Day 0 1 3 5 0 1 3 5
HDAC4
C-PARP
β-Actin
J
shCtrl
shHDAC7
Day 0 1 3 5 0 1 3 5
HDAC7
C-PARP
β-Actin

Figure 3-12. MARK2-HDAC inhibition synergizes with Taxol treatment to induce mitotic defects in PDAC cells

(A-E) Mitotic defects were quantified in PANC-1 cells under various treatments. Low concentrations of Taxol (5 nM) were used in all experiments. Under this condition, cells proliferate without arrest. SAHA and LBH589 were used at 5 μM and 0.2 μM, respectively. Experiments were done at 24 h post-treatment. N=3 from 40-60 mitotic cells of each condition. P values on each column indicate the statistical analysis comparing with Taxol-treated cells (Student's t-test). (F) Representative confocal microscopy images of mitotic defects in PANC-1.**G.** Mitotic defects were quantified in S2.013 cells. Treatments were the same as in PANC-1 cells. (H-J) MARK2-HDAC inhibition synergizes with Taxol (low concentration) treatment to induce apoptosis in PANC-1 cells. Cells were treated with DMSO, Taxol (5 nM for 0 h, 24 h, 72 h, and 120 h). Total cell lysates were probed with the indicated antibodies. C-PARP: cleaved PARP.

Table 1. shRNA target sequences

Gene	Target sequence (5'-3')
human MARK2	TGCACAGAGTATTTCGCCTAA
mouse MARK2	TGCACAGAGTATTTCGCCTAA
human HDAC4	CGACTCATCTTGTAGCTTATT
human HDAC7	CAAGTAGTTGGAACCAGAGAA
mouse HDAC7	GCTGAAGTGATCCTGAAGAAA

Table 2. MARK2 guide sequences

Oligo name	Sequence (5'-3')
MARK2 ex1 sgRNA A FWD	CACCGCCTACCCACGCTGAACGAGA
MARK2 ex1 sgRNA A REV	aaacTCTCGTTCAGCGTGGGTAGGC
MARK2 ex1 sgRNA B REV	aaacCCGAGATACCGGCGCCATGTC
MARK2 ex1 sgRNA B FWD	CACCGACATGGCGCCGGTATCTCGG
MARK2 ex2 sgRNA A FWD	CACCGAGCCCCACATTGGAAACTAC
MARK2 ex2 sgRNA A REV	aaacGTAGTTTCCAATGTGGGGCTC
MARK2 ex2 sgRNA B REV	aaacACATGATTCGGGGCCGCAAC
MARK2 ex2 sgRNA B FWD	CACCGTTGCGGCCCCGAATCATGT
Fwd, forward; Rev, reverse.	

Table 3. Antibodies used in this study

Vendor	Cat. Number	Antibody name
Cell Signaling Technology	3633	ALK (D5F3®) XP® Rabbit mAb
Cell Signaling Technology	3262	BLK Antibody
Cell Signaling Technology	55174	BRK/PTK6 (D4O2D) Rabbit mAb
Cell Signaling Technology	14162	ETK/BMX Antibody

Continued

Vendor	Cat. Number	Antibody name
Cell Signaling Technology	14582	M-CSF Receptor (E7S2S) Rabbit mAb
Cell Signaling Technology	4290	HER2/ERBB2 (D8F12) XP® Rabbit mAb
Cell Signaling Technology	4795	HER4/ERBB4 (111B2) Rabbit mAb
Cell Signaling Technology	8793	EPHA3/A4/A5 (D2C11) Rabbit mAb
Cell Signaling Technology	14389	EPHB2 Antibody
Cell Signaling Technology	14960	EPHB4 (D1C7N) Rabbit mAb
Cell Signaling Technology	2736	FES Antibody
Cell Signaling Technology	9740	FGF Receptor 1 (D8E4) XP® Rabbit mAb
Cell Signaling Technology	11835	FGF Receptor 2 (D4H9) Rabbit mAb
Cell Signaling Technology	4574	FGF Receptor 3 (C51F2) Rabbit mAb
Cell Signaling Technology	8562	FGF Receptor 4 (D3B12) XP Rabbit mAb
Cell Signaling Technology	2755	FGR Antibody
Cell Signaling Technology	3462	FLT3 (8F2) Rabbit mAb
Cell Signaling Technology	4023	FYN Antibody
Cell Signaling Technology	14643	HCK (E1I7F) Rabbit mAb
Cell Signaling Technology	2380	ITK (2F12) Mouse mAb
Cell Signaling Technology	9750	IGF-I Receptor β (D23H3) XP Rabbit mAb
Cell Signaling Technology	3344	JAK1 (6G4) Rabbit mAb
Cell Signaling Technology	8863	JAK3 (D7B12) Rabbit mAb
Cell Signaling Technology	2984	LCK (D88) XP® Rabbit mAb

Continued

Vendor	Cat. Number	Antibody name
Cell Signaling Technology	2796	LYN (C13F9) Rabbit mAb
Cell Signaling Technology	8198	MET (D1C2) XP® Rabbit mAb
Cell Signaling Technology	14556	RET (E1N8X) XP® Rabbit mAb
Cell Signaling Technology	2654	RON (C81H9) Rabbit mAb
Cell Signaling Technology	2109	SRC (36D10) Rabbit mAb
Cell Signaling Technology	4987	TEC Antibody
Cell Signaling Technology	14193	TYK2 (D4I5T) Rabbit mAb
Cell Signaling Technology	4691	Akt (pan) (C67E7) Rabbit mAb
Cell Signaling Technology	2795	AMPK-alpha-1 Rabbit mAb
Cell Signaling Technology	2757	AMPK-alpha-2 Rabbit Antibody
Cell Signaling Technology	4178	AMPKβ1 (71C10) Rabbit mAb
Cell Signaling Technology	4148	AMPKβ2 Rabbit Antibody
Cell Signaling Technology	4187	AMPKγ1 Rabbit Antibody
Cell Signaling Technology	2536	AMPKγ2 Rabbit Antibody
Cell Signaling Technology	2550	AMPKγ3 Rabbit Antibody
Cell Signaling Technology	3477	LATS1 (C66B5) Rabbit mAb
Cell Signaling Technology	5888	LATS2 (D83D6) Rabbit mAb
Cell Signaling Technology	3682	MST1 Rabbit Antibody
Cell Signaling Technology	3952	MST2 Rabbit Antibody
Cell Signaling Technology	12417	CK1δ Antibody

Continued

Vendor	Cat. Number	Antibody name
Cell Signaling Technology	4695	p44/42 MAPK (Erk1/2) (137F5) Rabbit mAb
Cell Signaling Technology	8943	IKKβ (D30C6) Rabbit mAb
Cell Signaling Technology	8242	NF-κB p65 (D14E12) XP® Rabbit mAb
Cell Signaling Technology	9252	SAPK/JNK Rabbit mAb
Cell Signaling Technology	3319	MARK1 Antibody
Cell Signaling Technology	9311	MARK3 Antibody
Cell Signaling Technology	4834	MARK4 Antibody
Cell Signaling Technology	4249	PI3 Kinase p110α (C73F8) Rabbit mAb
Cell Signaling Technology	3011	PI3 Kinase p110β (C33D4) Rabbit mAb
Cell Signaling Technology	5842	PKA C-α (D38C6) Rabbit mAb
Cell Signaling Technology	12297	PKR (D7F7) Rabbit mAb
Cell Signaling Technology	6997	EPHA2 (D4A2) XP Rabbit mAb
Cell Signaling Technology	4570	TNK1 (C44F9) Rabbit mAb
Cell Signaling Technology	3201S	YES Antibody
Cell Signaling Technology	64094	VEGF Receptor 1 (E7T9H) Rabbit mAb
Cell Signaling Technology	9698	VEGF Receptor 2 (D5B1) Rabbit mAb
Cell Signaling Technology	33566	VEGF Receptor 3 (D1J9Z) Rabbit mAb
Cell Signaling Technology	3174	PDGF Receptor α (D1E1E) XP® Rabbit mAb
Cell Signaling Technology	3169	PDGF Receptor β (28E1) Rabbit mAb
Cell Signaling Technology	3376	TRKC (C44H5) Rabbit mAb

Continued

Vendor	Cat. Number	Antibody name
Cell Signaling Technology	4603	TRKB (80E3) Rabbit mAb
Cell Signaling Technology	2510	TRKA (12G8) Rabbit mAb
Santa Cruz Biotechnology	sc-7291	GSK-3α/β (0011-A)
Santa Cruz Biotechnology	SC-28336	ACK (A-11)
Santa Cruz Biotechnology	SC-533	LSK (C-20)
Santa Cruz Biotechnology	SC-393465	LTK/TYK1 (B-6)
Santa Cruz Biotechnology	SC-166478	FRK/RAK (H-12)
Santa Cruz Biotechnology	SC-130386	ROR1 (60-D)
Santa Cruz Biotechnology	SC-342	TIE-1 (C-18)
Santa Cruz Biotechnology	SC-377202	TXK (B-2)
Santa Cruz Biotechnology	sc-8408	CHK1 (G-4)
Santa Cruz Biotechnology	sc-5278	CHK2 (A-12)
Santa Cruz Biotechnology	sc-365405	MARK2 (B-1)
Santa cruz biotechnology	sc-219	MEK-1(C-18)
Santa Cruz Biotechnology	sc-216	PKC ζ (C-20)
Santa Cruz Biotechnology	sc-1842	PKN(c-19)
Santa Cruz Biotechnology	sc-271971	PKN2
Santa cruz biotechnology	sc-231	RSK-1(C-21)
Santa Cruz Biotechnology	sc-1430	RSK-2 (C-19)
Santa Cruz Biotechnology	sc-8418	p70 S6 kinase α (H-9)

Continued

Vendor	Cat. Number	Antibody name
Santa Cruz Biotechnology	sc-6282	PKR (B-10)
Bethyl Labs Inc.	A301-660A-T	rabbit anti-CABL antibody
Bethyl Labs Inc.	A301-986A-T	rabbit anti-ARG antibody
Bethyl Labs Inc.	A304-231A-T	rabbit anti-CSK antibody
Bethyl Labs Inc.	A300-387A-T	rabbit anti-EGFR antibody
Bethyl Labs Inc.	A301-693A-T	rabbit anti-FAK antibody
Bethyl Labs Inc.	A304-310A-T	rabbit anti-FER antibody
Bethyl Labs Inc.	A303-712A-T	rabbit anti-insulin receptor beta
Bethyl Labs Inc.	A303-252A-T	rabbit anti-C-KIT antibody
Bethyl Labs Inc.	A302-178A-T	rabbit anti-JAK2 antibody
Bethyl Labs Inc.	A304-270A-T	rabbit anti-LMTK2 antibody
Bethyl Labs Inc.	A300-222A-T	rabbit anti-Mertk/C-Mer
Bethyl Labs Inc.	A304-451A-T	rabbit anti-PTK7 antibody
Bethyl Labs Inc.	A304-227A-T	rabbit anti-PYK2 antibody
Bethyl Labs Inc.	A304-242A-T	rabbit anti-ROR2 antibody
Bethyl Labs Inc.	A300-559A-T	rabbit anti-SYK antibody
Bethyl Labs Inc.	A300-242A-T	rabbit anti-TYRO3 antibody
Bethyl Labs Inc.	A301-818A-T	rabbit anti-ZAP70 antibody
Bethyl Labs Inc.	A302-191A	Rabbit anti-MINK1 antibody
Bethyl Labs Inc.	A302-453A-T	Rabbit anti-PKN3 Antibody

Continued

Vendor	Cat. Number	Antibody name
Bethyl Labs Inc.	A300-524A	Rabbit anti-TAOK1 antibody
Bethyl Labs Inc.	A302-168A	rabbit anti-AXL Antibody
Bethyl Labs Inc.	A302-025A	rabbit anti-EPHA2 Antibody
BD Bioscience	610201	GSK3β
Abnova	PAB2668	Anti-CIT antibody

CHAPTER 4 SUMMARY OF THE ROLE OF VGLL4 AND MARK2-HDAC AXIS IN MITOSIS AND CANCER

Our study elucidated the regulation and their role of VGLL4 and MARK2 in mitosis. These studies support a notion that Hippo-YAP signaling exerts its function in tumorigenesis through controlling the mitotic machinery (Fig. 4-1).

We demonstrated that VGLL4 is phosphorylated at Ser58, Ser155, Thr159, Ser280 by CDK1 during mitosis. Mitotic phosphorylation of VGLL4 inhibits its tumor-suppressing activity in pancreatic cancer by affecting YAP and β-catenin activity.

Our study also revealed a novel regulatory mechanism underlying MARK2-meditated YAP activation. We identified that MARK2 directly phosphorylates HDAC4 S246/467/632 during mitosis, and HDAC4 S246/467/632 phosphorylation promotes YAP activation via altering the LATS2/YAP complex (Fig. 4-1). Importantly, the MARK2-HDAC axis determines paclitaxel chemosensitivity in pancreatic cancer. Our findings could be quickly translated into the clinic. For example, combination treatment of HDAC inhibitor with nab-paclitaxel is expected to overcome drug resistance in metastatic PDAC patients.

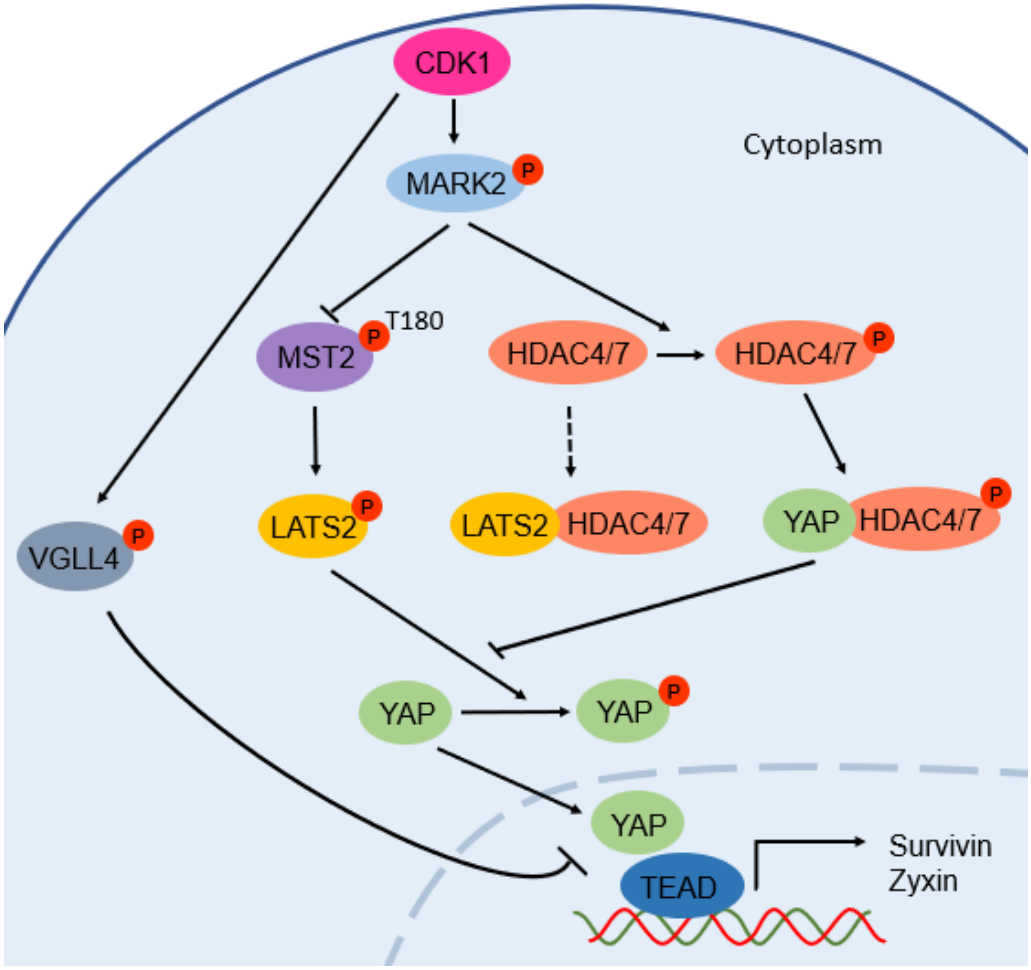

Figure 4-1 Schematic diagram of the role of VGLL4 and MARK2-HDAC axis in mitosis and cancer.

BIBLIOGRAPHY

1. Pan, D., *The hippo signaling pathway in development and cancer.* Dev Cell, 2010. **19**(4): p. 491-505.
2. Yu, F.X., B. Zhao, and K.L. Guan, *Hippo Pathway in Organ Size Control, Tissue Homeostasis, and Cancer.* Cell, 2015. **163**(4): p. 811-28.
3. Harvey, K.F., X. Zhang, and D.M. Thomas, *The Hippo pathway and human cancer.* Nat Rev Cancer, 2013. **13**(4): p. 246-57.
4. Zhao, B., et al., *TEAD mediates YAP-dependent gene induction and growth control.* Genes Dev, 2008. **22**(14): p. 1962-71.
5. Jiao, S., et al., *VGLL4 targets a TCF4-TEAD4 complex to coregulate Wnt and Hippo signalling in colorectal cancer.* Nat Commun, 2017. **8**: p. 14058.
6. Hansen, C.G., T. Moroishi, and K.L. Guan, *YAP and TAZ: a nexus for Hippo signaling and beyond.* Trends Cell Biol, 2015. **25**(9): p. 499-513.
7. Chiba, S., et al., *MST2- and Furry-mediated activation of NDR1 kinase is critical for precise alignment of mitotic chromosomes.* Curr Biol, 2009. **19**(8): p. 675-81.
8. Yabuta, N., et al., *The tumor suppressor Lats2 is pivotal in Aurora A and Aurora B signaling during mitosis.* Cell Cycle, 2011. **10**(16): p. 2724-36.
9. S, Y., et al., *CDK1 phosphorylation of YAP promotes mitotic defects and cell motility and is.* Cancer Res, 2013. **73**(22): p. 6722-33.
10. Dong, J., et al., *Elucidation of a universal size-control mechanism in Drosophila and mammals.* Cell, 2007. **130**(6): p. 1120-33.
11. Henriques, A.C., et al., *Mitosis inhibitors in anticancer therapy: When blocking the exit becomes a solution.* Cancer Lett, 2019. **440-441**: p. 64-81.
12. Dominguez-Brauer, C., et al., *Targeting Mitosis in Cancer: Emerging Strategies.* Mol Cell, 2015. **60**(4): p. 524-36.

13. Walsh, V. and J. Goodman, *From taxol to Taxol: the changing identities and ownership of an anti-cancer drug.* Med Anthropol, 2002. **21**(3-4): p. 307-36.

14. Janssen, A. and R.H. Medema, *Mitosis as an anti-cancer target.* Oncogene, 2011. **30**(25): p. 2799-809.

15. Jackson, J.R., et al., *Targeted anti-mitotic therapies: can we improve on tubulin agents?* Nat Rev Cancer, 2007. **7**(2): p. 107-17.

16. Sinn, M., et al., *CONKO-005: Adjuvant Chemotherapy With Gemcitabine Plus Erlotinib Versus Gemcitabine Alone in Patients After R0 Resection of Pancreatic Cancer: A Multicenter Randomized Phase III Trial.* J Clin Oncol, 2017. **35**(29): p. 3330-3337.

17. Conroy, T., et al., *FOLFIRINOX or Gemcitabine as Adjuvant Therapy for Pancreatic Cancer.* N Engl J Med, 2018. **379**(25): p. 2395-2406.

18. Ma, W.W. and M. Hidalgo, *The winning formulation: the development of paclitaxel in pancreatic cancer.* Clin Cancer Res, 2013. **19**(20): p. 5572-9.

19. Koontz, L.M., et al., *The Hippo effector Yorkie controls normal tissue growth by antagonizing scalloped-mediated default repression.* Dev Cell, 2013. **25**(4): p. 388-401.

20. Mann, K.M., et al., *Sleeping Beauty mutagenesis reveals cooperating mutations and pathways in pancreatic adenocarcinoma.* Proc Natl Acad Sci U S A, 2012. **109**(16): p. 5934-41.

21. Lee, K.M., et al., *Notch 2-positive progenitors with the intrinsic ability to give rise to pancreatic ductal cells.* Lab Invest, 2005. **85**(8): p. 1003-12.

22. Yang, S., et al., *Active YAP promotes pancreatic cancer cell motility, invasion and tumorigenesis in a mitotic phosphorylation-dependent manner through LPAR3.* Oncotarget, 2015. **6**(34): p. 36019-31.

23. Xiao, L., et al., *KIBRA regulates Hippo signaling activity via interactions with large tumor suppressor kinases.* J Biol Chem, 2011. **286**(10): p. 7788-96.

24. S, J., et al., *A peptide mimicking VGLL4 function acts as a YAP antagonist therapy against gastric cancer.* Cancer Cell, 2014. **25**(2): p. 166-80.

25. Yang, S., et al., *Phosphorylation of KIBRA by the extracellular signal-regulated kinase (ERK)-ribosomal S6 kinase (RSK) cascade modulates cell proliferation and migration.* Cell Signal, 2014. **26**(2): p. 343-51.

26. Elcheva, I., et al., *Direct induction of haematoendothelial programs in human pluripotent stem cells by transcriptional regulators.* Nat Commun, 2014. **5**: p. 4372.

27. Chen, X., et al., *Ajuba Phosphorylation by CDK1 Promotes Cell Proliferation and Tumorigenesis.* J Biol Chem, 2016. **291**(28): p. 14761-72.

28. Yang, S., et al., *CDK1 phosphorylation of YAP promotes mitotic defects and cell motility and is essential for neoplastic transformation.* Cancer Res, 2013. **73**(22): p. 6722-33.

29. Jube, S., et al., *Cancer cell secretion of the DAMP protein HMGB1 supports progression in malignant mesothelioma.* Cancer Res, 2012. **72**(13): p. 3290-301.

30. Zhang, L., et al., *CDK1 phosphorylation of TAZ in mitosis inhibits its oncogenic activity.* Oncotarget, 2015. **6**(31): p. 31399-412.

31. Ji, M., et al., *Phospho-regulation of KIBRA by CDK1 and CDC14 phosphatase controls cell-cycle progression.* Biochem J, 2012. **447**(1): p. 93-102.

32. Chen, X., Y. Chen, and J. Dong, *MST2 phosphorylation at serine 385 in mitosis inhibits its tumor suppressing activity.* Cell Signal, 2016. **28**(12): p. 1826-1832.

33. Nigg, E.A., *Cellular substrates of p34(cdc2) and its companion cyclin-dependent kinases.* Trends Cell Biol, 1993. **3**(9): p. 296-301.

34. Hornbeck, P.V., et al., *PhosphoSitePlus, 2014: mutations, PTMs and recalibrations.* Nucleic Acids Res, 2015. **43**(Database issue): p. D512-20.

35. Zhang, L., et al., *KIBRA regulates aurora kinase activity and is required for precise chromosome alignment during mitosis.* J Biol Chem, 2012. **287**(41): p. 34069-77.

36. Zhang, W., et al., *VGLL4 functions as a new tumor suppressor in lung cancer by negatively regulating the YAP-TEAD transcriptional complex.* Cell Res, 2014. **24**(3): p. 331-43.

37. Mann, K.M., et al., *Sleeping Beauty mutagenesis reveals cooperating mutations and pathways in pancreatic adenocarcinoma.* Proc Natl Acad Sci U S A, 2012. **109**(16): p. 5934-41.

38. Li, N., et al., *miR-222/VGLL4/YAP-TEAD1 regulatory loop promotes proliferation and invasion of gastric cancer cells.* Am J Cancer Res, 2015. **5**(3): p. 1158-68.

39. Li, H., et al., *VGLL4 inhibits EMT in part through suppressing Wnt/β-catenin signaling pathway in gastric cancer.* Med Oncol, 2015. **32**(3): p. 83.

40. Jiao, S., et al., *VGLL4 targets a TCF4-TEAD4 complex to coregulate Wnt and Hippo signalling in colorectal cancer. .* Nat Commun, 2017. **8**(14058).

41. B, Z., et al., *TEAD mediates YAP-dependent gene induction and growth control.* Genes Dev, 2008. **22**(14): p. 1962-71.

42. Yang, S., et al., *Oncoprotein YAP regulates the spindle checkpoint activation in a mitotic phosphorylation-dependent manner through up-regulation of BubR1.* J Biol Chem, 2015. **290**(10): p. 6191-202.

43. Tang, E.I., D.D. Mruk, and C.Y. Cheng, *MAP/microtubule affinity-regulating kinases, microtubule dynamics, and spermatogenesis.* J Endocrinol, 2013. **217**(2): p. R13-23.

44. Drewes, G., et al., *MARK, a novel family of protein kinases that phosphorylate microtubule-associated proteins and trigger microtubule disruption.* Cell, 1997. **89**(2): p. 297-308.

45. Ahrari, S., N. Mogharrab, and L. Navapour, *Interconversion of inactive to active conformation of MARK2: Insights from molecular modeling and molecular dynamics simulation.* Arch Biochem Biophys, 2017. **630**: p. 66-80.

46. Natalia, M.A., et al., *MARK1 is a Novel Target for miR-125a-5p: Implications for Cell Migration in Cervical Tumor Cells.* Microrna, 2018. **7**(1): p. 54-61.

47. Goodwin, J.M., et al., *An AMPK-independent signaling pathway downstream of the LKB1 tumor suppressor controls Snail1 and metastatic potential.* Mol Cell, 2014. **55**(3): p. 436-50.

48. Hubaux, R., et al., *Microtubule affinity-regulating kinase 2 is associated with DNA damage response and cisplatin resistance in non-small cell lung cancer.* Int J Cancer, 2015. **137**(9): p. 2072-82.

49. Pardo, O.E., et al., *miR-515-5p controls cancer cell migration through MARK4 regulation.* EMBO Rep, 2016. **17**(4): p. 570-84.

50. Magnani, I., et al., *Differential signature of the centrosomal MARK4 isoforms in glioma.* Anal Cell Pathol (Amst), 2011. **34**(6): p. 319-38.

51. Kato, T., et al., *Isolation of a novel human gene, MARKL1, homologous to MARK3 and its involvement in hepatocellular carcinogenesis.* Neoplasia, 2001. **3**(1): p. 4-9.

52. Jenardhanan, P., J. Mannu, and P.P. Mathur, *The structural analysis of MARK4 and the exploration of specific inhibitors for the MARK family: a computational approach to obstruct the role of MARK4 in prostate cancer progression.* Mol Biosyst, 2014. **10**(7): p. 1845-68.

53. Heidary Arash, E., et al., *MARK4 inhibits Hippo signaling to promote proliferation and migration of breast cancer cells.* EMBO Rep, 2017. **18**(3): p. 420-436.

54. Beghini, A., et al., *The neural progenitor-restricted isoform of the MARK4 gene in 19q13.2 is upregulated in human gliomas and overexpressed in a subset of glioblastoma cell lines.* Oncogene, 2003. **22**(17): p. 2581-91.

55. Mohseni, M., et al., *A genetic screen identifies an LKB1-MARK signalling axis controlling the Hippo-YAP pathway.* Nat Cell Biol, 2014. **16**(1): p. 108-17.

56. Kwan, J., et al., *DLG5 connects cell polarity and Hippo signaling protein networks by linking PAR-1 with MST1/2.* Genes Dev, 2016. **30**(24): p. 2696-2709.

57. Huang, H.L., et al., *Par-1 regulates tissue growth by influencing hippo phosphorylation status and hippo-salvador association.* PLoS Biol, 2013. **11**(8): p. e1001620.

58. Varelas, X., *The Hippo pathway effectors TAZ and YAP in development, homeostasis and disease.* Development, 2014. **141**(8): p. 1614-26.

59. Maugeri-Saccà, M. and R. De Maria, *The Hippo pathway in normal development and cancer.* Pharmacol Ther, 2018. **186**: p. 60-72.

60. Fu, V., S.W. Plouffe, and K.L. Guan, *The Hippo pathway in organ development, homeostasis, and regeneration.* Curr Opin Cell Biol, 2017. **49**: p. 99-107.

61. Dequiedt, F., et al., *New role for hPar-1 kinases EMK and C-TAK1 in regulating localization and activity of class IIa histone deacetylases.* Mol Cell Biol, 2006. **26**(19): p. 7086-102.

62. Wang, A.H., et al., *Regulation of histone deacetylase 4 by binding of 14-3-3 proteins.* Mol Cell Biol, 2000. **20**(18): p. 6904-12.

63. Grozinger, C.M. and S.L. Schreiber, *Regulation of histone deacetylase 4 and 5 and transcriptional activity by 14-3-3-dependent cellular localization.* Proc Natl Acad Sci U S A, 2000. **97**(14): p. 7835-40.

64. Roche, J. and P. Bertrand, *Inside HDACs with more selective HDAC inhibitors.* Eur J Med Chem, 2016. **121**: p. 451-483.

65. Hessmann, E., et al., *Epigenetic treatment of pancreatic cancer: is there a therapeutic perspective on the horizon?* Gut, 2017. **66**(1): p. 168-179.

66. Suraweera, A., K.J. O'Byrne, and D.J. Richard, *Combination Therapy With Histone Deacetylase Inhibitors (HDACi) for the Treatment of Cancer: Achieving the Full Therapeutic Potential of HDACi.* Front Oncol, 2018. **8**: p. 92.

67. Torres, M.P., et al., *Novel pancreatic cancer cell lines derived from genetically engineered mouse models of spontaneous pancreatic adenocarcinoma: applications in diagnosis and therapy.* PLoS One, 2013. **8**(11): p. e80580.

68. S, S., et al., *CDK1-mediated mitotic phosphorylation of PBK is involved in cytokinesis and inhibits its oncogenic activity.* Cell Signal, 2017. **39**: p. 74-83.

69. Zhang, L., et al., *The hippo pathway effector YAP regulates motility, invasion, and castration-resistant growth of prostate cancer cells.* Mol Cell Biol, 2015. **35**(8): p. 1350-62.

70. Zhao, Y. and X. Yang, *Regulation of sensitivity of tumor cells to antitubulin drugs by Cdk1-TAZ signalling.* Oncotarget, 2015. **6**(26): p. 21906-17.

71. J, Z., et al., *Zyxin promotes colon cancer tumorigenesis in a mitotic phosphorylation-dependent manner and through CDK8-mediated YAP activation.* Proc Natl Acad Sci U S A, 2018. **115**(29): p. E6760-E6769.

72. Qiu, W. and G.H. Su, *Development of orthotopic pancreatic tumor mouse models.* Methods Mol Biol, 2013. **980**: p. 215-23.

73. Duong-Ly, K.C. and J.R. Peterson, *The human kinome and kinase inhibition.* Curr Protoc Pharmacol, 2013. **Chapter 2**: p. Unit2.9.

74. Robinson, D.R., Y.M. Wu, and S.F. Lin, *The protein tyrosine kinase family of the human genome.* Oncogene, 2000. **19**(49): p. 5548-57.

75. Wang, Z., et al., *Cyclin-dependent kinase 1-mediated phosphorylation of YES links mitotic arrest and apoptosis during antitubulin chemotherapy.* Cell Signal, 2018. **52**: p. 137-146.

76. Stauffer, S., et al., *Cyclin-dependent kinase 1-mediated AMPK phosphorylation regulates chromosome alignment and mitotic progression.* J Cell Sci, 2019. **132**(20).

77. Woodring, P.J., T. Hunter, and J.Y. Wang, *Mitotic phosphorylation rescues Abl from F-actin-mediated inhibition.* J Biol Chem, 2005. **280**(11): p. 10318-25.

78. Ma, A., et al., *Serine phosphorylation of focal adhesion kinase in interphase and mitosis: a possible role in modulating binding to p130(Cas).* Mol Biol Cell, 2001. **12**(1): p. 1-12.

79. Kiyokawa, N., et al., *Mitosis-specific negative regulation of epidermal growth factor receptor, triggered by a decrease in ligand binding and dimerization, can be overcome by overexpression of receptor.* J Biol Chem, 1997. **272**(30): p. 18656-65.

80. Bagrodia, S., et al., *Altered tyrosine 527 phosphorylation and mitotic activation of p60c-src.* Nature, 1991. **349**(6305): p. 172-5.

81. B, Z., et al., *Inactivation of YAP oncoprotein by the Hippo pathway is involved in cell contact inhibition and tissue growth control.* Genes Dev, 2007. **21**(21): p. 2747-61.

82. Tsai, H.C., et al., *CTGF increases drug resistance to paclitaxel by upregulating survivin expression in human osteosarcoma cells.* Biochim Biophys Acta, 2014. **1843**(5): p. 846-54.

83. Lens, S.M., et al., *Survivin is required for a sustained spindle checkpoint arrest in response to lack of tension.* Embo j, 2003. **22**(12): p. 2934-47.

84. Aylon, Y., et al., *A positive feedback loop between the p53 and Lats2 tumor suppressors prevents tetraploidization.* Genes Dev, 2006. **20**(19): p. 2687-700.

85. Wang, Z., G. Qin, and T.C. Zhao, *HDAC4: mechanism of regulation and biological functions.* Epigenomics, 2014. **6**(1): p. 139-50.

86. Wanek, J., et al., *Pharmacological Inhibition of Class IIA HDACs by LMK-235 in Pancreatic Neuroendocrine Tumor Cells.* Int J Mol Sci, 2018. **19**(10).

87. Sild, M. and L. Booij, *Histone deacetylase 4 (HDAC4): a new player in anorexia nervosa?* Mol Psychiatry, 2019. **24**(10): p. 1425-1434.

88. Ni, X., L. Li, and G. Pan, *HDAC inhibitor-induced drug resistance involving ATP-binding cassette transporters (Review).* Oncol Lett, 2015. **9**(2): p. 515-521.

89. Zasadil, L.M., et al., *Cytotoxicity of paclitaxel in breast cancer is due to chromosome missegregation on multipolar spindles.* Sci Transl Med, 2014. **6**(229): p. 229ra43.

90. Weaver, B.A., *How Taxol/paclitaxel kills cancer cells.* Mol Biol Cell, 2014. **25**(18): p. 2677-81.

91. Wang, L., et al., *Targeting HDAC with a novel inhibitor effectively reverses paclitaxel resistance in non-small cell lung cancer via multiple mechanisms.* Cell Death Dis, 2016. **7**(1): p. e2063.

92. Dowdy, S.C., et al., *Histone deacetylase inhibitors and paclitaxel cause synergistic effects on apoptosis and microtubule stabilization in papillary serous endometrial cancer cells.* Mol Cancer Ther, 2006. **5**(11): p. 2767-76.

93. Dietrich, C.S., 3rd, et al., *Suberoylanilide hydroxamic acid (SAHA) potentiates paclitaxel-induced apoptosis in ovarian cancer cell lines.* Gynecol Oncol, 2010. **116**(1): p. 126-30.

94. Koutsounas, I., C. Giaginis, and S. Theocharis, *Histone deacetylase inhibitors and pancreatic cancer: are there any promising clinical trials?* World J Gastroenterol, 2013. **19**(8): p. 1173-81.

95. Bayat Mokhtari, R., et al., *Combination therapy in combating cancer.* Oncotarget, 2017. **8**(23): p. 38022-38043.

96. Yang, C.H. and S.B. Horwitz, *Taxol(®): The First Microtubule Stabilizing Agent.* Int J Mol Sci, 2017. **18**(8).